

**NPS ARCHIVE**  
**1966**  
**ALVAREZ, F.**

FLUID CONTROL SYSTEM BEHAVIOR  
IN A RANDOMLY VIBRATING ENVIRONMENT

by

LCDR. FRANKLIN F. ALVAREZ, U.S.N.

SUBMITTED IN PARTIAL FULFILLMENT

OF THE REQUIREMENTS FOR THE

DEGREE OF DOCTOR OF

SCIENCE

in

MECHANICAL ENGINEERING

at the

MASSACHUSETTS INSTITUTE OF

TECHNOLOGY

AUGUST, 1966

DUDLEY KNOX LIBRARY  
NAVAL POSTGRADUATE SCHOOL  
MONTEREY, CA 93943-5101

FLUID CONTROL SYSTEM BEHAVIOR  
IN A RANDOMLY VIBRATING ENVIRONMENT

by

LCDR. FRANKLIN F. ALVAREZ, U.S.N.

B.S., UNITED STATES NAVAL ACADEMY

(1957)

S.M., MASSACHUSETTS INSTITUTE OF TECHNOLOGY

(1964)

NAV.E., MASSACHUSETTS INSTITUTE OF TECHNOLOGY

(1964)

SUBMITTED IN PARTIAL FULFILLMENT

OF THE REQUIREMENTS FOR THE

DEGREE OF DOCTOR OF

SCIENCE

at the

MASSACHUSETTS INSTITUTE OF

TECHNOLOGY

AUGUST, 1966

NPS ARCHIVE

K166

ALVAREZ, F.

~~Thesis~~  
~~A4289~~

ABSTRACT

FLUID CONTROL SYSTEM BEHAVIOR IN A RANDOMLY VIBRATING ENVIRONMENT

LCDR. Franklin F. Alvarez, U.S.N.

Submitted to the Department of Mechanical Engineering on August 15,  
1966 in partial fulfillment of the requirements for the degree of  
Doctor of Science.

A fluid control system is analysed while operating in a vibrating environment. The introduction and transmission of noise signals in the way of unwanted pressures are examined for passive transmission line elements and an active flapper-nozzle control valve when subjected to environmental random or periodic translational vibrations. Methods are presented for predicting the levels and frequencies of induced pressures using distributed and lumped parameter techniques, including some damping effects. Analytic results evaluated with the help of a digital and analog computer are presented along with experimental data obtained for vibrating pneumatic transmission lines and for a small pneumatic control valve. Also included is a procedure for testing a given system's susceptibility to vibration induced noise sources.

It is found that pressure peaks proportional to the fluid density, speed of sound in the fluid, and degree of excitation are generated in transmission lines over a wide band of frequencies. The peaks occur at the system resonant frequencies, and are due to induced fluid flow caused by pipe boundary nonuniformities (bends and area changes) moving relative to the fluid. The noise signals are excited by either longitudinal or transverse piping vibrations making the system susceptible to noise introduction regardless of its orientation with respect to the vibrating field.

Noise is introduced into the control valve by means of the vibrating supply line, inertial forcing of the valve flapper, and for high pressure systems, by vibrations of the transmission line to the load. The greatest noise transmission takes place at low frequencies and near the flapper resonance. Force feedback by means of a bellows arrangement decreases the amplitudes at the lower frequencies, but reinforces those near the flapper resonance and can cause noise power amplification.

Thesis Supervisor: Henry M. Paynter

Title: Professor of Mechanical Engineering



ACKNOWLEDGEMENT

I wish to express my appreciation to my committee, Professor Henry M. Paynter, Professor Patrick Leehey, and Professor Dean C. Karnopp, whose many helpful suggestions, guidance, and encouragement made it possible for me to complete this endeavor.

I am also indebted to Professor Richard J. Gurski for his valuable assistance and to Mr. Wilbur A. Windsor and Mr. Robert M. Haley of the Engineering Projects Laboratory for their excellent help with instrumentation.

I also want to acknowledge the United States Navy which financed my education and allowed me the two extra years past the Master's in order to obtain this degree.

Lastly I want to thank the many others, including my family, who have helped me to reach this goal.

This work was done in part at the Computer Center at the Massachusetts Institute of Technology, Cambridge, Massachusetts.





TABLE OF CONTENTS

	<u>Page</u>
List of Figures -----	6
List of Tables -----	8
<u>Chapter 1.</u> Introduction -----	9
1.1 Background -----	9
1.2 Objectives and Procedure -----	10
<u>Chapter 2.</u> Vibration Induced Transmission Line Noise -----	12
2.1 Introduction -----	12
2.2 Concept -----	12
2.3 Method of Modelling Vibration Induced Flow Sources -----	14
2.4 Development for Longitudinal Vibrations -----	15
2.5 Development for Transverse Vibrations -----	24
2.6 Damping and Its Effects -----	33
2.7 Random Excitation -----	35
2.8 Experimental Results -----	36
2.9 Summary -----	45
<u>Chapter 3.</u> Control Valve Analysis -----	65
3.1 Introduction -----	65
3.2 Mathematical Models -----	66
3.2.1 Valve Chamber -----	66
3.2.2 Valve Flapper -----	68
3.2.3 Transmission Line, Distributed Parameters -----	72
3.2.4 Transmission Line, Lumped Parameters, and Analog Computer Modelling Techniques -----	74
3.3 Experimental Work and Discussion of Results -----	79
3.4 Procedure for Testing Control Valve Susceptibility to Noise -----	84
<u>Chapter 4.</u> Conclusions -----	97
4.1 Vibration Induced Transmission Line Noise -----	97
4.2 Control Valve -----	98
<u>Chapter 5.</u> Recommendations -----	100
5.1 Future Work -----	100
5.2 Application -----	100
Appendix -----	102
<u>Appendix A</u> Transmission Matrices -----	103
A.1 Transmission Matrix Development -----	103
A.2 Transmission Matrix Using Relative Flow or Displacement Variables -----	105
A.3 Transmission Matrix with Transport -----	106



	<u>page</u>
<u>Appendix B</u> Unsteady Momentum Term Evaluation -----	111
B.1 Approximate Solution -----	111
<u>Appendix C</u> Comments on Experimental Procedure and Instrumentation -----	115
C.1 Transmission Line Noise Experimentation -----	115
C.2 Control Valve Noise Experimentation -----	116
Bibliography -----	118
Biographical Note -----	121



LIST OF FIGURES

<u>Figure</u>	<u>Page</u>
2.1 Basic Fluid System -----	49
2.2 Fluid Control Volume -----	49
2.3 Pipe Element -----	50
2.4 Sample Problem -----	50
2.5 Pressure Frequency Response for Sample Problem -----	51
2.6 Shape of Damped Resonant Peaks -----	52
2.7 Test Setup for Longitudinal Pipe Vibrations -----	53
2.8 Test Setup for Transverse Pipe Vibrations -----	53
2.9 Experimental Arrangement -----	54
2.10 Pressure Frequency Response in a Pipe Vibrating Longitudinally -----	55
2.11 Velocity of Sound Frequency Dependence -----	56
2.12 Acceleration Frequency Response for a Pipe Vibrating Longitudinally -----	57
2.13 Pressure Spectrum in a Pipe Forced Longitudinally with White Noise Excitation -----	58
2.14 Pressure Spectrum in a Pipe Forced Longitudinally with White Noise Excitation -----	58
2.15 Explanation and Scale For Reading Db -----	59
2.16 Voltage Spectrum of White Noise Generator -----	60
2.17 End Acceleration Spectrum of Pipe Forced Longitudinally with White Noise Excitation -----	60
2.18 Normalized Spectrum of Figure 2.14 -----	61
2.19 Pressure Spectrum in a Pipe Forced Longitudinally with White Noise Excitation -----	62



<u>Figure</u>	<u>Page</u>
2.20 Pressure Spectrum in a Pipe Forced Transversely with White Noise Excitation -----	62
2.21 Pressure Spectrum in a Pipe Forced Transversely with White Noise Excitation -----	63
2.22 End Acceleration Spectrum in a Pipe Forced Transversely with White Noise Excitation -----	63
2.23 Pressure Spectrum in a Pipe Forced Both Longitudinally and Transversely with White Noise Excitation -----	64
2.24 End Acceleration Spectrum of a Pipe Forced Both Longitudinally and Transversely with White Noise Excitation -----	64
3.1 Control Valve Arrangement -----	87
3.2 Flapper-Nozzle Control Volume -----	88
3.3 Nozzle Relation Approximation -----	89
3.4 Valve Chamber Impedence as Seen by the Load Line -----	90
3.5 Lumped Parameter Model of Load Transmission Line -----	91
3.6 Analog Computer Operational Block Diagram -----	92
3.7 Flapper-Nozzle Control Valve -----	93
3.8 Experimental Setup -----	93
3.9 Chamber Pressure Frequency Response to Supply Line Noise -----	94
3.10 Chamber Pressure Frequency Response to Induced Flapper Motion -----	95
3.11 Chamber Pressure Frequency Response to Load Line Longitudinal Vibrations -----	96
B.1 Elemental Volumes -----	114





LIST OF TABLES

<u>Table</u>	<u>Page</u>
2.1 Pipe Longitudinal End Movement Due to Bending -----	31
2.2 Ratio of Mid-Pipe Transverse Displacement to Pipe Length -----	31
2.3 Ratio of Pipe End Longitudinal Acceleration to Platform Transverse Acceleration -----	32
2.4 Comparison of Experimental and Theoretical Ratios of Pipe End Longitudinal Acceleration to Platform Transverse Acceleration -----	43
2.5 Experimental Damping Ratios -----	45



## 1. INTRODUCTION

### 1.1 BACKGROUND

High performance hydraulic and pneumatic control systems are in wide use today because of the high speeds of response they offer. These systems can be found in missiles, aircraft, and ships, each of which is at times subject to random vibrations from either internal or external sources such as rocket combustion, engine vibration, or random seas. A fluid control system operating in this environment is subject to noise, unwanted pressure signals, excited by induced motion of the system structure and of the working fluid itself. How this noise is introduced into the system and how it effects the transmission of command signals are the two main questions this thesis will try to answer. Other important considerations are the dependence of noise generation on the orientation of the system to the vibration field, coupling between the fluid and structure, and transmission coupling into directions other than that of the primary vibrations.

Studies of fluid control valve forces both steady-state and transient have been conducted in the past [1, 2, 3] . However, none of the cases studied have included any environmental vibrations of the valve assembly itself with inertial forces being of significant importance.

Likewise, transmission line behavior has been investigated [4, 5, 6] for a line that is in an inertial system. D'Souza and Oldenburger [7] included some coupling between the piping and fluid, but they still did not consider any vibrating environment induced motion.



Silberman [8] did vibrate a tube with fluid flowing through it, but this investigation was solely to find the effect on pressure loss between two points, and it did not look at any pressures induced by the vibrations.

In Lipner and Fay [9] one finds the first mention of environmental induced pressures. This paper discusses the transient behavior of acoustic waves generated by a seismic shock. The simplified analysis begins with a pipe of infinite extent and ignores end conditions even when boundaries are established. Thus fluid resonances are not considered.

Random vibration studies have been conducted investigating parts failures in electronics equipment [10], structural response to random forcing [11, 12, 13], and fatigue failure of materials [12, 13, 14]. Once again, however, there is a lack of information dealing with fluid power elements while operating in a randomly vibrating environment.

## 1.2 OBJECTIVES AND PROCEDURE

The objectives of this thesis are three fold. The first is to investigate the sources of noise production and its transmission in fluid systems subject to environmental vibrations. The second is to analyse the behavior of an active element, a control valve, when it is part of this system, and to be able to give procedures for estimating its susceptibility to this type of noise. The third is to be able to recommend the most profitable avenues for further investigation in this area.



In order to conduct meaningful experiments in conjunction with the analysis, the following procedures were adopted. Air was used for the working fluid because of the large quantities of pressurized air available and the simplicity of exhausting directly to the atmosphere. A nozzle-flapper control valve was decided upon as the active element due to its ease of construction and the availability of previous analytical information. Also, it was decided to use a choked orifice, a pure resistance, for the load as no further insight would be gained by having the transmission line terminate in a more complicated impedance. Both analog and digital computers were used to help interpret the analytic results.

Throughout this thesis the units of pounds mass, pounds force, inches, and seconds are used for mass, force, length, and time respectively. This introduces in Newton's Second Law the factor  $g_0$ , relating pounds force to pounds mass, which is equal to  $386 \text{ lbf sec}^2 / \text{lbm in}$ .

The thesis contains in Chapter 2 a study of vibration induced noises in transmission lines subject to both longitudinal and transverse vibrations. The last section of the chapter contains a summary due to the relative importance of this chapter to the thesis. Chapter 3 includes the analysis of a control valve operating in a vibrating environment, discussing the sources and transmission of noise. Also included is a procedure for testing a given system's susceptibility to vibration induced noises. The final conclusions and recommendations are presented in Chapters 4 and 5 respectively, and supplementary work is contained in the Appendix.





## 2. VIBRATION INDUCED TRANSMISSION LINE NOISE

### 2.1 INTRODUCTION

The basic system to be investigated consists of a supply line leading from a constant pressure reservoir to a flapper-nozzle control valve. The load controlled by the valve, in this case a pure resistance, is located at the end of a transmission line, Fig. 2.1. The entire system is assumed to be on a rigid base that can experience translational vibrations in all directions. Since the base is rigid, all supports, where joined to the base, experience the same motion independent of positions. The entire system is subject to induced vibrations due to the forced motion of the base that for this investigation assumes the role of a rocket frame, plane fuselage, or ship hull excited by periodic or random accelerations. Due to the induced vibrations of the structure, noise is introduced into the system by means of motion of the control valve flapper relative to the nozzle and by the motion of the structure, containing the fluid, relative to the fluid. The valve flapper and actuator comprise a second order system and therefore are susceptible to noise when excited near the resonant frequency. Since their behavior is dependent upon the control valve properties, this source of induced noise will be investigated in Chapter 3. The rest of this Chapter will be devoted to fluid pressures induced by structure motion.

### 2.2 CONCEPT

When a vibrating pipe contains a fluid under pressure, the boundary condition at the interfaces is that the fluid has the same



motion as the piping. Thus for pipes experiencing vibrations along their longitudinal axis, if the contained fluid is of low viscosity such as air, the boundary layer is thin, and the main mass of fluid is at rest. However, the fluid at end junctions such as bends or area changes would be experiencing motion because of the longitudinal vibration of the solid boundaries. These junctions act as flow sources to the fluid in the same way as a piston oscillating in a stationary pipe. These flow sources excite fluid vibrations causing quite high pressures to be obtained at the resonant frequencies.

For liquids, the boundary layer is thicker than for air, but the same general behavior takes place. Cavitation bubbles can form at the solid boundaries, however, reducing the effectiveness of the structure motion.

When the induced vibrations are transverse, all the fluid is forced in a transverse motion along with the pipe. However, due to mechanical coupling the pipe sets up longitudinal vibrations at the bending resonant frequencies and at double the resonant frequencies. Then as before, any junctions act as flow sources to the fluid and impose longitudinal vibrations on top of the transverse motion.

For this investigation, the base is assumed rigid and all support excitation is the same independent of position. However, in actual practice the piping structure can be excited independently at different locations especially if the distance between points is large. Thus each junction can act as an independent flow source, and the total fluid response will be the superposition of the responses to each of the sources. Likewise, if the excitation is both longitudinal and

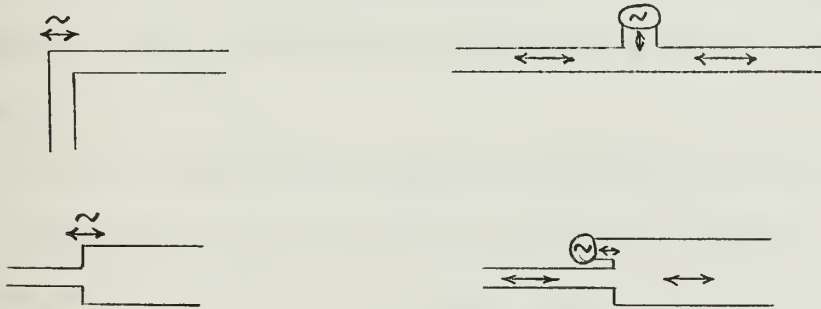


transverse, the pressure response is the superposition of the two types, and each can therefore be treated separately in the analysis.

These concepts will be expanded upon in the following sections.

### 2.3 METHOD OF MODELLING VIBRATION INDUCED FLOW SOURCES

The representation of the flow source concept by a physical system which can be modelled is shown in the following sketch.



The representation allows a vibrating bend or area change to be modelled as two transmission lines forced at their junction by a flow source. Thus normal analytic techniques such as developed by Paynter [15] for energy transmission elements can be used. The forcing functions are then obtained when the additional conditions for the interaction between the fluid and piping are included in the analysis. These forcing terms which are peculiar to systems under the influence of environmental vibrations will be identified in a sample problem formulated in the next section.



## 2.4 DEVELOPMENT FOR LONGITUDINAL VIBRATIONS

First to be considered is piping forced in a longitudinal motion. Since the fluid is forced at junctions it is the conditions at these junctions that are of most interest. Thus the analysis leads to the use of transmission matrices between junctions which can then be cascaded to obtain the overall effects. This method will be used here. A development of uniform, one-dimensional, linear, distributed system transmission matrices, along with extensions to systems in noninertial frames and with mean transport, is contained in Appendix A.

In order to apply the transmission matrix, Eq. (A.1-3), to the fluid in a transmission line it is first necessary to obtain a relation for the variables in differential equation form. That is,

$$\frac{dp}{dx} = - Z w$$

and

$$\frac{dw}{dx} = - Y p.$$

This is necessary in order to identify the system parameters  $Z$  and  $Y$  when the power variables  $p$ , pressure, and  $w$ , mass flow rate, are used.

Friction and damping will be ignored for the present as well as viscous transfer of motion from the pipe wall to the fluid.

Using the continuity equation for a small elemental control volume of length  $dx$  in a uniform pipe gives, Fig. 2.2,

$$0 = \frac{\partial w}{\partial x} dx + \frac{\partial p A}{\partial t} dx$$





or

$$0 = \frac{\partial w}{\partial x} + A \frac{\partial \rho}{\partial t} + \rho \frac{\partial A}{\partial t} \quad (2.4-1)$$

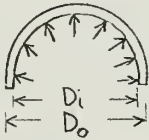
where  $\rho$  is the fluid density and  $A$  is the flow area.

When using the acoustic assumptions of small pressure fluctuations and an adiabatic process, the equation of state becomes

$$d\rho = \frac{\rho}{\beta} d\rho$$

where  $\beta$  is the bulk modulus of the fluid.

The change in area is found by conducting a stress analysis on a section of the thin-walled elastic pipe. This gives



$$\sigma(D_o - D_i)dx = D_i p dx$$

or

$$d\sigma(D_o - D_i) = D_i dp$$

where  $\sigma$  is the circumferential stress in the pipe and  $D_o$  and  $D_i$  are the outside and inside diameters of the pipe respectively.

Now the change in circumference with area is

$$dC = \frac{2}{D_o} dA,$$

and the stress-strain relation is

$$d\sigma = \frac{dC}{C} E$$

where  $E$  is the modulus of elasticity and  $C$  is the circumference.

Therefore the change of area with pressure becomes



$$dA = \frac{2A}{D} \frac{dp}{E\left(\frac{D_o}{D_i} - 1\right)}$$

Putting this and the equation of state into Eq. (2.4-1) gives

$$\frac{\partial w}{\partial x} = - \frac{\rho A}{\beta_e} \frac{\partial p}{\partial t} \quad (2.4-2)$$

where

$$\frac{1}{\beta_e} = \frac{1}{\beta} + \frac{2}{E(D_o/D_i - 1)} \quad (2.4-3)$$

It is to be noted that any compliance of the pipe is taken into account in Eq. (2.4-3) by decreasing the fluid equivalent bulk modulus and thus decreasing the speed of sound in the fluid. This effect is important in liquids which have a high bulk modulus. However, it can be neglected in air unless the pipe is very compliant and has a low modulus of elasticity.

Now applying the momentum equation to the same elemental control volume gives,

$$- A \frac{\partial p}{\partial x} dx = \frac{1}{g_o} \frac{\partial vw}{\partial x} dx + \frac{1}{g_o} \frac{\partial w}{\partial t} dx$$

or

$$- \frac{\partial p}{\partial x} = \frac{v}{g_o A} \frac{\partial w}{\partial x} + \frac{w}{g_o A} \frac{\partial v}{\partial x} + \frac{1}{g_o A} \frac{\partial w}{\partial t} \quad (2.4-4)$$

where  $v$  is the velocity of the fluid particles.

From continuity,

$$\frac{\partial w}{\partial x} = \rho A \frac{\partial v}{\partial x} + v A \frac{\partial \rho}{\partial x} = - \frac{\rho A}{\beta_e} \frac{\partial p}{\partial t}$$



Putting the equation of state in this expression gives,

$$\frac{\partial v}{\partial x} = - \frac{1}{\beta_e} \frac{\partial p}{\partial t} - \frac{v}{\beta_e} \frac{\partial p}{\partial x} . \quad (2.4-5)$$

Now putting Eqs. (2.4-2) and (2.4-5) into Eq. (2.4-4) and noting from the equation of state that  $g_o \frac{\beta_e}{\rho} = g_o \frac{dp}{d\rho} = c^2$ , one can obtain

$$\left( \frac{v^2}{c^2} - 1 \right) \frac{\partial p}{\partial x} = - \frac{2v}{c^2} \frac{\partial p}{\partial t} + \frac{1}{g_o A} \frac{\partial w}{\partial t} .$$

Since  $\frac{v}{c} \ll 1$ , this becomes

$$\frac{\partial p}{\partial x} = - \frac{1}{g_o A} \frac{\partial w}{\partial t} . \quad (2.4-6)$$

Using the differential operator  $D \equiv \frac{\partial}{\partial t}$ , Eqs. (2.4-2) and (2.4-6) can now be written in the desired form. Thus,

$$\frac{dp}{dx} = - Z w$$

and

$$\frac{dw}{dx} = - Y p \quad (2.4-7)$$

where

$$Z = \frac{D}{g_o A} \quad \text{and} \quad Y = \frac{g_o A D}{c^2} .$$

Then  $Z_c \equiv \sqrt{Z/Y}$ , defined as the characteristic impedance, becomes

$$Z_c = \frac{c}{g_o A},$$

and  $\gamma \equiv \sqrt{YZ}$ , the propagation operator, becomes

$$\gamma = \frac{D}{c} .$$

It is also desirable to express these relations in terms of a relative flow variable  $w_r$ . Thus from Eqs. (2.4-7) one obtains



$$\frac{dp}{dx} = -Zw_r = Z\rho_o A dx_o$$

and

(2.4-8)

$$\frac{dw_r}{dx} = -Yp,$$

$$\text{since } w = w_r + \rho_o A dx_o.$$

$x_o$  is the component of motion of the base in the direction of the longitudinal axis of the pipe,  $\rho_o$  is the mean fluid density, and  $Z$ ,  $Y$ ,  $Z_c$ , and  $\gamma$  have the same values as above.

The two sets of Equations, (2.4-7) and (2.4-8), can now be put directly into there corresponding transmission matrix forms, Eqs. (A.1-3) and (A.2-3). Thus for the two cases they become

$$\begin{bmatrix} p(0) \\ w(o) \end{bmatrix} = \begin{bmatrix} \cosh \gamma x & Z_c \sinh \gamma x \\ \frac{1}{Z_c} \sinh \gamma x & \cosh \gamma x \end{bmatrix} \begin{bmatrix} p(x) \\ w(x) \end{bmatrix} \quad (2.4-9)$$

and

$$\begin{bmatrix} p(o) \\ w_r(o) \end{bmatrix} = \begin{bmatrix} \cosh \gamma x & Z_c \sinh \gamma x \\ \frac{1}{Z_c} \sinh \gamma x & \cosh \gamma x \end{bmatrix} \begin{bmatrix} p(x) \\ w_r(x) \end{bmatrix} + \begin{bmatrix} Z_c \sinh \gamma x (\rho_o A dx_o) \\ (\cosh \gamma x - 1) (\rho_o A dx_o) \end{bmatrix}. \quad (2.4-10)$$

If transport is important, the transmission matrices can be obtained from Eqs. (2.4-9) and (2.4-10) by using the multiplicative factor as discussed in Appendix A.

For the piping containing the fluid, the variables  $f$ , force, and  $\xi$ , absolute displacement will be used. Once more friction and damping will be ignored at present. Using Newton's Second Law for an element of pipe, Fig. 2.3, gives

$$-\frac{\partial f}{\partial x} dx = \frac{\rho_p A}{g_o} \frac{\partial^2 \xi}{\partial t^2}$$

or

$$\frac{\partial f}{\partial x} = -\frac{\rho_p A}{g_o} \frac{\partial^2 \xi}{\partial t^2} \quad (2.4-11)$$





where  $A_p$  and  $\rho_p$  are the pipe cross sectional area and pipe density respectively. Now since  $f$  is positive when compressive, Hooke's Law becomes

$$E \frac{\partial \xi}{\partial x} = - \frac{f}{A_p} \quad (2.4-12)$$

where  $E$  is the modulus of elasticity.

Rewriting Eqs. (2.4-11) and (2.4-12) using differential operators, one obtains

$$\frac{df}{dx} = - Z \xi$$

and (2.4-13)

$$\frac{d\xi}{dx} = - Y f$$

where

$$Z = \frac{\rho_p A_p D^2}{g_o} \quad \text{and} \quad Y = \frac{1}{EA_p} .$$

Thus, the characteristic impedance and propagation operator are

$$Z_{cp} = A_p D \sqrt{\frac{\rho_p E}{g_o}}$$

and

$$\gamma_p = D \sqrt{\frac{\rho_p}{g_o E}} \quad \text{respectively.}$$

Once again it is desirable to obtain these relations in terms of a relative flow variable  $\xi_r$ . Thus Eqs. (2.4-13) become

$$\frac{df}{dx} = - Z \xi_r - Z x_o$$

and (2.4-14)

$$\frac{d\xi_r}{dx} = - Y f ,$$



and  $Z$ ,  $Y$ ,  $Z_{cp}$ , and  $\gamma_p$  have the same values as above when the substitution,  $\xi = \xi_r + x_o$ , is made.

Then since Eqs. (2.4-13) and (2.4-14) are in the proper forms of Appendix A, they can be directly expressed as transmission matrices.

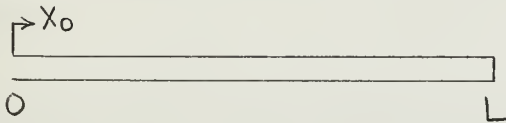
Thus for the two cases,

$$\begin{bmatrix} f(o) \\ \xi(o) \end{bmatrix} = \begin{bmatrix} \cosh \gamma_p x & Z_{cp} \sinh \gamma_p x \\ \frac{1}{Z_{cp}} \sinh \gamma_p x & \cosh \gamma_p x \end{bmatrix} \begin{bmatrix} f(x) \\ \xi(x) \end{bmatrix} \quad (2.4-15)$$

and

$$\begin{bmatrix} f(o) \\ \xi_r(o) \end{bmatrix} = \begin{bmatrix} \cosh \gamma_p x & Z_{cp} \sinh \gamma_p x \\ \frac{1}{Z_{cp}} \sinh \gamma_p x & \cosh \gamma_p x \end{bmatrix} \begin{bmatrix} f(x) \\ \xi_r(x) \end{bmatrix} + \begin{bmatrix} Z_{cp} \sinh \gamma_p x x_p \\ (\cosh \gamma_p x - 1)x_p \end{bmatrix} \quad (2.4-16)$$

Using the relations developed above it is now possible to investigate the behavior of fluid contained in a vibrating pipe. Consider first the simple problem of a pipe open to the atmosphere at one end and closed at the other. Let the open end experience vibrations in the direction of the pipe axis.



The end conditions are,

$$\xi_r(o) = 0, p(o) = 0, f(L) = -p(L)A, \text{ and } w_r(L) = \rho_o AD \xi_r(L).$$

Using Eq. (2.4-16) gives



$$\xi_r(L) = \frac{(1 - \cosh \Gamma_p) x_o}{\cosh \Gamma_p} + \frac{\frac{A}{Z_{cp}} \sinh \Gamma_p p(L)}{\cosh \Gamma_p}$$

where  $\Gamma_p = \gamma L$ .

Then from Eq. (2.4-10) one obtains,

$$0 = \left[ \cosh \Gamma \cosh \Gamma_p + \frac{Z_c}{Z_{cp}} (\rho_o A^2 D) \sinh \Gamma \sinh \Gamma_p \right] p(L) \\ + Z_c \sinh \Gamma (\rho_o A D) (1 - \cosh \Gamma_p) x_o + Z_c \sinh \Gamma \cosh \Gamma_p (\rho_o A D x_o)^*$$

or

$$p(L) = \frac{-Z_c \rho_o A \sinh \Gamma D x_o}{\cosh \Gamma \cosh \Gamma_p + \frac{Z_c}{Z_{cp}} (\rho_o A^2 D) \sinh \Gamma \sinh \Gamma_p}$$

where  $\Gamma = \gamma L$ . Now if the excitation is measured in terms of a  $g$  of acceleration, which is 386 in per sec<sup>2</sup>, this becomes

$$p(L) = \frac{-386 Z_c \rho_o A \sinh \Gamma G}{D \left[ \cosh \Gamma \cosh \Gamma_p + \frac{Z_c}{Z_{cp}} \rho_o A^2 D \sinh \Gamma \sinh \Gamma_p \right]}$$

The frequency response of  $\frac{p(L)}{G}$  can be obtained by substituting  $i\omega$  for  $D$ . Thus,

---

\* The last two terms of this equation are the flow sources caused by the pipe's vibrating. The next to last term is due to the closed end of the pipe moving relative to the open end, while the last term is due to the translational motion of the pipe.



$$\frac{p(L)}{G} = \frac{-c\rho_o \sin \frac{L}{c} \omega}{\omega \left[ \cos \frac{L}{c} \omega \cos \sqrt{\frac{\rho_p}{g_o E}} L \omega - \frac{\rho_o c}{g_o} \frac{A}{A_p} \sqrt{\frac{g_o}{\rho_p E}} \sin \frac{L}{c} \omega \sin \sqrt{\frac{\rho_p}{g_o E}} L \omega \right]}$$

This equation shows that the pressure levels are proportional to fluid density, equivalent speed of sound, and excitation. High pressures will be induced at the frequencies at which the denominator minimums occur. Relative minimums occur at the resonant frequencies of both the fluid and the pipe, and absolute minimums occur at the overall system resonances. Damping would decrease the induced pressure levels somewhat, but would not change the overall appearance of the response.

Another system might have the pipe mounted to the base by means of cantilevered supports. The pipe might then be supplied from a reservoir and exhaust through a choked orifice. Such a system, Fig. 2.4, was analysed, and the theoretical frequency response for  $\left| \frac{p(L)}{20G} \right|$  is plotted in Fig. 2.5. It can be seen that relatively high pressures have been induced by the vibrating environment at all the odd numbered fluid resonances. The large peak near 800 cps is due to resonance of the pipe on the cantilever supports. This also causes the fluid resonance near 850 cps to be much higher than the others as it is reinforced by the near resonant motion.

When the cantilevers are stiffened by a factor of two, the resonant peak is moved far enough to the right that it is off the Figure. Also it is noticed that all but the first fluid resonant pressures have been decreased slightly.

The Figure also contains a plot which includes a fluid mean



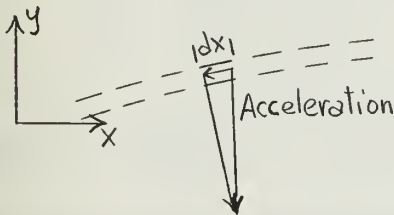


transport velocity of one tenth the speed of sound for the stiffened system. It is seen to have very little effect. This indicates that small values of transport are not too important.

It is to be noted that in the Figure the resonant peaks are damped by the orifice resistance and by an assumed damping of approximately .04.

## 2.5 DEVELOPMENT FOR TRANSVERSE VIBRATIONS

The generation of pressures in pipes undergoing transverse vibrations is more complicated than in the previously developed longitudinal case. The pipe does exert a small component of force on the fluid in the direction of the pipe axis due to the bowed shape,



$$- A \frac{\partial p}{\partial x} dx = \frac{\rho_o A}{g_o} dx \left( \frac{\partial y}{\partial x} \right) \frac{\partial^2 y}{\partial t^2}$$

but this does not produce any significant pressures as the slope (force component) is too small. Coriolis and radial accelerations are also insignificant for this particular configuration. Experimentally, however, relatively high induced pressures were observed along with longitudinal vibrations of the pipe ends even though they were braced. Significant end motion was observed at the pipe bending resonant frequencies and at double these frequencies indicating considerable coupling between transverse and longitudinal motion.

One means of coupling can be attributed to the pipe maintaining approximately the same length while undergoing transverse vibrations.



The pipe curvature thus causes longitudinal motion of the ends in order to maintain this length. This type of coupling will be investigated now for a pipe under two different types of end conditions, pinned-pinned and clamped-clamped. In so doing the maximum transverse displacement of the pipe will be determined and used to find the change in projected length. The Bernoulli-Euler model for beams will be used.\*

Consider first a pipe pinned at both ends. Jacobsen and Ayre [17] give

$$Y = c_1 \cos \mu x + c_2 \sin \mu x + c_3 \cosh \mu x + c_4 \sinh \mu x \quad (2.5-1)$$

for the space part of the solution of the beam equation,

$$\frac{\partial^4 y}{\partial x^4} + \frac{\rho_p A}{g_o EI} \frac{\partial^2 y}{\partial t^2} = 0 \quad **$$

where  $\mu = \left( \frac{\rho_p A \omega^2}{g_o EI} \right)^{1/4}$ ,  $y(x,t)$  is the transverse displacement,

$Y(x)$  is the space dependent part of the displacement, and the  $c$ 's are the integration constants.  $I$  is the pipe cross-sectional moment of inertia.

---

\* Reference [16] p. 332 states that if the radius of gyration of the cross section of the beam,  $\gamma = \sqrt{I/A}$ , is small compared to the wavelength investigated, then the Bernoulli-Euler model is adequate.

\*\* The normal beam equation without any fluid terms can be used as Long [18] has shown that the fluid has very little effect on transverse vibrations. This is especially true for air.



Now if the platform holding the end supports undergoes motion in a transverse direction, the end conditions will be

$$\text{at } x = 0, Y = y_o \text{ and } \frac{d^2 Y}{dx^2} = 0,$$

$$\text{and at } x = L, Y = y_o \text{ and } \frac{d^2 Y}{dx^2} = 0$$

where  $y_o$  is the transverse motion of the supports.

Putting these expressions into Eq. (2.5-1) and into its second derivative gives

$$c_1 = c_3 = \frac{y_o}{2} ,$$

$$c_2 = \frac{y_o}{2} \tan \frac{\mu L}{2} ,$$

and

$$c_4 = - \frac{y_o}{2} \tanh \frac{\mu L}{2} .$$

Since this type of forcing causes resonances only at the symmetric, odd numbers, modes the maximum displacement will always occur at mid span. Thus writing Eq. (2.5-1) at  $x = \frac{L}{2}$  in terms of relative displacement,  $y_r = Y - y_o$ , it becomes

$$y_r \left( \frac{L}{2} \right) = \left[ \frac{1}{2 \cos \frac{\mu L}{2}} + \frac{1}{2 \cosh \frac{\mu L}{2}} - 1 \right] y_o$$

Written in terms of  $g$ 's of acceleration the frequency response becomes

$$\frac{y_r \left( \frac{L}{2} \right)}{G} = \frac{386}{w^2} \left[ \frac{1}{2 \cos \frac{\mu L}{2}} + \frac{1}{2 \cosh \frac{\mu L}{2}} - 1 \right] \quad (2.5-2)$$

This then gives the maximum relative transverse displacement of the pipe at various frequencies.

Now following the same procedure for a pipe clamped at both



ends, reference [17] gives

$$Y = c_1(\cos \mu x + \cosh \mu x) + c_2(\cos \mu x - \cosh \mu x) \\ + c_3(\sin \mu x + \sinh \mu x) + c_4(\sin \mu x - \sinh \mu x) \quad (2.5-3)$$

as a more convenient form for the space part of the beam equation solution when complicated end conditions are encountered.

The end conditions are now

$$\text{at } x = 0, Y = y_0 \text{ and } \frac{dY}{dx} = 0,$$

$$\text{and at } x = L, Y = y_0 \text{ and } \frac{dY}{dx} = 0.$$

Putting these into Eq. (2.5-3) and into its first derivative gives,

$$c_1 = \frac{y_0}{2},$$

$$c_3 = 0,$$

$$c_2 = y_0 c'_2 = \frac{y_0}{2} \left( \frac{\sin \mu L \sinh \mu L + \cos \mu L - \cosh \mu L}{1 - \cos \mu L \cosh \mu L} \right),$$

and

$$c_4 = y_0 c'_4 = \frac{y_0}{2} \left[ \frac{\sin \mu L (1 - \cosh \mu L) + \sinh \mu L (1 - \cos \mu L)}{1 - \cos \mu L \cosh \mu L} \right]$$

As before, writing Eq. (2.5-3) at  $x = \frac{L}{2}$  in terms of relative displacement and  $g$ 's, gives for the frequency response

$$\frac{y_r(\frac{L}{2})}{G} = \frac{386}{\omega^2} \left[ 1/2 \left( \cos \frac{\mu L}{2} + \cosh \frac{\mu L}{2} \right) + c'_2 \left( \cos \frac{\mu L}{2} - \cosh \frac{\mu L}{2} \right) \right. \\ \left. + c'_4 \left( \sin \frac{\mu L}{2} - \sinh \frac{\mu L}{2} \right) - 1 \right].$$

Reference [17] states that the shape of a pinned-pinned beam forced

at the supports at resonance approaches the normal-mode shape,

$\sin \frac{n\pi x}{L}$ , corresponding to the resonant frequency. Since it is

resonance that is of interest the pinned-pinned pipe displacement is



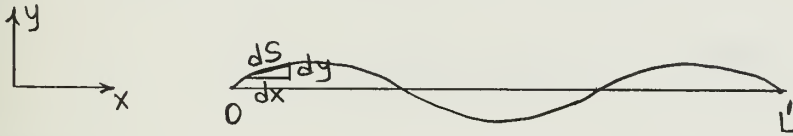


taken to be

$$y_r = y_{ro} \sin \frac{n\pi x}{L} \sin \omega t \quad (2.5-5)$$

where  $n = 1, 3, 5, \dots$  is the number of the mode and  $y_{ro}$  is the relative maximum displacement obtained from Eq. (2.5-2) for a given assumed damping.

Using this equation the change in length of pipe with pinned-pinned end conditions can be found as follows:



$$dS = \sqrt{1 + \left(\frac{\partial y_r}{\partial x}\right)^2} dx$$

or

$$dS = \left[ 1 + \frac{1}{2} \left( \frac{\partial y_r}{\partial x} \right)^2 \right] dx$$

as

$$\frac{\partial y_r}{\partial x} \ll 1.$$

Then

$$S = \int_0^{L'} \left[ 1 + \frac{1}{2} \left( \frac{\partial y_r}{\partial x} \right)^2 \right] dx .$$

Now the assumption of this section is  $S = L$  so that

$$L = \int_0^{L'} \left[ 1 + \frac{1}{2} \left( \frac{\partial y_r}{\partial x} \right)^2 \right] dx .$$

However since  $L \approx L'$ , with little loss in accuracy this can be written

$$L = \int_0^L \left[ 1 + \frac{1}{2} \left( \frac{\partial y_r}{\partial x} \right)^2 \right] dx$$

or



$$\Delta L = \frac{1}{2} \int_0^L \left( \frac{\partial y_r}{\partial x} \right)^2 dx \quad (2.5-6)$$

Putting in Eq. (2.5-5) gives

$$\frac{\partial y_r}{\partial x} = y_{ro} \frac{n\pi}{L} \cos \frac{n\pi x}{L} \sin \omega t,$$

and

$$\begin{aligned} \left( \frac{\partial y_r}{\partial x} \right)^2 &= \left( y_{ro} \frac{n\pi}{L} \right)^2 \cos^2 \frac{n\pi x}{L} \sin^2 \omega t \\ &= \frac{1}{2} \left( y_{ro} \frac{n\pi}{L} \right)^2 \sin^2 \omega t \left( 1 + \cos \frac{2n\pi x}{L} \right). \end{aligned}$$

Therefore,

$$\begin{aligned} \Delta L &= \frac{1}{4} \left( \frac{y_{ro} n\pi}{L} \right)^2 \sin^2 \omega t \int_0^L \left( 1 + \cos \frac{2n\pi x}{L} \right) dx \\ &= \frac{1}{4} \left( \frac{y_{ro} n\pi}{L} \right)^2 \sin^2 \omega t \left( x + \frac{L}{2n\pi} \sin \frac{2n\pi x}{L} \right) \Big|_0^L \end{aligned}$$

or

$$\Delta L = L \left( \frac{y_{ro} n\pi}{2L} \right)^2 \sin^2 \omega t. \quad (2.5-7)$$

Now following the same procedure for the clamped-clamped pipe the normal-mode shape [17] is

$$y_r = y_{ro} \left[ \sinh \mu x - \sin \mu x + \alpha (\cosh \mu x - \cos \mu x) \right] \sin \omega t$$

where

$$\alpha = \frac{\sinh \mu L - \sin \mu L}{\cosh \mu L - \cos \mu L},$$

and  $y_{ro}$ , the maximum relative displacement, is obtained from Eq. (2.5-4).

Differentiating, squaring, and integrating the expression in Eq. (2.5-6) gives



$$\begin{aligned} \Delta L = \frac{\mu L}{2} \left( \frac{y_{ro}}{L} \right)^2 L \left\{ \frac{1}{2} \left( \frac{1}{2} \sinh 2\mu L + \mu L \right) - \sin \mu L \cos \mu L + \cosh \mu L \sin \mu L \right. \\ + \frac{1}{2} (\mu L + \sin \mu L \cos \mu L) + 2\alpha \left[ \frac{1}{4} \cosh 2\mu L + \frac{1}{2} + \frac{1}{4} \cos 2\mu L \right. \\ + \left. \frac{1}{2} (\sinh \mu L \sin \mu L - \cosh \mu L \cos \mu L) - \frac{1}{2} (\cosh \mu L \cos \mu L + \sinh \mu L \sin \mu L) \right] \\ + \alpha^2 \left[ \frac{1}{2} \left( \frac{1}{2} \sinh 2\mu L - \mu L \right) + (\cosh \mu L \sin \mu L - \sinh \mu L \cos \mu L) \right. \\ + \left. \left. \frac{1}{2} (\mu L - \sin \mu L \cos \mu L) \right] \right\} \sin^2 \omega t. \quad (2.5-8) \end{aligned}$$

Since Eq. (2.5-8) only holds for the resonant frequencies which are

$$\mu L)_1 = 4.730,$$

$$\mu L)_3 = 10.996,$$

$$\mu L)_5 = 17.279,$$

and  $\mu L)_7 = 23.562,$

and since  $\cosh 10.0 = \sinh 10.0 = 11,013.2$  so that  $\alpha = -1$ , the Equation can be simplified for all the resonant modes above the first. Cancelling terms it is found that

$$\Delta L = \frac{\mu L}{2} \left( \frac{y_{ro}}{L} \right)^2 L \left[ \mu L - 1 - \frac{1}{2} \cos 2\mu L \right] \sin^2 \omega t. \quad (2.5-9)$$

Thus the change in pipe length is determined for the two types of end conditions, and Table 2.1 can be constructed using Eqs. (2.5-7), (2.5-8), and (2.5-9).

Now since  $\sin^2 \omega t = \frac{1}{2} - \frac{1}{2} \cos 2\omega t$ , the experimentally found end double resonant frequencies can be attributed to this means of coupling, and the end accelerations can now be calculated as soon as the pipe length and ratio of maximum displacement to length are known.

Some typical values of  $\frac{y_{ro}}{L}$  were obtained using Eqs. (2.5-2) and (2.5-4) for a sinusoidal platform acceleration of one g and an approximate damping ratio of .04, and are presented in Table 2.2.



TABLE 2.1

Pipe Longitudinal End Movement Due to Bending

<u>Pinned-Pinned</u>			<u>Clamped-Clamped</u>		
<u>Mode</u>	<u><math>\Delta L</math></u>		<u>Mode</u>	<u><math>\Delta L</math></u>	
1	$2.47 \left( \frac{y_{ro}}{L} \right)^2 L \sin^2 \omega t$		1	$6.35 \left( \frac{y_{ro}}{L} \right)^2 L \sin^2 \omega t$	
3	22.21	"	3	57.71	"
5	61.68	"	5	144.95	"
7	120.90	"	7	271.69	"

TABLE 2.2

Ratio of Mid-Pipe Transverse Displacement to Pipe Length  
(pipe is 1/4" copper tubing filled with air at 200 psia)

<u>Pinned-Pinned</u>				<u>Clamped-Clamped</u>			
<u>Mode</u>	<u>Cps</u>	<u>L</u>	<u><math>\frac{y_{ro}}{L}</math></u>	<u>Mode</u>	<u>Cps</u>	<u>L</u>	<u><math>\frac{y_{ro}}{L}</math></u>
1	34	23	$7.5 \times 10^{-3}$	1	76	23	$1.9 \times 10^{-3}$
3	218	27	$4.5 \times 10^{-4}$	3	296	27	$1.1 \times 10^{-4}$
5	606	27	$2.3 \times 10^{-5}$	5	733	27	$0.6 \times 10^{-5}$
7	240	60	$6.2 \times 10^{-6}$	7	276	60	$1.6 \times 10^{-6}$

Now using the results of Tables 2.1 and 2.2 some typical values of the ratio of end double frequency accelerations to base accelerations are calculated and given in Table 2.3.





TABLE 2.3

Ratio of Pipe End Longitudinal

Acceleration to Platform Transverse Acceleration

(pipe is 1/4" copper tubing filled with air at 200 psia)

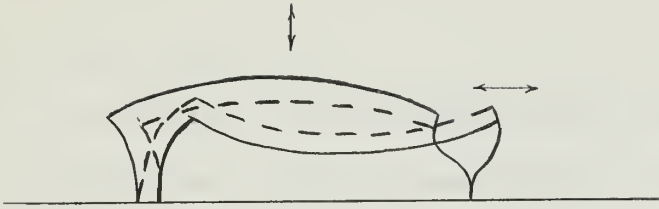
<u>Pinned-Pinned</u>			<u>Clamped-Clamped</u>		
<u>Mode</u>	<u>2xCps</u>	<u>Accel</u> $\frac{g_{end}}{g_{base}}$	<u>Mode</u>	<u>2xCps</u>	<u>Accel</u> $\frac{g_{end}}{g_{base}}$
1	68	.76	1	152	.62
3	436	1.18	3	592	.34
5	1212	.07	5	1466	.016
7	480	.0033	7	552	.00065

The values from the Table will be a little high due to the restraining action of the end supports. However, they show that the end accelerations are of a relatively high value for the first and third modes, but that they drop off quickly after that. This trend and the above values will be compared with experimental results in Section 2.8.

While the above analysis gives valid results for the twice resonant frequency end motion, only a qualitative explanation can be given for the even stronger coupling at the resonant frequency.

This effect can be due to nonsymmetry in the system since an unsymmetrically supported pipe can be forced into longitudinal motion by transverse vibrations as shown.





Thus any nonsymmetry could cause the longitudinal vibrations to begin, and once started, they very probably would be maintained.

If the platform is excited with components along both the longitudinal and transverse axis, the longitudinal end motion will be the additive effect due to both.

## 2.6 DAMPING AND ITS EFFECTS

The previous sections have shown that all the important phenomenon occur at resonances. Therefore, in order to have any feeling for the amplitudes involved it is essential to know the amount of damping. So far very little has been said about this for several reasons. First, most of the mathematical developments become considerably more complicated when losses are taken into account. Secondly, it is difficult to determine what form the losses should take, i.e. internal friction, external friction, etc. Lastly, the correct values for the parameters are very hard to determine, and sometimes vary by as much as a factor of twenty. An example would be support damping of beams which changes greatly depending on the tightness of the connection. Thus the most satisfactory way to gain an understanding of the damping involved in a given situation is experimentally.



The definition for lightly damped systems,\*

$$\Delta\omega = 2\zeta\omega_n = \frac{\omega_n}{Q}, \quad (2.6-1)$$

where  $\Delta\omega$  is the bandwidth,  $\zeta$  is the damping ratio, and  $\omega_n$  is the resonant frequency, gives a means of experimentally determining damping by measuring the bandwidths of resonant peaks. This measurement is made at the half power point which is .707 of the peak amplitude.

A plot of Eq. (2.6-1), Fig. 2.6, shows that as damping increases the peak amplitude decreases and the peak broadens out. Brown [19] had also shown theoretically that fluid damping is frequency dependent and increases significantly as  $\omega$  goes up.

Eq. (2.6-1) gives good approximate values of damping from experimentally obtained amplitude verses frequency plots. However, it is desirable to be able to predict the effects of damping on amplitude in analytical discussions as well. This can also be done by using Eq. (2.6-1) and experimentally obtained values of damping. The zero damped infinite peaks of a plot can be rounded off by making its shape conform to the correct shape, in Fig. 2.6, for the given damping. This will give a good estimation of the peak amplitudes if the values of damping used are close to that actually experienced by the system. Good repeatable damping values for both the fluid and mechanical systems were obtained experimentally as discussed in Section 2.8.

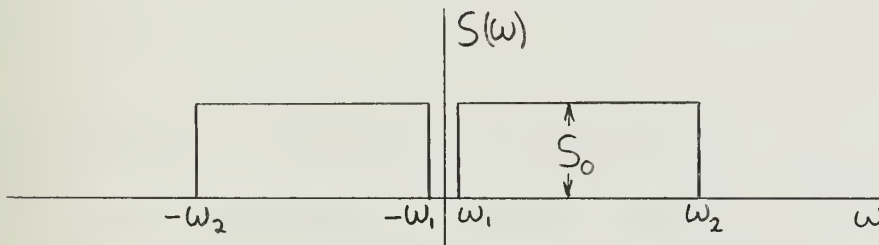
---

\* The fluid and mechanical systems in this investigation are all lightly damped.



## 2.7 RANDOM EXCITATION

The developments in sections 2.4 and 2.5 were conducted using sinusoidal excitation to the base. Although rockets, airplanes, and ships are often subject to narrow-band periodic disturbances, a majority of the time the excitation will be of a wide-band random nature. A convenient means of characterizing a wide-band random signal is to use a stationary process which has a uniform, band-limited spectral density. This is known as white noise.



White noise is a close approximation to the desired physical process, and as long as the frequency band of interest of the system to be investigated falls between  $\omega_1$  and  $\omega_2$  it will give the desired results.

One can develop the relation for a system response spectral density when the excitation spectral density is known. A development is contained in Crandall and Mark [14], pages 70-71, and the transformation notation used is

$$S(\omega) = \frac{1}{2\pi} \int_{-\infty}^{\infty} R(\tau) e^{-i\omega\tau} d\tau \quad (2.7-1)$$

where  $S(\omega)$  is the spectral density and  $R(\tau)$  is the autocorrelation function. The results given are

$$S_y(\omega) = H(-\omega)H(\omega)S_x(\omega)$$





or

$$S_y(\omega) = |H(\omega)|^2 S_x(\omega), \quad (2.7-2)$$

where  $S_y(\omega)$  is the response spectral density,  $S_x(\omega)$  is the excitation spectral density, and  $H(\omega)$  is the frequency response of the system.

The response spectral density is relatively simple to obtain from Eq. (2.7-2) since the frequency response for the system can be found using the techniques developed in Sections 2.4 and 2.5, and  $S_x(\omega)$  is simply

$$\begin{aligned} S_o & \quad \omega_1 \leq |\omega| \leq \omega_2 \\ 0 & \quad \text{elsewhere} \end{aligned}$$

for the excitation assumed in this investigation.

It is to be noted that the spectral density covers both positive and negative values of frequency and is in the units of quantity squared divided by circular frequency. Therefore if experimental work is being done and only positive values of frequency are used and one is working with cycles instead of radians, then in order for the excitations to have the same value a factor of  $4\pi$  must be used, or

$$W_x(f) = 4\pi S_x(\omega).$$

Then

$$W_y(f) = |H(f)|^2 W_x(f), \quad (2.7-3)$$

where  $W_x$  and  $W_y$  are the excitation and response spectral densities in terms of cps.

## 2.8 EXPERIMENTAL RESULTS

In order to verify the theory developed in the previous sections,



experiments were conducted by actually vibrating pipes. The pipes were vibrated longitudinally and transversely with both periodic and random excitation while containing air under pressures of 100 and 200 psia. In some cases the air had a small mean transport and in others it had no flow. Some preliminary work was done with water in the pipes, but this was discontinued due to the difficulties encountered in trying to remove the entrapped air bubbles. The piping used was standard one quarter inch copper tubing. The vibration generator was built from a high fidelity speaker, and the pressures and accelerations were obtained by using piezoelectric transducers. Data was taken up to 1000 cps since above this frequency the system response is almost nil.

Figs. 2.7 and 2.8 show the piping arrangement for longitudinal and transverse vibrations respectively. One end of the piping is connected by flexible hose to a constant pressure reservoir while the other end terminates at the pressure transducer, Fig. 2.9. Additional details of the experimental procedures and instrumentation are contained in Appendix C.

Fig. 2.10 shows good agreement between the experimental and theoretical frequency responses for a system of total length 51.6 inches forced by longitudinal vibrations while containing air under 200 psia pressure. There is a choked orifice near the transducer end of .032 inches diameter which gives a mean velocity of 14 feet per second or about one one-hundredth the speed of sound. The Figure shows fluid pressure peaks at all the odd resonances due to a cosine



function characteristic equation, and a peak near 850 cps due to the longitudinal resonance of the pipe. The resonances are not multiples of each other because of the frequency dependence of boundary layer friction which causes the boundary layer to be thinner at higher frequencies. The analysis used in this investigation did not take this change in boundary layer thickness into account so that a frequency correction to the equivalent speed of sound must be made from Fig. 2.11.\* It is necessary to use this Figure to obtain the correct value of  $c$  in order to compute the correct values of the resonant frequencies.

From Fig. 2.10 it is seen that high enough pressures are generated per  $g$  of acceleration at the first several resonances to be of concern if the system were subjected to any substantial environmental excitation. Also, from the first two peaks, using Eq. (2.6-1), the fluid damping ratios are found to be approximately .03 and .04 respectively.

Fig. 2.12 is the frequency response for the pipe longitudinal accelerations at the nonforced end. This Figure shows good agreement in resonant frequency between the theory and experimental results, but the agreement in bandwidth is not too good due to limitations in the equipment resolution capabilities. The resolution at high frequencies is only one tenth as good as at low frequencies. The pipe end had to be mass loaded in order to bring the first resonance down

---

\* This Figure was taken from Brown 19, where  $c$  is the actual speed of sound,  $c_0$  is the isentropic speed of sound,  $a$  is the pipe radius in inches, and  $\nu_0$  is the kinematic viscosity in  $\text{in}^2/\text{sec}$ .



to below 1000 cps. It is seen that relatively high accelerations can be obtained which if they occurred at low enough frequencies or if they corresponded to fluid resonant frequencies would cause pressure signals large enough to be of great concern. From this Figure the pipe damping ratio can be seen to be about .04.

Now the same system was excited with white noise input. Figs. 2.13 and 2.14 show the pressure response for reservoir pressures of 100 and 200 psia respectively. Notice that the two Figures are exactly the same except the first is everywhere between five and seven db less than the second.\* This is exactly what would be expected as the induced pressure is proportional to density which for a gas is proportional to pressure. Thus when the pressure is doubled there should be a rise of six db in induced pressure noise, Fig. 2.15. These two Figures also show the fluid resonant frequencies at 60, 200, 355, 455, 600, and 740 cps. Notice that the resonances at 455 and 740 cps are much smaller than the others. This showed up in the theory also. The resonance at 600 cps is higher than it would normally be since although white noise was put into the vibration generator, the generator had resonances around 370 and 530 cps which show up throughout the graphs. The peak at 850 cps is due to the pipe longitudinal resonance.

The several runs attempted with water filled pipes produced pressure levels approximately four times as high as for the 200 psia

---

\* An explanation on reading db graphs is given in Fig. 2.15.





air for a given excitation. The increased density and speed of sound would predict level increases by a factor of ten. However, increased damping lowers the resonant peaks so that the factor of four seems reasonable with the theory.

There is a misleading upward trend to all the graphs made by the analyser and recorder. This is because the filter bandwidth is always a constant percentage of the mid frequency being swept, in all these cases 6%. Thus the filter bandwidth doubles each octave, and in the case of white noise, twice as much signal is being averaged. Thus there is a 3 db rise per octave since  $10 \log \frac{g_{\text{oct}}^2}{g} = 10 \log 2 = 3$ . This 3 db rise can be seen in Fig. 2.16 which is the random white noise input to the vibration generator.

Fig. 2.17 shows the acceleration at the nonforced end of the pipe. The peak near 900 cps is due to the pipe longitudinal resonance, and the two peaks at 370 and 530 cps are the resonances of the shaker.

In order to better understand these last several results, Fig. 2.14 has been replotted in Fig. 2.18. In this Figure the 3 db rise has been eliminated and the pressure has been normalized by the input acceleration. Theoretical results are also plotted and agree favorably. This Figure shows the big drop in pressure after the first two resonances, and also shows that the resonances at 455 and 740 cps are almost nil. The resonance at 600 cps is much higher than predicted as explained before. Because of the wideness of the filter at higher frequencies, the resonance at 875 cps is masked in the pipe resonance in the experimental results.



Before leaving longitudinal excitation, Fig. 2.19 is included to show that the fluid resonances are dependent on the total pipe length and not on the forcing flow source positions. For this case, the distance between flow sources (pipe bends) was left the same as above while increasing the total distance between the reservoir and pressure transducer. It can be seen that the fluid resonances are at lower frequencies, 40, 156, 250, 350, 450, and 550 cps, corresponding to the greater length. As before the high peak at 550 cps is due to the shaker resonance and the peak near 850 cps is once again the pipe resonance.

Figs. 2.20 and 2.21 show the pressure response to random transverse excitation for clamped-clamped pipes of lengths 27 and 23 inches respectively. The overall lengths from reservoir to pressure transducer are 46.1 and 42.1 inches, and in both cases there is zero mean flow. These pipes were not excited by inertial forces as the vibration generator was not large enough to move the whole system. Instead the pipes were forced directly at a point near one end. This method proved satisfactory. However, since the forcing was not symmetric as in the case of inertial loading, all the resonances are present and not just the odd numbered ones.

Notice the difference between the two Figures. The first has many small resonances while the second has several large ones. This is because in the case of the 23 inch pipe, the fluid resonances and pipe bending resonances coincided. The two graphs are similar in that the first resonances are large while the higher ones fall off quickly. This is more noticable if the 3 db rise per octave is subtracted. This



fall off was predicted and is much more severe than for longitudinal excitation.

Now looking at Fig. 2.20 in detail, the first peak at 44 cps is excited by the first bending resonance<sup>\*</sup> for a pipe of this length with clamped-pinned end conditions. Therefore, even though the pipe ends where clamped, forcing the pipe near one end excited this mode of bending also since the support moved torsionally. The peak at about 86 cps is due to the double resonant frequency as predicted. The second and third resonant frequencies cause the peaks at 130 and 260 cps respectively, but both their double frequencies are masked by other peaks. The one is masked by the third resonant frequency and the other by the shaker resonance around 530 cps. The peak at 57 cps is excited by the first resonant frequency for clamped-clamped end conditions. Its double frequency shows up near 120 cps. The fluid resonances are at 68, 220, 368, 515, 660, and 803 cps respectively. Only one, 517 cps, corresponds with any of the acceleration peaks.

In Fig. 2.21 the fluid resonances can be observed at 80, 242, 410, 585, 741, and 920 cps. The bending resonances for clamped-clamped end conditions are at 73, 216, 420, and 691 cps. Since the first several correspond almost exactly with the fluid resonances, the peaks are seen to be relatively large. A small peak is seen at the first double resonant frequency also, about 152 cps. There is some motion of this beam in the clamped-pinned mode, but since these

---

\* The pipe bending resonances were computed by directly using the formulas listed in Den Hartog [20] .



frequencies do not correspond to any fluid resonant frequencies, the small peaks are masked out.

Fig. 2.22 shows the longitudinal accelerations at one support of this pipe. For the clamped-clamped mode the first resonance and its double frequency show at 73 and 158 cps respectively. Likewise for the clamped-pinned mode the first two resonances and their double frequencies are seen at 58, 111, 184, and 360 cps. The peak at 39 cps must be due to the first resonance of the pinned-pinned mode.

In these last three Figures it is seen that the primary bending frequencies do excite pressures through longitudinal motions. Also, the double bending frequency accelerations are present, but they are of smaller magnitude and only show up for the first few resonances. Table 2.4 compares some of the experimental and theoretical results.

TABLE 2.4

Comparison of Experimental and Theoretical Ratios of Pipe End Longitudinal Acceleration to Platform Transverse Acceleration\*

(pipe is 1/4" copper tubing filled with air at 200 psia)

<u>Clamped-Clamped</u>				<u>Clamped-Pinned</u>					
<u>Cps</u>	<u>Exp</u>	$\frac{g_{end}}{g_{base}}$	<u>Theo</u>	$\frac{g_{end}}{g_{base}}$	<u>Cps</u>	<u>Exp</u>	$\frac{g_{end}}{g_{base}}$	<u>Theo</u>	$\frac{g_{end}}{g_{base}}$
120	.32		.74		98	.40		.74	
156	.28		.62		111	.23		.71	

\*The experimental data had to be converted to g's per base acceleration since the pipe was not inertially forced. This was done by using Eq. (2.5-2) and a similar one for clamped-pinned end conditions.





This Table shows the theoretical results to be a little high because the end support stiffness in reality places some restraint on the motion. However, the results are of the right order of magnitude and show that the techniques of Section 2.5 could be used to determine an upper bound for the end accelerations.

On the other hand the magnitude of the longitudinal end accelerations due to the primary bending resonances can not be determined at the present time. Considerably more experiments with various end conditions and base supports will have to be conducted in order to be able to predict this effect. The most that can be said now is that the first resonance is the most important and seems to induce a pressure peak of approximately the same magnitude as that induced by comparable longitudinal excitation.

The last two Figures included are to show the combined effects of both longitudinal and transverse accelerations. The pipe was excited near one end at an angle of 45 degrees to its axis, giving both types of forcing. Fig. 2.23 shows the pressure response to have the general upward trend, on the recorder graph, of longitudinal excitation, with fluid resonances near 80, 242, and 400 cps. However, the bending resonances are also present. For the clamped-pinned mode the first resonance and its double frequency are at 59 and 121 cps respectively, but those for the clamped-clamped mode are masked behind peaks. They can be seen, however, in Fig. 2.24 at 77 and 154 cps along with the second bending resonance at 216 cps. These two Figures show that both longitudinal and transverse vibrations can excite fluid pressures at the same time, making the system susceptible to noise



regardless of the orientation of the system with respect to the vibration field.

Finally, Table 2.5 is included with a summary of the experimentally determined damping ratios.

TABLE 2.5

Experimental Damping Ratios

<u>Fluid-no mean flow</u> (200 psia)		<u>Fluid-mean flow</u> (200 psia, 14 ft/sec)		<u>Pipe-long</u> (1/4" copper tubing, air at 200 psia)		<u>Pipe-trans</u>	
<u>Cps</u>	<u>ζ</u>	<u>Cps</u>	<u>ζ</u>	<u>Cps</u>	<u>ζ</u>	<u>Cps</u>	<u>ζ</u>
45	.03	42	.04	850	.04	73	.04
80	.03	155	.04	900	.04*	78	.05
232	.04	197	.04				
390	.04	350	.04				

It can be seen that the values are fairly consistant, having a slight increase with frequency. Also, the fluid damping with no flow is smaller than with flow since the orifice adds resistance when it is in the system.

## 2.9 SUMMARY

In Chapter 2 it has been shown that piping systems containing fluid can excite large pressures when their supporting environment is subjected to vibrations. Energy transfer to the fluid is by means of

---

\* This value was corrected from a recorder output value of .07. Since the filter bandwidth is approximately 50 cps at this point it gives a misleading broadening of the peak which must be corrected.



flow sources caused by pipe boundary nonuniformities such as bends and area changes moving relative to the fluid. When subject to a white noise environment the pressure spectrum is composed of numerous resonant peaks over a wide band of frequencies, the peaks being due to the various resonances in the system.

The piping supports can be forced longitudinally, transversely, or in combination. In all cases it is the longitudinal motion of the end nonuniformities that forces the fluid since the pipe transverse bending vibrations also cause longitudinal motion of its ends. These longitudinal end motions are excited at the bending resonant frequencies and at twice the bending resonant frequencies.

The induced pressures due to longitudinal environmental vibrations were predicted and the experimental data gave excellent agreement with the theory. The excitation coupling to the twice bending resonant frequency end motion was first observed and then a theory developed which allows one to predict pressure levels with a fair degree of accuracy. The coupling effect at the primary bending resonant frequencies was not anticipated, but the theory for longitudinal vibrations can be applied once the coupled longitudinal motion has been measured. The experimental results show this coupling to be such as to induce pressures of the same order of magnitude as those induced by comparable longitudinal excitation.

Since both longitudinal and transverse accelerations of the piping supports induce fluid pressures, the system is susceptible to noise regardless of its orientation to the vibration field. Motion components in more than one of the directions simply cause an additive



effect to the longitudinal forcing motion.

The level of pressure induced for a given excitation was seen to be proportional to the effective speed of sound in the fluid and to the density which is proportional to the pressure for compressible fluids. For the particular system investigated, air at 200 psia, pressures of approximately .6 psi per g of environmental acceleration were observed for the first several resonant peaks. These pressures would have been even greater for fluids of higher density as was indicated by the scanty data obtained for water filled pipes. Reference [13] contains acceleration spectra for aircraft, rockets, and ships which can be used to estimate the levels of induced pressures that systems in actual operation can experience.

Extremely high pressures can be excited when a fluid resonance coincides with that of the piping system. For a more complicated system it is impossible to distinguish between these two types of resonances, but there are still absolute system resonant peaks that are higher than the others. This phenomenon can cause significant induced pressures at the higher frequencies even though the fluid resonant peak levels normally fall off sharply after the first two or three.

Experimental results show the fluid resonant peaks to be fairly sharp, and both the fluid and piping damping ratios appear to be .04 for the cases tested.

The good agreement between the theoretical and experimental results indicates that the assumption made neglecting the viscous boundary





layer transfer from pipe to air is permissible over a wide band of frequencies.

Reducing the production and transmission of these induced pressures is not simple. Use of a typical acoustic filter would not be satisfactory since the filter connections would only furnish more nonuniformities with which to generate more noise. The use of a compliant section at the valve end of the supply transmission line might, however, prove to be useful. Also, low pressure systems are less susceptible to the noise due to their low density, and perhaps should be exclusively used where very high accelerations will be encountered. Securing the piping to stiff structure at short intervals would also reduce the transverse vibrations and make the system susceptible to vibrations in only one axis, longitudinal. Lastly, a thorough vibration test of the empty piping system should be made since high induced pressures can be expected at any frequency where strong structural resonances exist.



Figure 2.1 Basic Fluid System

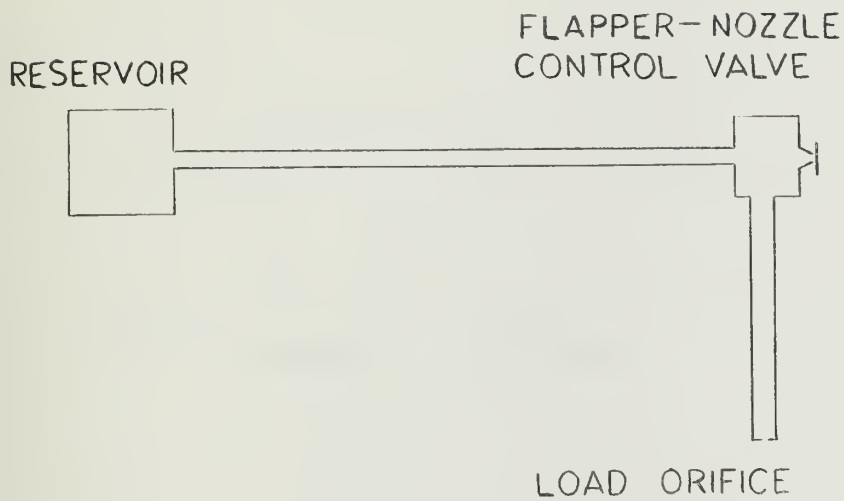


Figure 2.2 Fluid Control Volume

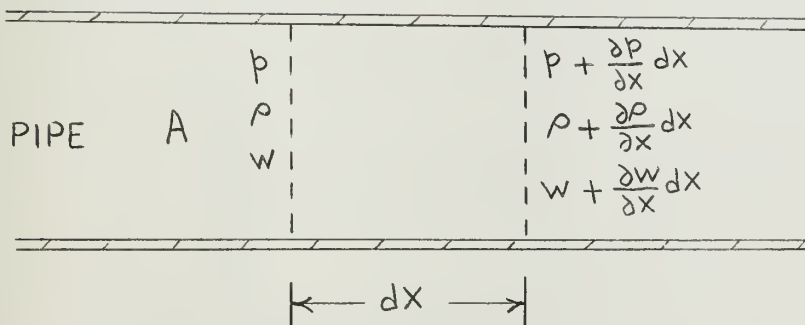




Figure 2.3 Pipe Element

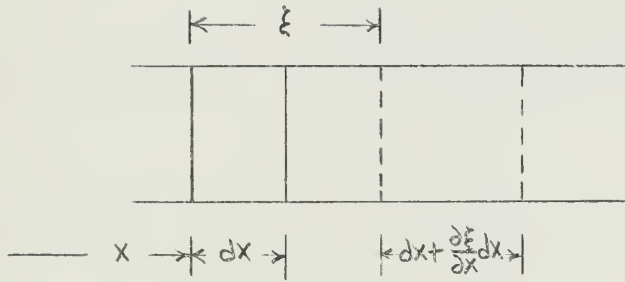


Figure 2.4 Sample Problem

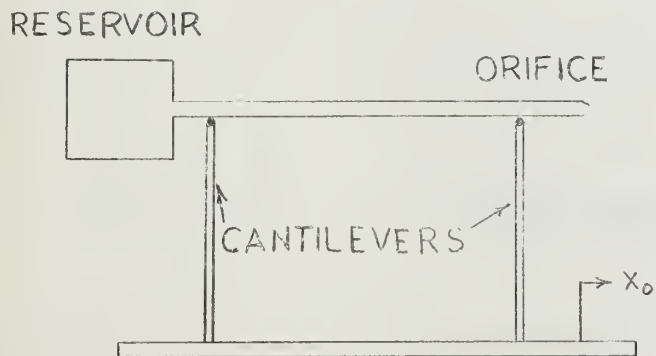




Figure 2.5 Pressure Frequency Response For Sample Problem

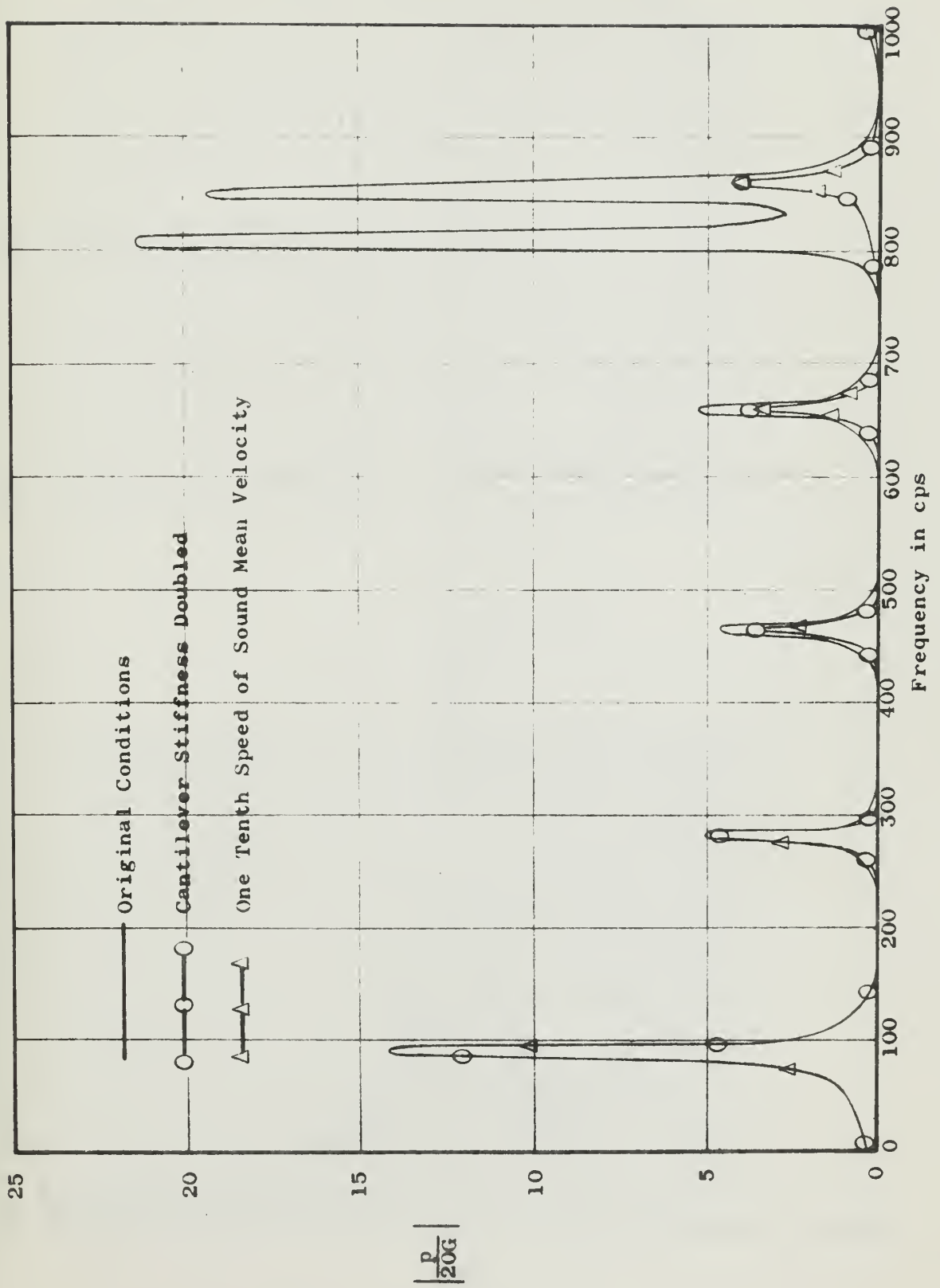






Figure 2.6 Shape of Damped Resonant Peaks

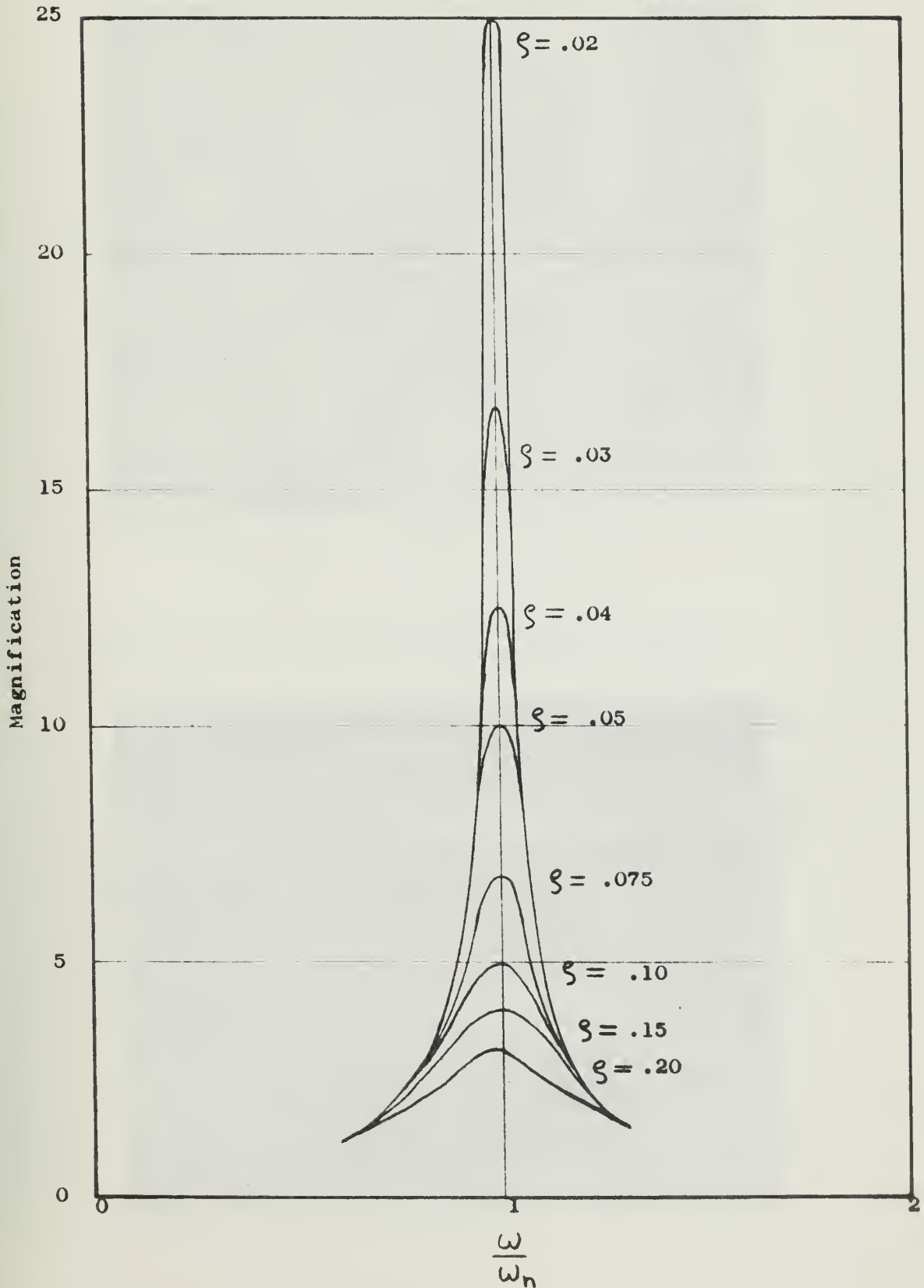




Figure 2.7 Test Setup for Longitudinal Pipe Vibrations

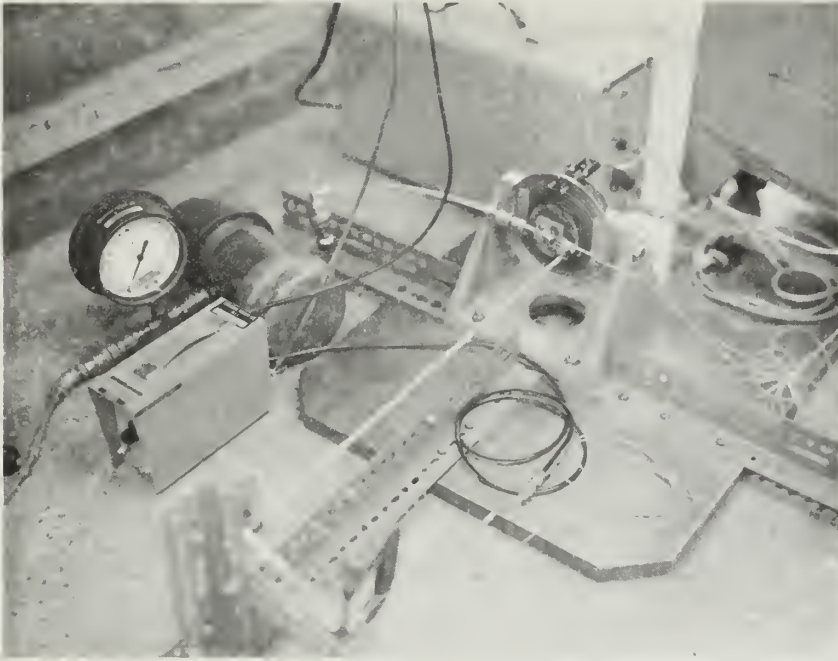


Figure 2.8 Test Setup for Transverse Pipe Vibrations

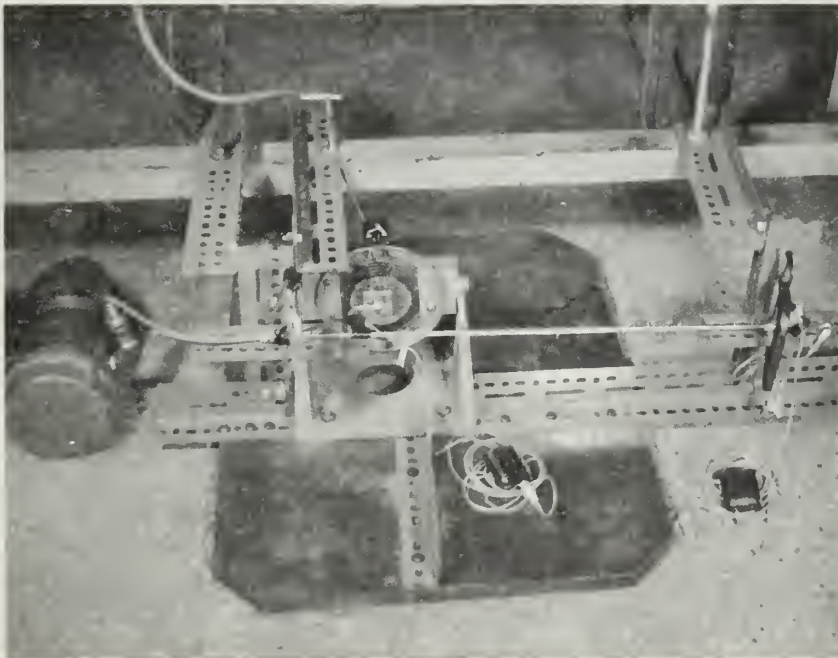
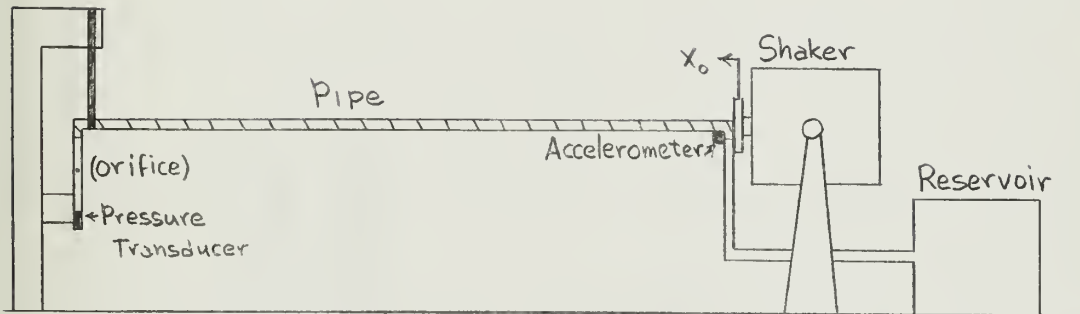




Figure 2.9 Experimental Arrangement

### LONGITUDINAL



$L_1$  = length of line between reservoir and pressure transducer.

$L_2$  = length of pipe between bends.

$L_3$  = distance between end supports.

### TRANSVERSE

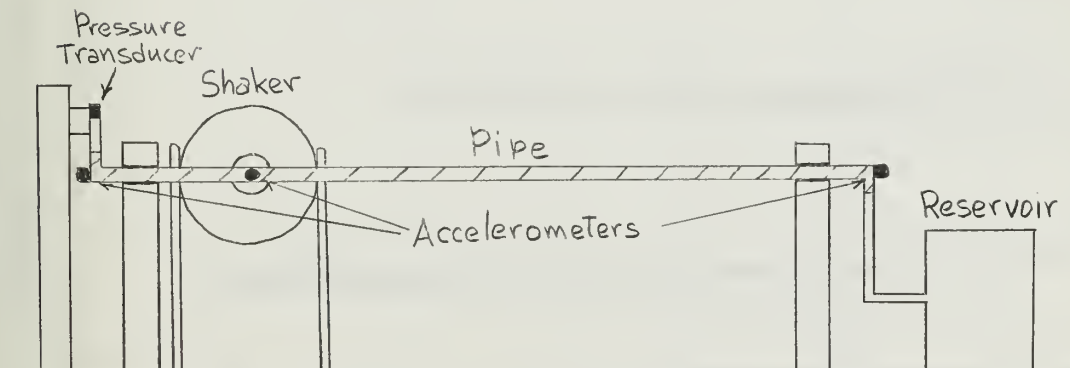




Figure 2.10 Pressure Frequency Response in a Pipe Vibrating Longitudinally

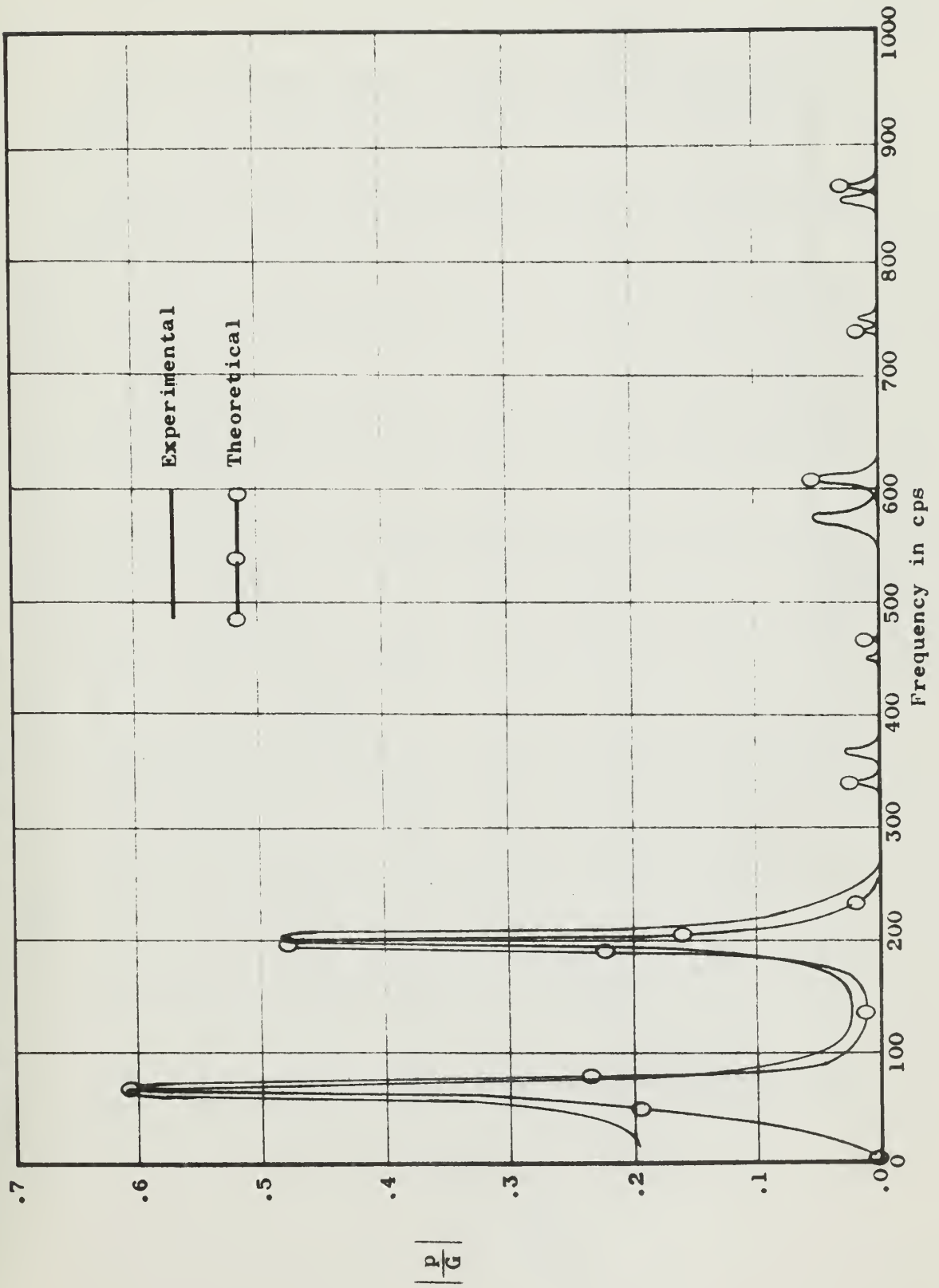






Figure 2.11 Velocity of Sound Frequency Dependence

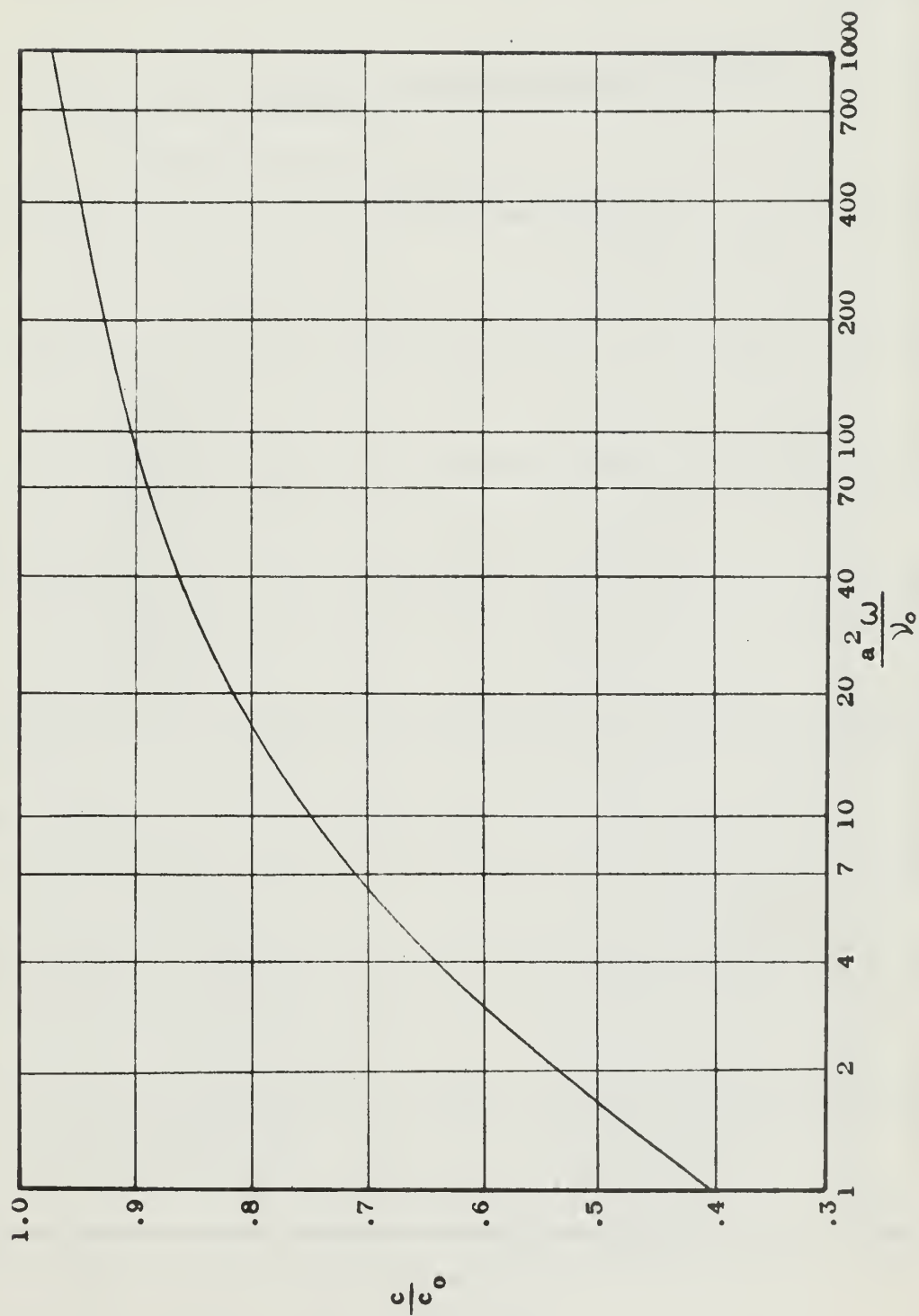




Figure 2.12 Acceleration Frequency Response For a Pipe Vibrating Longitudinally

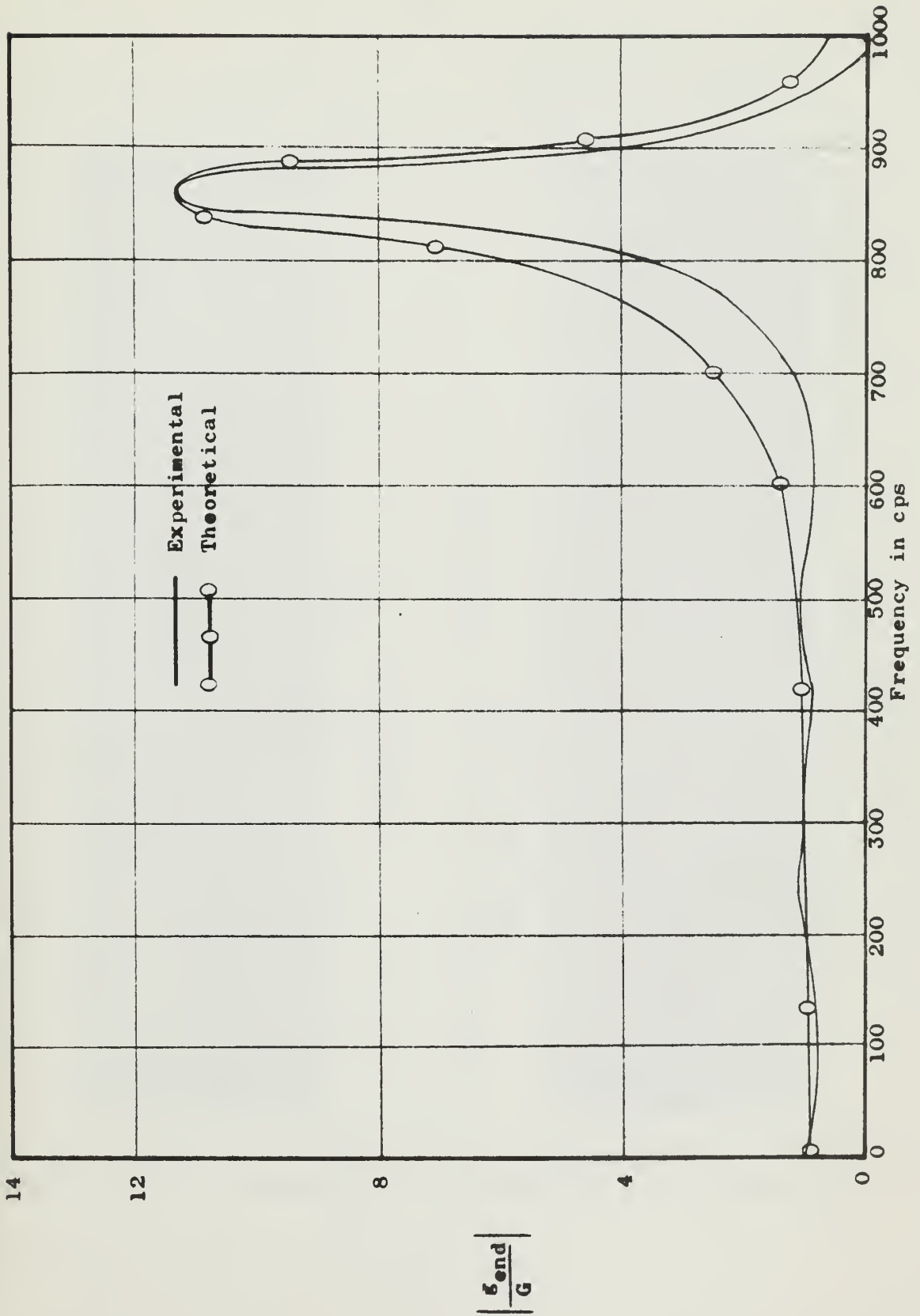




FIGURE 2.13 PRESSURE SPECTRUM IN A PIPE FORCED LONGITUDINALLY WITH WHITE NOISE EXCITATION

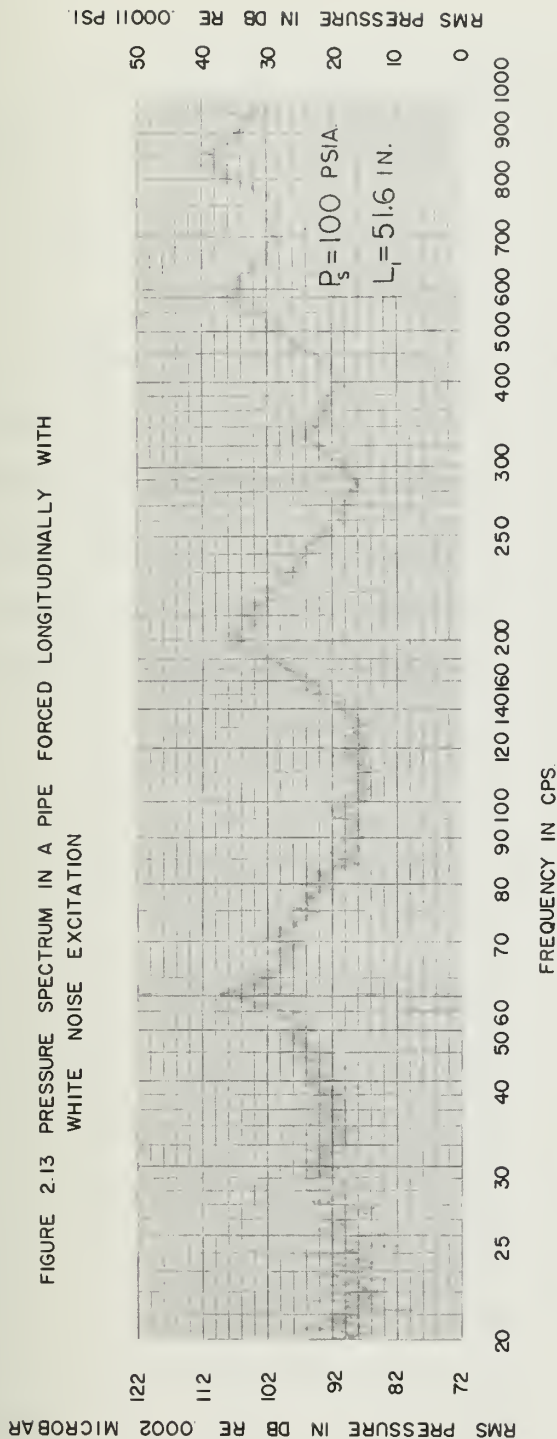


FIGURE 2.14 PRESSURE SPECTRUM IN A PIPE FORCED LONGITUDINALLY WITH WHITE NOISE EXCITATION

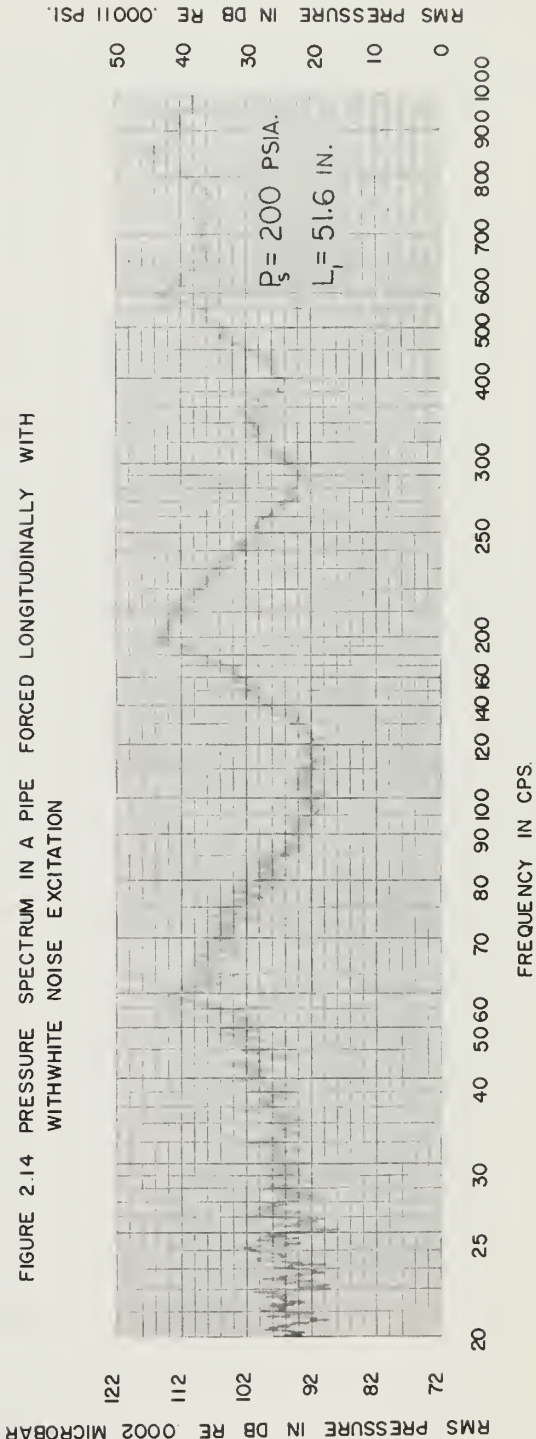




Figure 2.15 Explanation and Scale for Reading db

$db = 10 \log \frac{q}{q_0}$  where  $q_0$  is the reference quantity. Spectrum, however, are in units of quantity squared. Therefore,

$$db = 10 \log \frac{q^2}{q_0^2} = 20 \log \frac{q}{q_0}$$

Graphs that are presented in db can be easily read by using the scale below. The correct quantity for a given db is obtained by multiplying the reference quantity by the appropriate factor in the scale. For units between decades, the decade factor is first multiplied by the appropriate unit factor and then times the reference quantity. i.e.  $23 \text{ db} = 10 \times 1.41 \text{ } q_0 = 14.1 \text{ } q_0$ .

db	$q_0 \times$	db	$q_0 \times$
0	1.00	20	10.0
1	1.12	30	31.6
2	1.26	40	100
3	1.41	50	316
4	1.58	60	1000
5	1.78	70	3160
6	2.00	80	10000
7	2.25	90	31600
8	2.51	100	100000
9	2.82	110	316000
10	3.16	120	1000000





FIGURE 2.16 VOLTAGE SPECTRUM OF WHITE NOISE GENERATOR

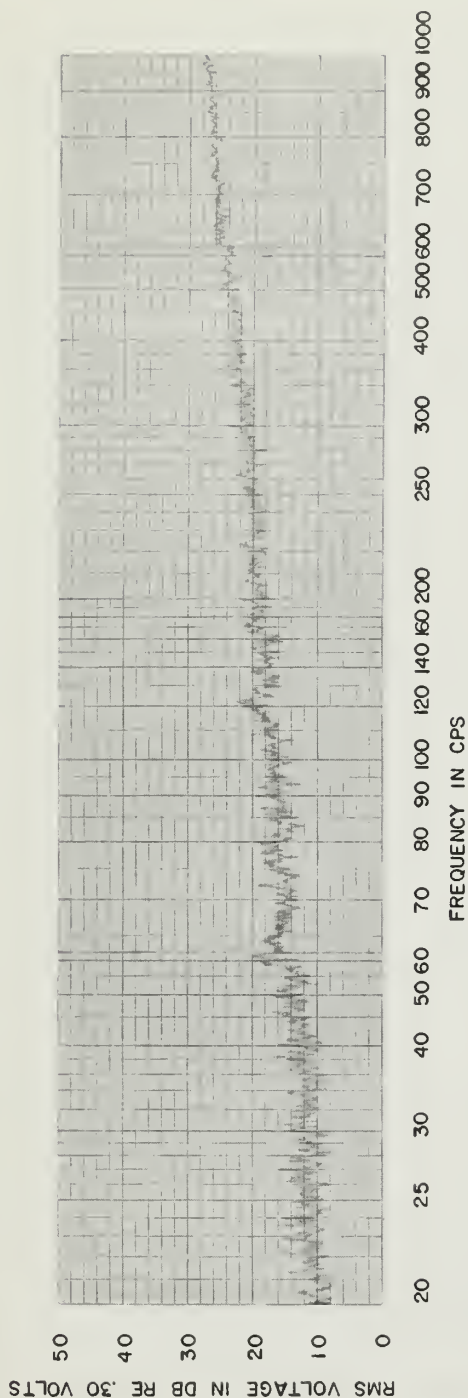


FIGURE 2.17 END ACCELERATION SPECTRUM OF PIPE FORCED LONGITUDINALLY WITH WHITE NOISE EXCITATION

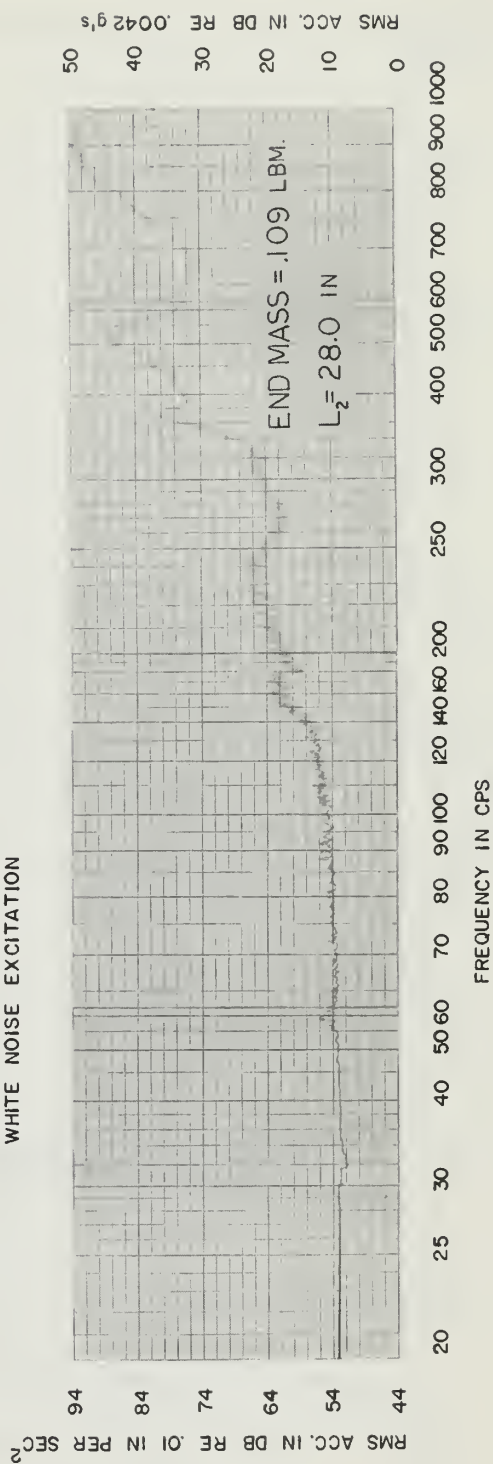
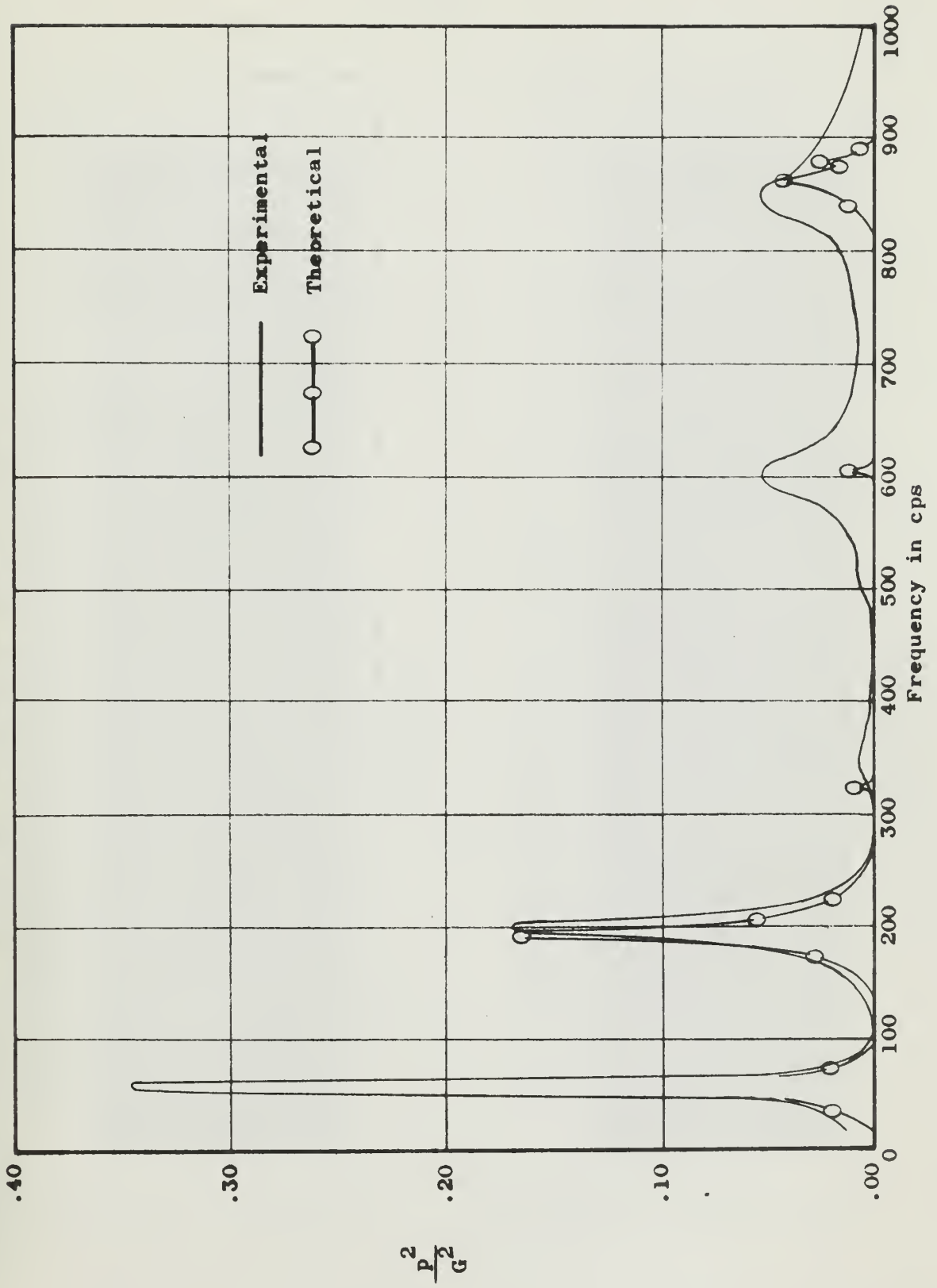




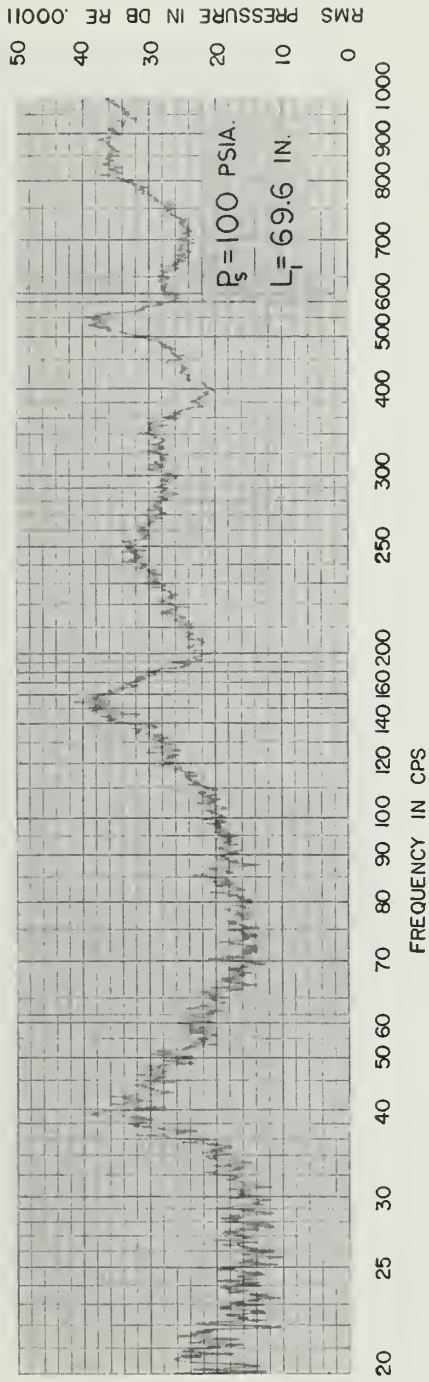
Figure 2.18 Normalized Spectrum of Figure 2.14





RMS PRESSURE IN DB RE .0002 MICROBAR

FIGURE 2.19 PRESSURE SPECTRUM IN A PIPE FORCED LONGITUDINALLY WITH WHITE NOISE EXCITATION



RMS PRESSURE IN DB RE .0002 MICROBAR

FIGURE 2.20 PRESSURE SPECTRUM IN A PIPE FORCED TRANSVERSELY WITH WHITE NOISE EXCITATION

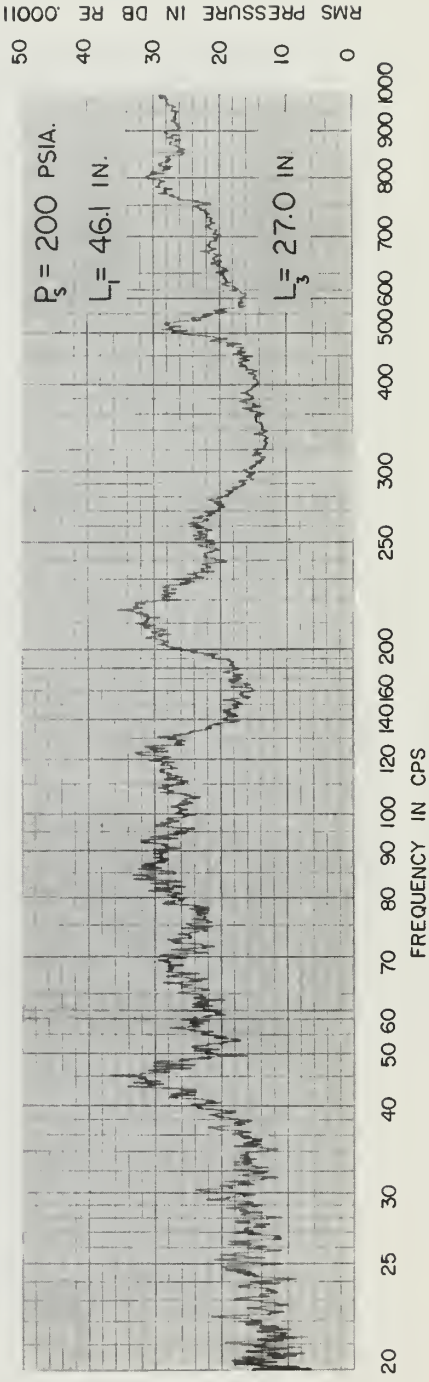
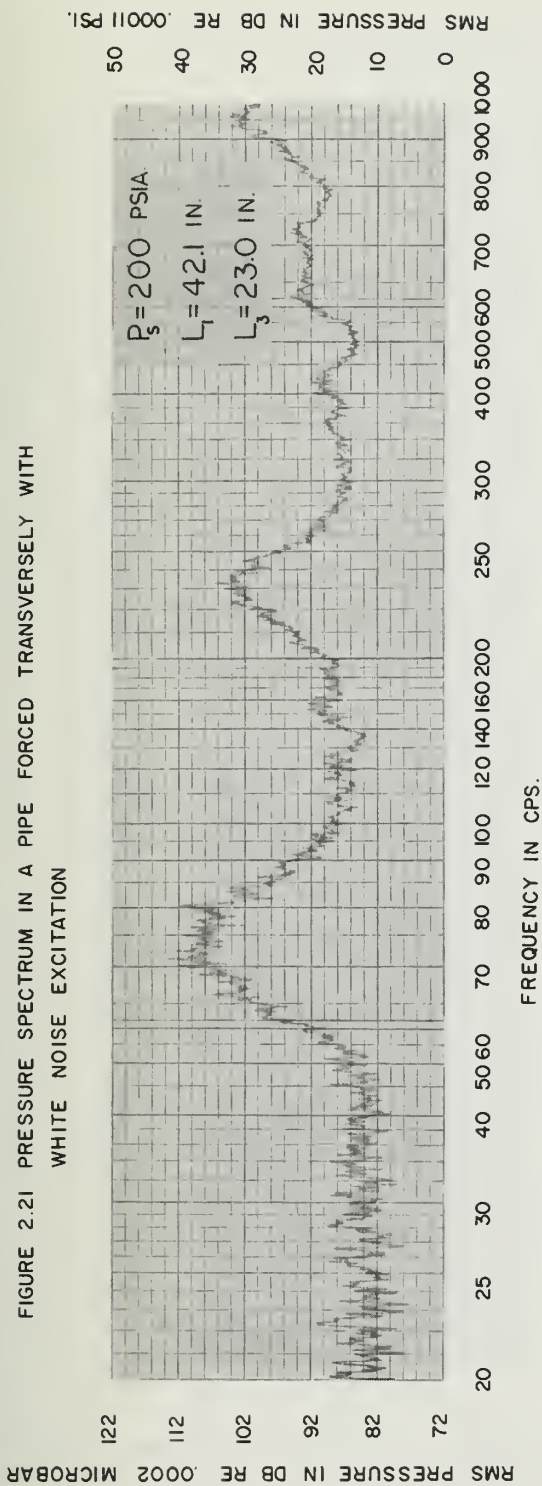






FIGURE 2.21 PRESSURE SPECTRUM IN A PIPE FORCED TRANSVERSELY WITH  
WHITE NOISE EXCITATION



- 63 -

FIGURE 2.22 END ACCELERATION SPECTRUM IN A PIPE FORCED TRANSVERSELY WITH  
WHITE NOISE EXCITATION

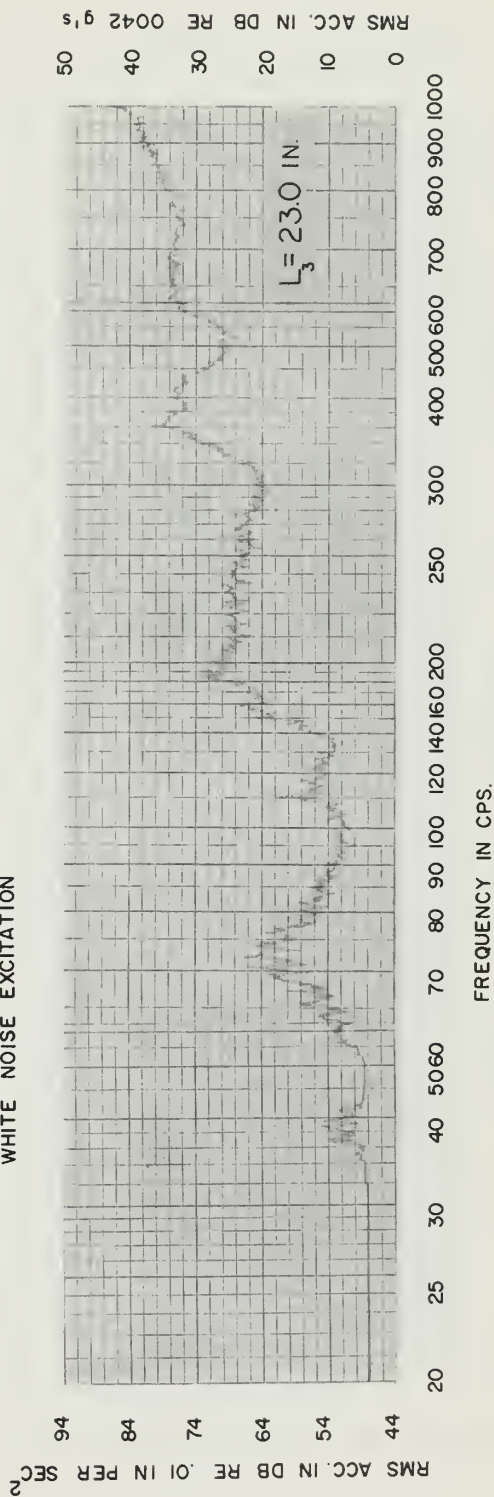






FIGURE 2.23 PRESSURE SPECTRUM IN A PIPE FORCED BOTH LONGITUDINALLY AND TRANSVERSELY WITH WHITE NOISE EXCITATION

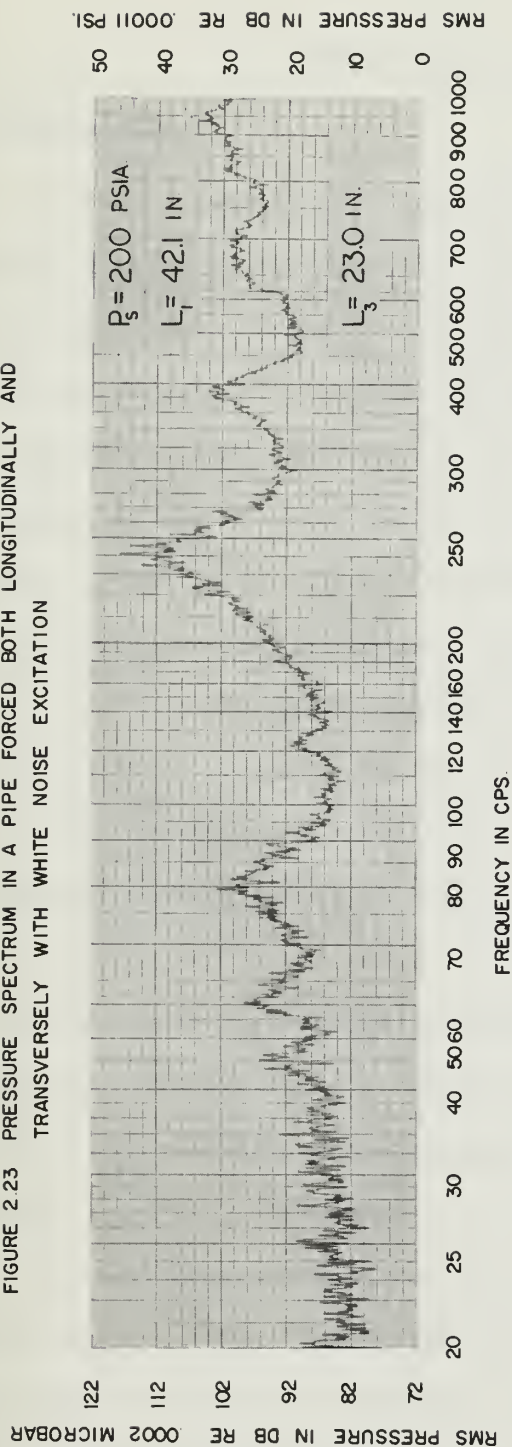
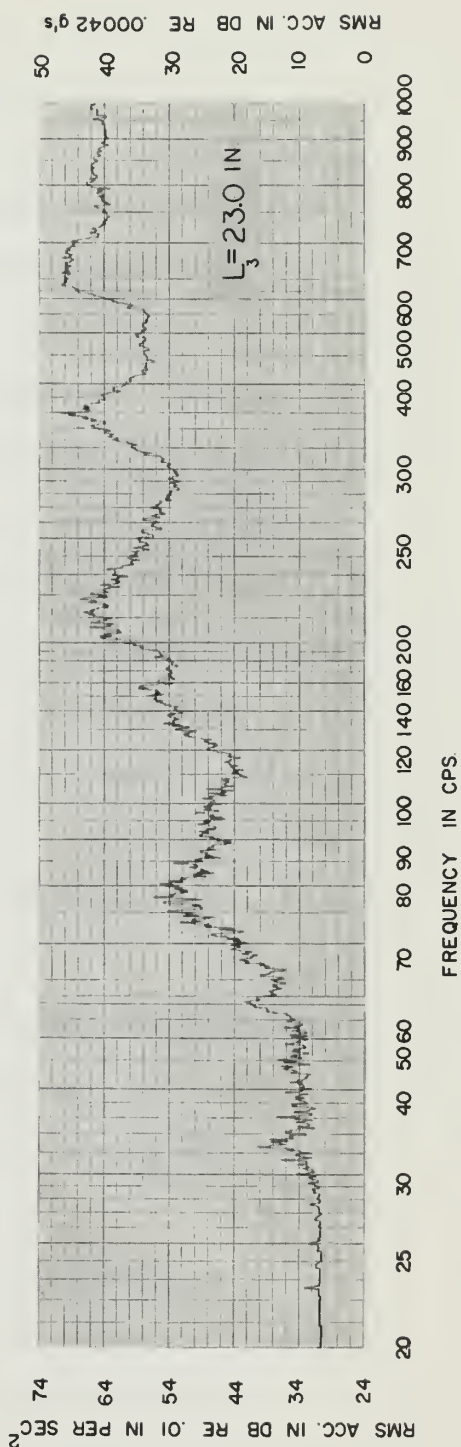


FIGURE 2.24 END ACCELERATION SPECTRUM OF A PIPE FORCED BOTH LONGITUDINALLY AND TRANSVERSELY WITH WHITE NOISE EXCITATION





### 3. CONTROL VALVE ANALYSIS

#### 3.1 INTRODUCTION

In Chapter 2, fluid noise introduction through the environmental vibrations of a passive transmission line element was developed. In this Chapter an active element, a flapper-nozzle control valve, will be investigated while in the same vibrating environment. There are two transmission lines associated with the control valve, the supply line leading to the upstream orifice and the load line that transmits the signal to the load orifice. Noise can be introduced into the system in either or both of these. Induced relative motion of the valve flapper also creates a noise problem and will be investigated along with the two other sources. The small dimensions of a control valve prohibit the generation of structural induced internal pressures since the resonant frequencies are so high as to make the pressures insignificant.

A quasi-linear approach will be used whenever nonlinearities are encountered by linearizing the relation around the operating point. This method gives satisfactory results for small excursions of the variables.

In the following sections the valve chamber and flapper will be analysed first. Then two different models, distributed and lumped, will be constructed for the load line. Finally, the experimental results will be presented and discussed.



## 3.2 MATHEMATICAL MODELS

### 3.2.1 VALVE CHAMBER

In a flapper-nozzle control valve the variable orifice is the curtain area between the nozzle and flapper. This orifice is located downstream of a fixed orifice so that any change in its area alters the mass flow rate out of the valve and causes the pressure in the chamber to vary, see Fig. 3.1. For the valve analysed, both the fixed and variable orifices have choked flow through them and behave as pure resistances.

Writing the continuity equation for the valve chamber of Fig. 3.1 gives

$$w_n + w_\ell - w_s + \frac{\partial}{\partial t} \rho_c V_c = 0, \quad (3.2-1)$$

where  $w_s = \frac{.532N_s A_s p_s}{\sqrt{T_o}}$  and  $w_n = \frac{.532N_n \pi D_n x_r p_c}{\sqrt{T_o}}$  are the choked mass

flow rates through the upstream supply orifice and the variable nozzle orifice respectively. In these relations the N's are the orifice discharge coefficients,  $T_o$  is the absolute temperature, and  $A_s$  and  $\pi D_n x_r$  are the areas of the respective orifices.  $w_\ell$  is the mass flow rate into the transmission line, and the valve chamber volume,  $V_c$ , is taken to include that of the bellows.

Let  $w_i = \frac{.532N_s A_s p_{si}}{\sqrt{T_o}} = \frac{p_{si}}{R_s}$  be the initial supply steady

state mass flow rate at the design operating point, where  $R_s$  is the resistance of the orifice, and the subscript i is used to denote initial steady state condition. Then using the equation of state,



$\rho_c = \frac{p_c}{R_o T_o}$  , and the differential operator, D, Eq. (3.2-1) can be nondimensionalized to give

$$N \frac{x_r p_c}{x_{ri} p_{si}} + \frac{R_s w_l}{p_{si}} - \frac{p_s}{p_{si}} + \tau D \frac{p_c}{p_{si}} + \tau_b \frac{p_{ci} D x_r}{p_{si} x_{ri}} = 0 \quad (3.2-2)$$

and for the steady state,

$$\frac{p_{ci}}{p_{si}} = \frac{1 - \frac{R_s w_{li}}{p_{si}}}{N} \quad (3.2-3)$$

In these equations

$$N = \frac{N_n \pi D x_{ri}}{N_s A_s} \quad , \quad \tau = \frac{V_{ci} p_{si}}{w_i R_o T_o} \quad , \quad \text{and} \quad \tau_b = \frac{A_b x_{ri} p_{si} l_b}{w_i R_o T_o l_n}$$

where  $R_o$  is the gas constant and  $A_b$  is the area of the bellows. The lengths  $l_b$  and  $l_n$  are defined in Fig. 3.1.

In order to get rid of the nonlinearity in the first term, Eq. (3.2-2) can be put into a quasi-linear form. Thus,

$$\frac{p_{ci}}{p_{si}} (\tau_b D + N) \frac{\Delta x_r}{x_{ri}} + (\tau D + N) \frac{\Delta p_c}{p_{si}} + R_s \frac{\Delta w_l}{p_{si}} - \frac{\Delta p_s}{p_{si}} = 0$$

or

$$\frac{\Delta p_c}{p_{si}} = \frac{\frac{\Delta p_s}{p_{si}} - \frac{p_{ci}}{p_{si}} (\tau_b D + N) \frac{\Delta x_r}{x_{ri}} - R_s \frac{\Delta w_l}{p_{si}}}{\tau D + N} \quad (3.2-4)$$

In this equation it is seen that the valve chamber gives a first order lag to the pressure response. For optimum operation, the time constant  $\tau$  should be small and the signal to be transmitted introduced through the flapper displacement,  $\Delta x_r$ . However, with the valve in a vibrating environment, noise can be introduced by the transmission lines





in the form of  $\Delta p_s$  and  $\Delta w_\ell$ , and also as an additional induced flapper displacement.

$\Delta p_s$  is the variation in pressure at the upstream orifice induced by the supply line vibrations. Since the orifice is choked, its impedance as seen by the line is a constant resistance and independent of the valve characteristics. Therefore,  $\Delta p_s$  can be independently determined by the methods of Chapter 2 and applied as a forcing function in Eq. (3.2-4).

On the other hand the flapper motion,  $\Delta x_r$ , is very dependent on the rest of the control valve variables. This is also true of  $\Delta w_\ell$ . For although it is a transmission line induced mass flow, it cannot be independently determined since the impedance as seen by the line is the valve chamber. This complicated impedance is wholly dependent on the other variables. Therefore, to completely describe the system, relations for the flapper and load line will have to be developed.

### 3.2.2 VALVE FLAPPER

Consider now the behavior of the flapper. The force of the air jet acting on it can be found by applying the noninertial momentum equation\* to the control volume in Fig. 3.2, and taking into account the unsteady terms which previously have been left out [23]. This gives

---

\* The noninertial momentum equation is

$$F = \oint_{c.s.} \frac{v_r (\rho v_r \cdot dA)}{g_o} + \iiint_{c.v.} \frac{\partial^2 x_o}{\partial t^2} \frac{dV}{g_o} + \frac{\partial}{\partial t} \iiint_{c.v.} \frac{v_r (\rho dV)}{g_o}$$

where the r stands for relative to the accelerating control volume.



$$(p_n - p_a)A_n - f_f = \frac{1}{2} \frac{\partial x_r}{\partial t} \frac{w_n}{g_o} - \frac{\rho_n v_n^2 A_n}{g_o} + \frac{m_a}{g_o} \frac{\partial^2 x_o}{\partial t^2} + \frac{\partial}{\partial t} \iiint_{c.v.} \frac{v_{xr} \rho dV}{g_o} \quad (3.2-5)$$

where  $f_f$  is the force of the flapper on the fluid (or the fluid on the flapper),  $m_a$  is the mass of air in the control volume, and  $x_o$  is the motion of the platform.

The above equation was obtained by noticing that the pressure forces cancel each other everywhere except over the nozzle area,  $A_n$ . Also in the first term on the right hand side, it is assumed that the air flowing outward through the curtain area has a mean axial relative velocity of one half the flapper relative velocity. In the last term, the integrand vanishes everywhere except in the volume between the flapper and nozzle. In order to evaluate this term a simple approximate, one-dimensional flow solution can be integrated over this volume. This has been done in Appendix B with the results that

$$\frac{\partial}{\partial t} \iiint_{c.v.} \frac{v_{xr} \rho dV}{g_o} = \frac{\partial}{\partial t} \left( \frac{2}{3} \frac{x_r w_n}{g_o} \right). \quad (3.2-6)$$

Also from the equation of state,

$$\rho_n v_n^2 = \frac{p_n v_n^2}{R_o T_o} = g_o k p_n M_n^2 \quad (3.2-7)$$

where  $k$  is the ratio of specific heats, and  $M_n$  is the Mach number. Since the chamber area is much larger than that of the nozzle, the relation for stagnation pressure can be used to give

$$\frac{p_n}{p_c} = \left( 1 + \frac{k-1}{2} M_n^2 \right)^{-\frac{k}{k-1}} \quad (3.2-8)$$



Thus substituting Eqs. (3.2-6), (3.2-7), and (3.2-8) into (3.2-5), one obtains

$$f_f = p_c A_n \left[ \frac{1 + k M_n^2}{(1 + \frac{k-1}{2} M_n^2)^{\frac{k}{k-1}}} \right] - p_a A_n + \frac{m_a}{g_o} \frac{\partial^2 x_o}{\partial t^2} - \frac{7}{6} \frac{\partial x_r}{\partial t} \frac{w_n}{g_o} - \frac{2}{3} \frac{\partial w_n}{\partial t} \frac{x_r}{g_o} \quad (3.2-9)$$

The term in brackets is merely a function of  $k$  and  $M_n$  and thus a function of  $\frac{A_n^*}{A_n}$ , where  $A_n^*$  is the curtain area for choked flow.

However,

$$\frac{A_n^*}{A_n} = \frac{4x_r}{D_n} \quad .$$

Therefore this term can be replaced with an empirical expression that is a function of  $\frac{4x_r}{D_n}$ . This was done by fitting a second order relation to it, Fig. 3.3. The result,

$$.243 \left( \frac{4x_r}{D_n} \right)^2 + 1$$

gives excellent agreement up to  $\frac{4x_r}{D_n} = .7$ . Virtually all flapper-nozzle valve operation is well below this point.

Now writing Eq. (3.2-9) in quasi-linear form after substituting in the above relation, the differential operator, and  $w_n$ , gives

$$\Delta f_f = A_n \left[ .243X + 1 \right] \Delta p_c + .486X A_n p_{ci} \frac{\Delta x_r}{x_{ri}} + \frac{m_a}{g_o} D^2 x_o - \frac{11}{6} \frac{w_i N}{g_o p_{si}} \frac{p_{ci}}{p_{si}} D \Delta x_r - \frac{2}{3} \frac{w_i N x_{ri}}{g_o p_{si}} \frac{D \Delta p_c}{p_{si}} \quad , \quad (3.2-10)$$



the expression for the force the fluid exerts on the flapper, where

$$x = \left( \frac{4x_r}{D_n} \right)^2.$$

The flapper is positioned by a torque motor and bellows feedback, Fig. 3.1. Because the torque motor mass, damping, and stiffness are considerably greater than those of the flapper, a lumped model for the flapper can be used giving the system a single degree of freedom. From the Figure it can be seen that an inertial force will act on the flapper if the platform experiences accelerations in the direction of the control valve principle axis. This will also be true for the torque motor rotor if it is not symmetrically balanced.

The differential equation for the balanced condition is

$$\begin{aligned} \frac{F_t}{\ell} + A_b p_c - (k_b \ell_b + k_s \ell_s) \frac{x_r}{\ell_n} + f_f - \frac{m_f D^2 x_o}{g_o} \\ = \frac{1}{g_o} \left( m_f + \frac{j_t}{\ell^2} \right) D^2 x_r + \left( b_f + \frac{b_t}{\ell^2} \right) D x_r + \left( k_f + \frac{k_t}{\ell^2} \right) x_r \end{aligned} \quad (3.2-11)$$

where  $F_t$  is the signal torque applied to the torque motor and  $k_b$  and  $k_s$  are the stiffnesses of the bellows and spring respectively.  $m_f$ ,  $j_t$ ,  $b_f$ ,  $b_t$ ,  $k_f$ , and  $k_t$  are the mass, inertia, damping, and stiffness of the flapper and torque motor, and the lengths  $\ell$ ,  $\ell_b$ ,  $\ell_n$ , and  $\ell_s$  are defined in Fig. 3.1. When this equation is written in the quasi-linear form, put into Eq. (3.2-10) and the whole expression nondimensionalized by  $kx_{ri}$ , one obtains,

$$\begin{aligned} \Delta F - \Delta I = \left[ \frac{D^2}{\omega_n^2} + \left( 2\zeta + \frac{11}{6} \eta N \frac{p_{ci}}{p_{si}} \right) \frac{D}{\omega_n} + (1 + \kappa - .485\alpha X \frac{p_{ci}}{p_{si}}) \right] \frac{\Delta x_r}{x_{ri}} \\ + \left[ \frac{2}{3} \eta N \frac{D}{\omega_n} - \alpha (.243X + \frac{A_b}{A_s} + 1) \right] \frac{\Delta p_c}{p_{si}}. \end{aligned} \quad (3.2-12)$$





In this Equation,

$$\Delta F = \frac{\Delta F_t}{2kx_{ri}}, \quad \Delta I = \frac{m_f D^2 x_o}{g_o kx_{ri}} = \frac{m_f \Delta G}{kx_{ri}}, \quad \kappa = \frac{k_b^l + k_s^l}{k\ell_n},$$

$$\alpha = \frac{A_n^p s_i}{kx_{ri}}, \quad \eta = \frac{w_i}{\sqrt{g_o m_e k_e}}, \quad \zeta = \frac{b_e}{2 \sqrt{\frac{m_e k_e}{g_o}}}, \quad \text{and } \omega_n = \sqrt{\frac{g_o k_e}{m_e}},$$

$$\text{where } m_e = m_a + m_f + \frac{j_t}{\ell^2}, \quad b_e = b_f + \frac{b_t}{\ell^2}, \quad \text{and } k_e = k_f + \frac{k_t}{\ell^2}.$$

Eq. (3.2-12) shows that the flapper motion is dependent on the chamber pressure. It also shows that the pressure is a function of the inertia force and susceptible to noise introduction by it.

Still one more equation is needed in addition to (3.2-3), (3.2-4), and (3.2-12) to completely describe the system. This is the relation for the load transmission line. Models for this line will be constructed in the next two sections.

### 3.2.3 TRANSMISSION LINE, DISTRIBUTED PARAMETERS

The transmission line leads from the valve chamber to the choked load orifice. Depending on the vibration field, it can be excited longitudinally, transversely, or in a combination. Regardless of the excitation or the piping supports, the methods of Chapter 2 can be used to obtain a relation for  $\Delta w_\ell$  in terms of  $\Delta p_c$ . Here the pipe will be assumed rigid and forced, along with the valve, in a longitudinal direction with an acceleration of  $D^2 \Delta y_o$ .

Using the relative transmission matrix from Section 2.4 for the fluid, one obtains



$$\Delta p_c = \cosh \Gamma \Delta p(L) + Z_c \sinh \Gamma \Delta w_r(L) + Z_c \rho_o A D \sinh \Gamma \Delta y_o$$

and (3.2-13)

$$\Delta w_l = \frac{1}{Z_c} \sinh \Gamma \Delta p(L) + \cosh \Gamma \Delta w_r(L) + \rho_o A D (\cosh \Gamma - 1) \Delta y_o,$$

where  $\Delta w_l$  is the relative mass flow rate out of the chamber, Eq. (3.2-1).

Since the load orifice is choked,  $w_r(L) = \frac{p(L)}{R}$ , where  $R$  is the orifice resistance. Therefore,

$$\Delta w_l = \left( \frac{1/Z_c \sinh \Gamma + 1/R \cosh \Gamma}{\cosh \Gamma + \frac{Z_c}{R} \sinh \Gamma} \right) \Delta p_c + 386 \rho_o A \frac{(1 - \cosh \Gamma - \frac{Z_c}{R} \sinh \Gamma) \Delta G}{D (\cosh \Gamma + \frac{Z_c}{R} \sinh \Gamma)} \quad (3.2-14)$$

and in the steady state,

$$w_{li} = \frac{p_{ci}}{R}.$$

Putting this last expression into Eq. (3.2-3) gives,

$$\frac{p_{ci}}{p_{si}} = \frac{1}{N + \frac{R_s}{R}} \quad (3.2-15)$$

Eqs. (3.2-14) and (3.2-15) along with (3.2-4) and (3.2-12) completely define the system. Eq. (3.2-14) is for one specific type of load line and excitation while the other three Equations are general. The system behavior will be analysed using these Equations in Section 3.3.

Before going on to a lumped model development for the transmission line, it is of interest to consider the impedance the line sees looking into the valve. Once this is known the load transmission line is completely determined and can be independently analysed. The impedance only has meaning when the valve is passive or  $\Delta F$ ,  $\Delta I$ , and  $\Delta p_s$  are zero. For this case, since  $Z_v = \frac{\Delta p_v}{\Delta w_r} = \frac{\Delta p_c}{\Delta w_l}$ , combining Eqs. (3.2-4), (3.2-12), and (3.2-15) gives



$$Z_v = - \frac{R_s \left( \frac{D^2}{\omega^2 n} + a \frac{D}{\omega n} + b \right)}{(\tau D + N) \left( \frac{D^2}{\omega^2 n} + a \frac{D}{\omega n} + b \right) + \left( \frac{\tau_b D + N}{R + \frac{s}{N}} \right) \left( c \frac{D}{\omega n} + d \right)}, \quad (3.2-16)$$

where  $a = 2\zeta + \frac{11}{6} \eta \frac{N}{R + \frac{s}{N}}$ ,  $b = 1 + \kappa - .486\alpha X \frac{1}{R + \frac{s}{N}}$ ,  $c = -\frac{2}{3} \eta N$ ,

and  $d = \alpha \left( .243X + \frac{A_b}{A_s} + 1 \right)$ .

From Eq. (3.2-16), the impedance and real and imaginary parts are plotted in Fig. 3.4 for the particular control valve used in the experimental work. Also included is the impedance for when there is no bellows feedback, or  $\tau_b = \kappa = A_b = 0$ . It is seen that feedback emphasizes the flapper resonance, but that it decreases the impedance at lower frequencies.

It is to be noted that the real part of the impedance is positive up to the resonant frequency where it becomes negative, and the imaginary part is negative for all frequencies. Using this figure along with the known orifice resistance, Eqs. (3.2-13) can be used to solve the load line pressure and mass flow rate at any frequency.

#### 3.2.4 TRANSMISSION LINE, LUMPED PARAMETERS, AND ANALOG COMPUTER MODELLING TECHNIQUES

In addition to the distributed model for the line, it is also desirous to construct a lumped model which allows the system to be



analysed on the analog computer. The advantage of using the computer is that each of the parameters can be easily changed and its effect on the rest of the system readily seen.

The line is modelled as lumped inertias, resistances, and compliances. The inertias and resistances are combined into series impedance elements and the compliances constitute shunt admittance elements, see Fig. 3.5.

Causality must be taken into account when constructing the model so that the problem can be solved on the analog computer without using differentiation which causes difficulties. The specified variable, pressure or mass flow rate, at each end of the line determines what the nearest lumped element must be. Pressure requires a series impedance while mass flow rate requires a shunt admittance. Also, the number of line resonances a person desires to model determines the number of inertia elements that must be used. Thus since the transmission line in this investigation starts with a known pressure,  $\Delta p_c$ , and terminates with an induced flow source due to the motion of the line, and since it is desired to model the first two resonances of the line, the model in Fig. 3.5 is appropriate.

The transmission matrix for the first half of the line is

$$\begin{bmatrix} \Delta p_c \\ \Delta w_{r\ell} \end{bmatrix} = \begin{bmatrix} 1 & \frac{ZL}{2} \\ 0 & 1 \end{bmatrix} \begin{bmatrix} 1 & 0 \\ \frac{YL}{2} & 1 \end{bmatrix} \begin{bmatrix} \Delta p_m \\ \Delta w_m \end{bmatrix},$$

and that for the second half is





$$\begin{bmatrix} \Delta p_m \\ \Delta w_m \end{bmatrix} = \begin{bmatrix} 1 & \frac{ZL}{2} \\ 0 & 1 \end{bmatrix} \begin{bmatrix} 1 & 0 \\ \frac{YL}{2} & 1 \end{bmatrix} \begin{bmatrix} \Delta p(L) \\ \Delta w(L) \end{bmatrix}.$$

In relative coordinates, since  $\Delta w = \Delta w_r + \rho_o AD \Delta y_o$ , these become

$$\begin{bmatrix} \Delta p_c \\ \Delta w_{rl} \end{bmatrix} = \begin{bmatrix} 1 + \frac{YLZL}{4} & \frac{ZL}{2} \\ \frac{YL}{2} & 1 \end{bmatrix} \begin{bmatrix} \Delta p_m \\ \Delta w_{rm} \end{bmatrix} + \begin{bmatrix} \frac{ZL}{2} \rho_o AD \Delta y_o \\ 0 \end{bmatrix}$$

and

$$\begin{bmatrix} \Delta p_m \\ \Delta w_{rm} \end{bmatrix} = \begin{bmatrix} 1 + \frac{YLZL}{4} & \frac{ZL}{2} \\ \frac{YL}{2} & 1 \end{bmatrix} \begin{bmatrix} \Delta p(L) \\ \frac{\Delta p(L)}{R} \end{bmatrix} + \begin{bmatrix} \frac{ZL}{2} \rho_o AD \Delta y_o \\ 0 \end{bmatrix}$$

respectively, when the substitution  $\Delta w_r(L) = \frac{\Delta p(L)}{R}$  is made.

Now extending the results in Section 2.4, the series impedance becomes

$$\begin{aligned} ZL &= \frac{DL}{g_o A} = R_\ell \\ &= Z_c \frac{LD}{c} + R_\ell \\ &= Z_c T_e D + R_\ell \end{aligned} \tag{3.2-17}$$

where  $T_e = \frac{L}{c}$  is the transmission time for a wave to travel the length of the pipe, and  $R_\ell$  is the total frictional resistance. Also, the shunt admittance becomes

$$\begin{aligned} YL &= \frac{g_o ADL}{c^2} \\ &= \frac{1}{Z_c} \frac{L}{c} D \\ &= \frac{1}{Z_c} T_e D. \end{aligned} \tag{3.2-18}$$



Putting Eqs. (3.2-17) and (3.2-18) into the transmission matrices

then gives

$$\begin{bmatrix} \Delta p_c \\ \Delta w_\ell \end{bmatrix} = \begin{bmatrix} \frac{T_e^2 D^2}{4} + \frac{R_\ell T_e D}{4Z_c} + 1 & \frac{Z_c T_e D}{2} + \frac{R_\ell}{2} \\ \frac{T_e D}{2Z_c} & 1 \end{bmatrix} \begin{bmatrix} \Delta p_m \\ \Delta w_m \end{bmatrix} + \begin{bmatrix} \frac{Z_c T_e \rho_o A D^2 \Delta y_o}{2} \\ 0 \end{bmatrix} \quad (3.2-19)$$

and

$$\begin{bmatrix} \Delta p_m \\ \Delta w_m \end{bmatrix} = \begin{bmatrix} \frac{T_e^2 D^2}{4} + \frac{R_\ell T_e D}{4Z_c} + 1 & Z_c T_e D + \frac{R_\ell}{2} \\ \frac{T_e D}{2Z_c} & 1 \end{bmatrix} \begin{bmatrix} \Delta p(L) \\ \frac{\Delta p(L)}{R} \end{bmatrix} + \begin{bmatrix} \frac{Z_c T_e \rho_o A D^2 \Delta y_o}{2}^* \\ 0 \end{bmatrix}$$

For the steady state, Eqs. (3.2-19) give

$$w_{li} = \frac{p_{ci}}{R + R_\ell}$$

which when combined with Eq. (3.2-3) becomes,

$$\frac{p_{ci}}{p_{si}} = \frac{1}{N + \frac{R_s}{R+R_\ell}} \quad (3.2-20)$$

Although Eqs. (3.2-19) could be cascaded to give one overall transmission matrix, this should not be done for the same reason as mentioned previously, namely the resulting equations would not be able to be solved on the analog computer without the use of differentiation. Therefore, regardless of the number of lumped sections the line is divided into, each section should be handled separately.

---

\* The resistance is not included in the forcing term since only the flow relative to the pipe causes a loss of pressure.



In order to determine  $R_\ell$  for use in the above equations, it is necessary to use a quasi-linear approach since the frictional resistance is nonlinear. The pressure loss equation is

$$p = \frac{4fL\rho_o v^2}{2g_o D_\ell}$$

where  $f$  is the friction factor,  $\rho_o$  is the mean fluid density, and  $D_\ell$  is the pipe diameter. Now putting in mass flow rate gives

$$p = \frac{4fL\rho_o w^2}{2g_o D_\ell \rho_o^2 A^2}$$

where  $A$  is the flow area.

Putting this into the quasi-linear form it becomes

$$\Delta p = \frac{8fL\rho_o w_i \Delta w}{2g_o D_\ell \rho_o^2 A^2} \cdot$$

Therefore,

$$\frac{\Delta p}{\Delta w} = R_\ell = \frac{4fLw_i}{g_o D_\ell \rho_o^2 A^2} \cdot \quad (3.2-21)$$

Using Eqs. (3.2-4), (3.2-12), (3.2-19), and (3.2-20) it is now possible to set up the problem on the analog computer. An operational block diagram for this setup is contained in Fig. 3.6. Since everything is nondimensionalized, including time, scaling is not too difficult and is indicated on the Figure. The various inputs are also marked as well as the system variables that are of interest. It is noted that the load line induced noise input,  $\Delta y_o$ , enters in at two different points due to the load line being modelled in two parts.

This analog model now allows one to vary the input and system parameters, and to investigate their effect on the system variables.



Results thus obtained are discussed along with the other analytic and experimental results in the following section.

### 3.3 EXPERIMENTAL WORK AND DISCUSSION OF RESULTS

A small flapper-nozzle control valve was built in order to verify experimentally the analytical results. It was equipped with a removable bellows feedback system, Fig. 3.7. The flapper displacement could be measured by means of a capacitance pickup, and the chamber pressure and supply line pressure just upstream of the orifice were obtained with a piezoelectric transducer. The flapper displacement was controlled by means of a torque motor supplied from a servo amplifier. A view of the general arrangement and instrumentation are shown in Fig. 3.8, and further discussion is contained in Appendix C.

Since a vibration generator large enough to shake the whole system was not available, it was necessary to simulate the noise inputs. The pressures in the supply line were generated by supplying the valve through the load line of another flapper-nozzle valve operating at a higher pressure. In this manner pressures at any frequency could be imposed on top of the mean supply pressure of 100 psia, simulating resonant noise peaks.

The behavior of the control valve transfer function of,  $\Delta p_c$ , when subjected to supply line noise,  $\Delta p_s$ , is shown in the frequency response curves of Fig. 3.9. The Figure contains an experimentally obtained curve for the valve operating with bellows feedback as well as theoretical curves with and without feedback.





The theoretical results were obtained by combining Eqs. (3.2-4), (3.2-12), (3.2-14), and (3.2-15). After putting in the appropriate values for the valve used, this distributed model equation becomes

$$\Delta p_c = \frac{a\Delta p_s + .59b\Delta G_f + .012ac\Delta G_\ell}{ae + 6.75b + 1.82ad} \quad (3.3-1)$$

where  $\Delta p_c$  is in psi,  $\Delta p_s$  is the supply line pressure noise in psi,  $\Delta G_f$  is the acceleration in g's experienced by the valve in the direction of its principle axis, and  $\Delta G_\ell$  is the acceleration of the load line in g's. Any one of the three noise transfer functions can be obtained by setting the other two noise inputs to zero. In this equation,

$$a = .35 \frac{\omega}{\omega_n} i + 1.12 - \frac{\omega^2}{\omega_n^2},$$

$$b = .02 \frac{\omega}{\omega_n} i + .22,$$

$$c = \frac{\omega_n}{\omega} \left[ \left( \cos \frac{\omega}{1100} - 1 \right) i + .23d \sin \frac{\omega}{1100} \right],$$

$$d = \frac{\cos \frac{\omega}{1100} + 4.40 i \sin \frac{\omega}{1100}}{\cos \frac{\omega}{1100} + .23 i \sin \frac{\omega}{1100}},$$

$$e = 7.36 \frac{\omega}{\omega_n} i + .50,$$

and

$$\omega_n = 2520 \text{ radians per second.}$$

When there is no bellow feedback, the denominator of Eq. (3.3-1) becomes  $ae + 1.30b + 1.82ad$ ,

$$\text{and} \quad a = .35 \frac{\omega}{\omega_n} i + 1.00 - \frac{\omega^2}{\omega_n^2}$$

$$\text{while} \quad b = .22.$$



In the Figure, the transfer function is seen to behave as a first order lag cascaded with a second order system. This is due to the valve chamber and flapper respectively. Feedback increases the effect of the flapper resonance, but it decreases the pressure at lower frequencies. The experimental curve is not continued past 700 cps because the response of the first (noise producing) flapper-nozzle valve drops off to zero at this frequency, and no noise could be introduced to the test valve.

The system appears to have slightly more damping than was estimated, and therefore the experimental peak is not as high as predicted, and it is at a slightly lower frequency. From the Figure, the damping is calculated to be approximately .08 and .10 for the theoretical and experimental results respectively. It is to be noted that the flow noise in the valve created a region of uncertainty in the experimental results having a width of approximately .02 on the Figure.

It appears that if the flapper-torque motor arrangement had less damping and if the bellows feedback were increased, then the noise transfer function would become much larger near the flapper resonance. In order to study the effect of varying these two parameters, analog computer solutions were obtained using the lumped model formulated in Section 3.2.4.

It was found that the noise signal could be increased as expected. However of much more interest, it was also found that the total noise power could be amplified in the valve at frequencies near the flapper



resonance. That is to say that the noise power associated with the bellows, force times velocity, was greater than the noise power entering the valve, pressure times flow. This amplification can take place because some of the steady power flowing into the valve is converted into noise power. This is a danger of noise in an active element and differs from what can happen in a passive element. In a passive element high noise signals can be obtained through resonances as in the transmission lines studied, but the total noise power cannot increase. It is of interest that the increased power was measured in the bellows which is a direct analogy to a load piston operating with the control valve. Thus it is seen that the noise can be amplified into actually displacing a load. Also, increased motion of the flapper due to the feedback of the supply line noise can cause the flapper to strike the nozzle. This flapper motion saturation makes the valve inoperative to command signals.

In terms of numbers, the threshold of amplification was observed when damping was decreased by a factor of .7 and feedback was increased by a factor of 1.7. Another combination was found when damping was decreased by a half and feedback was increased by a factor of 1.2. These factors decreased the flapper system damping ratios to .25 and .17 respectively for the two cases. These are not excessively low values and might well be encountered in many systems. These results could not be checked experimentally using the test valve because the feedback and torque motor damping had fixed values. When the torque motor was removed to decrease the amount of damping, the system became unstable. Since the feedback could not be increased, it also was not



possible to make the flapper motion saturate. The maximum flapper motion that could be excited was about .0015 inches while the steady state nozzle clearance was .005 inches.

In order to simulate inertial excitation to the flapper, a white noise signal was added into the servo amplifier input. This showed the first resonant peak as expected, but it also showed smaller peaks at the equalizing spring resonances and at the second resonance of the flapper. Fig. 3.10 is the frequency response transfer function of the chamber pressure per g of induced flapper excitation. The characteristics are very much like those discussed in conjunction with Fig. 3.9. There is, however, a small peak at 300 cps in the experimental result due to the equalizing spring, and the pressures at the lower frequencies are larger than predicted. Increasing feedback and decreasing damping would have the same effects with regards to amplifying this induced noise as was discussed with supply line noise. It is also possible to get flapper motion saturation.

Since there was no driver available that would work against the pressure in the load line, it was not possible to simulate load line induced vibrations. The line was hooked up to the vibration generator, but this did not induce signals large enough to be recorded. Fig. 3.11 shows that the theory predicts that these pressures will be very small. Even for 100 g's of excitation the induced pressure would be less than one psi even at the flapper resonant frequency. The smallness of the induced pressure is due to the capacitive effect of the valve chamber volume, and to the low pressure of the load line, approximately 35 psia, causing the air density to be quite low. A valve operating at higher





pressures would be much more susceptible to this type of noise.

The above results have shown that the control valve is susceptible to noise from the supply line and inertial forcing of the flapper. The noise amplitude is greatest at low frequencies and near the flapper resonant frequency. When the flapper system damping is low enough, bellows force feedback can cause amplification of the noise power to the valve and saturation of the flapper motion.

External vibrations of the load line do cause resonant frequency peaks, but because of the reduced pressure of this line, it is only of concern in valves with very high supply pressures.

### 3.4 PROCEDURE FOR TESTING CONTROL VALVE SUSCEPTIBILITY TO NOISE

Of considerable interest to the person who must specify a particular control valve for a given job, is whether or not the valve will be highly susceptible to vibration induced noise. Therefore, it should become standard procedure to test any such control valve before it is assigned for use. Since there are three ways noise can be induced into the system, there are primarily three tests.

The first test deals with noise introduced through the supply line. For this test, the supply line noise can be generated in the same manner used in this theses. Supply the valve through the load line of a second control valve operating at a higher pressure. In this way sinusoidal noise signals can be imposed on the mean supply pressure for any frequency. The frequency response for  $\left| \frac{\Delta p_c}{\Delta p_s}(\omega) \right|$  should then be obtained as well as the response for  $\left| \frac{\Delta x_r}{\Delta p_s}(\omega) \right|$ , making sure to test



at the maximum feedback that will be used in practice. If either of these two responses is excessively large, the control valve should not be used where environmental vibrations could be a problem.

The second test is for vibration induced flapper motion. If a large vibration shaker is available the valve can be vibrated directly and  $\left| \frac{\Delta x}{\Delta G} r \right| (\omega)$  and  $\left| \frac{\Delta p}{\Delta G} c \right| (\omega)$  recorded. Otherwise the frequency response for both of these can be obtained by applying a signal to the torque motor as was done in this thesis. In this case  $G = \frac{\Delta F_t}{\ell m_f}$  where  $F_t$  is the torque applied to the motor,  $m_f$  is the equivalent forced mass of the flapper, and  $\ell$  is the lever arm of the rotor. If either of the responses is too large, an effort can be made to balance the rotor and flapper assembly. If one is fortunate enough to have the large shaker, any reduction in response due to balancing will show up directly. However, if one is simulating the vibration, balancing will reduce the value of  $m_f$  used in calculating  $\Delta G$ . If  $m_f$  is reduced enough,  $\Delta G$  will be excessive in order to force a response, and the control valve will be safe for use. If balancing is not successful the valve should not be used.

The third test is for load line induced pressures. If the control valve chamber does not operate above several hundred psia, this type of noise should not be a problem. A test can be made with a small vibration generator used to vibrate the end of a flexible line in a longitudinal direction and the response,  $\left| \frac{\Delta p}{\Delta G} c \right| (\omega)$ , recorded. The amplitude of this response will dictate whether the valve is safe or not.

One additional test can be conducted with the fluid transmission



lines. A thorough vibration test of the empty piping system should be made since high induced pressures can be expected at any frequency where strong structural resonances exist. If any of these resonances are near the flapper resonant frequency of the proposed control valve, a different valve should be used.



Figure 3.1 Control Valve Arrangement

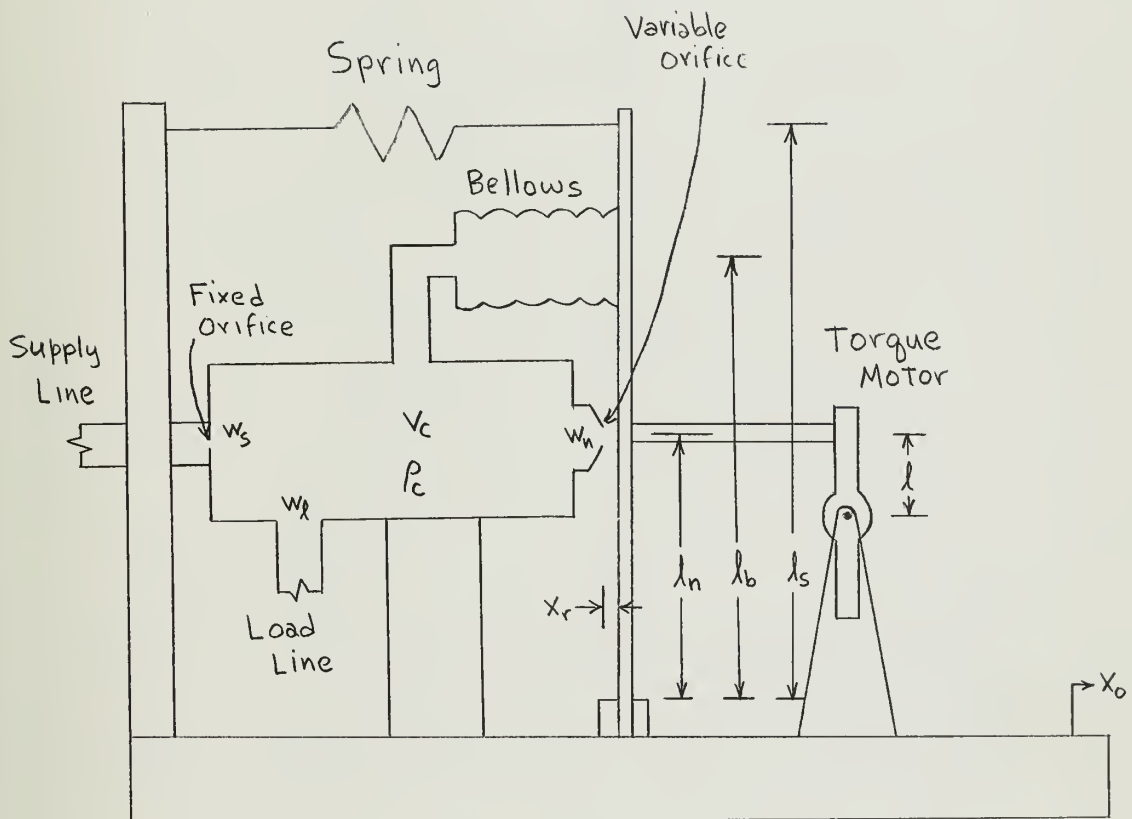






Figure 3.2 Flapper-Nozzle Control Volume

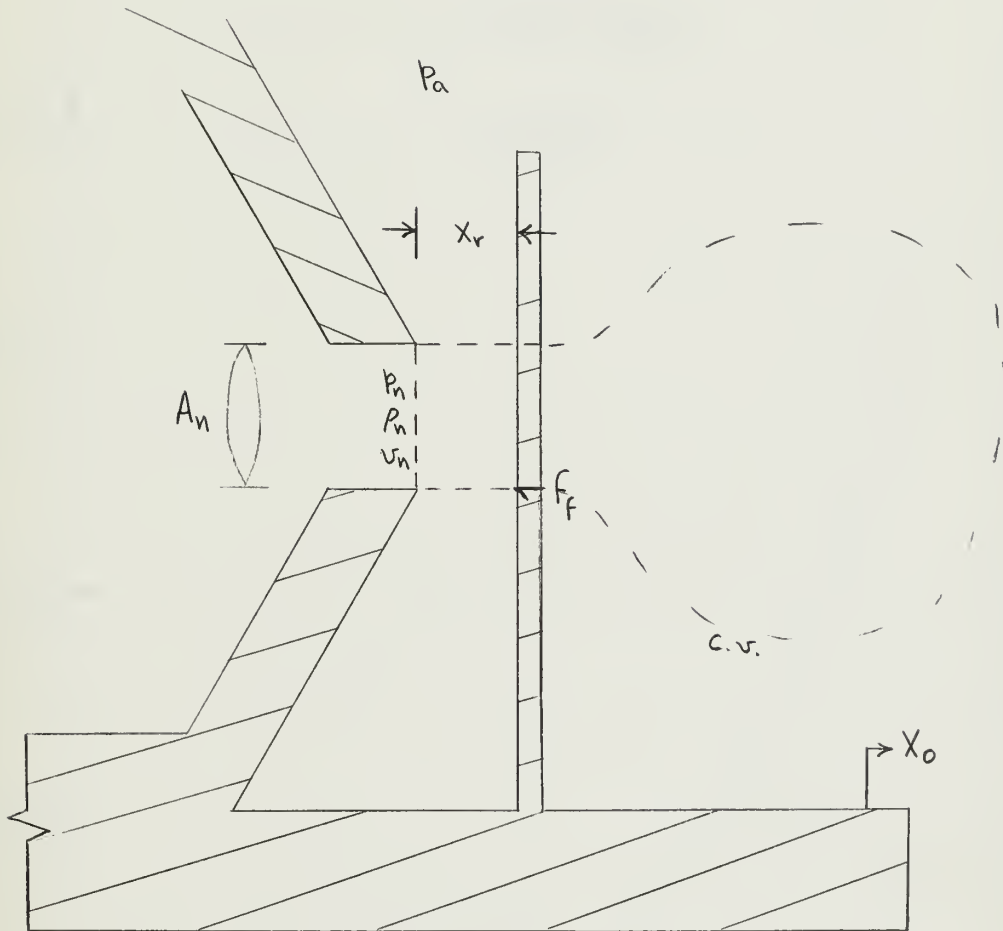




Figure 3.3 Nozzle Relation Approximation

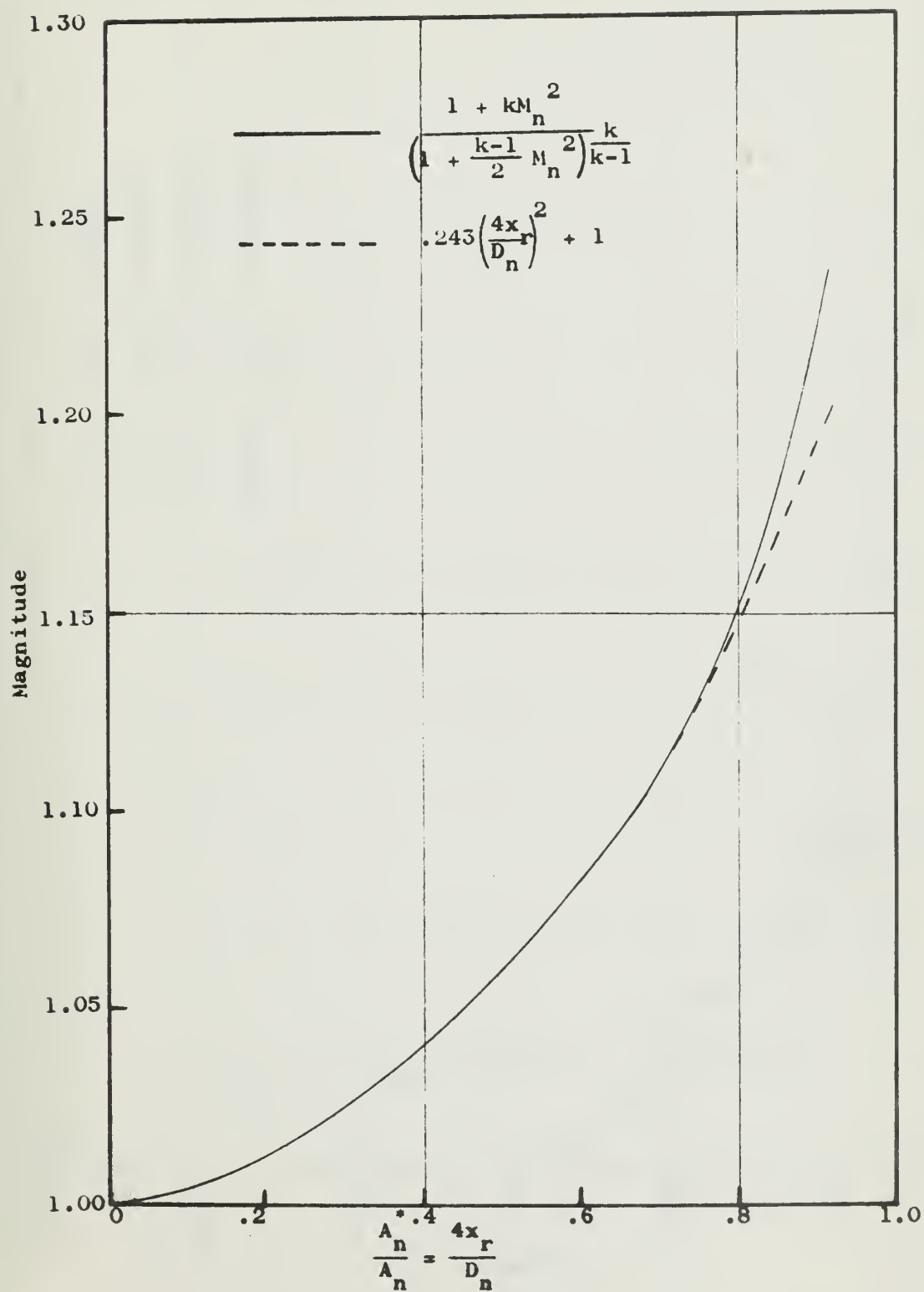




Figure 3.4 Valve Chamber Impedance as Seen by the Load Line

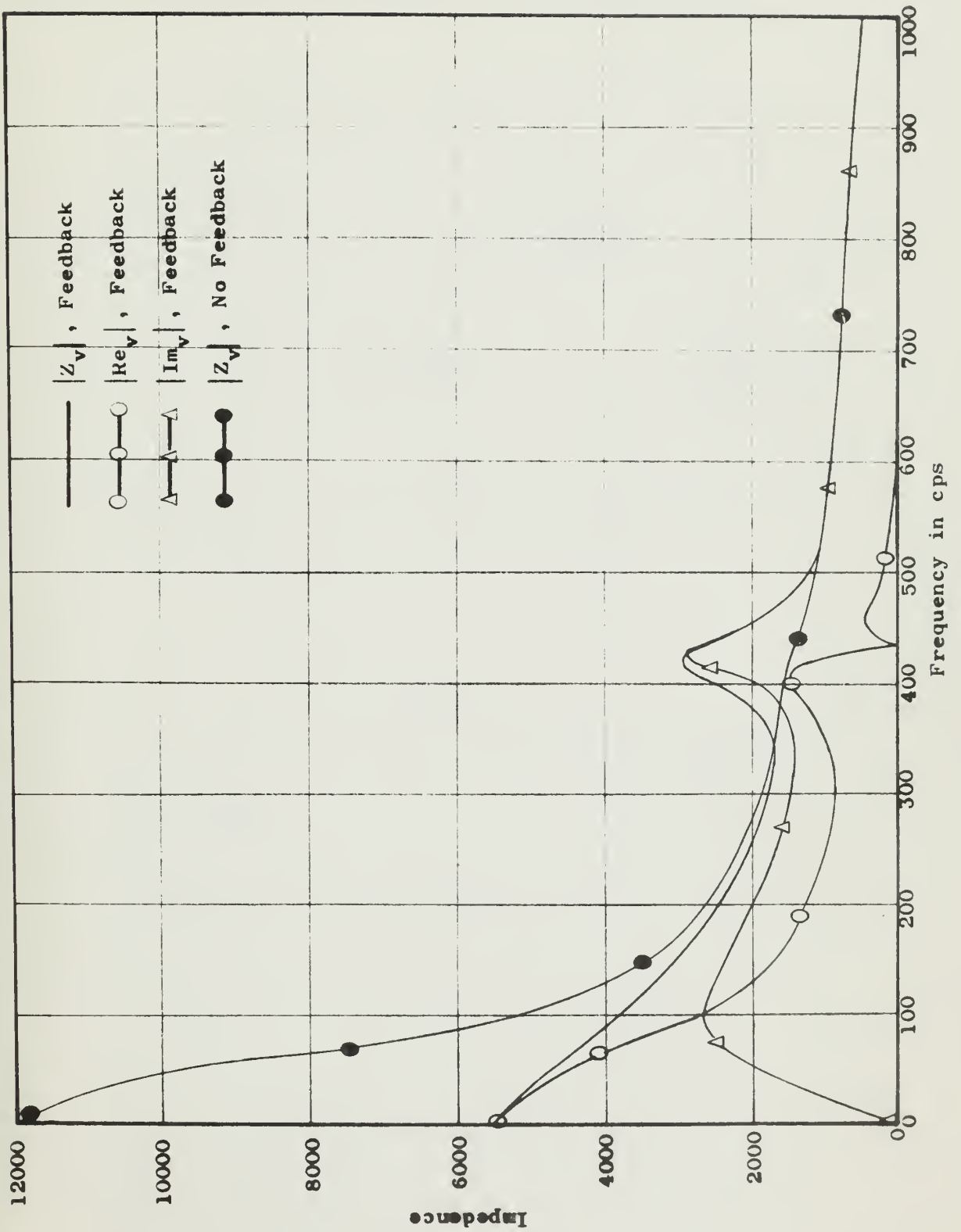




Figure 3.5 Lumped Parameter Model of Load Transmission Line

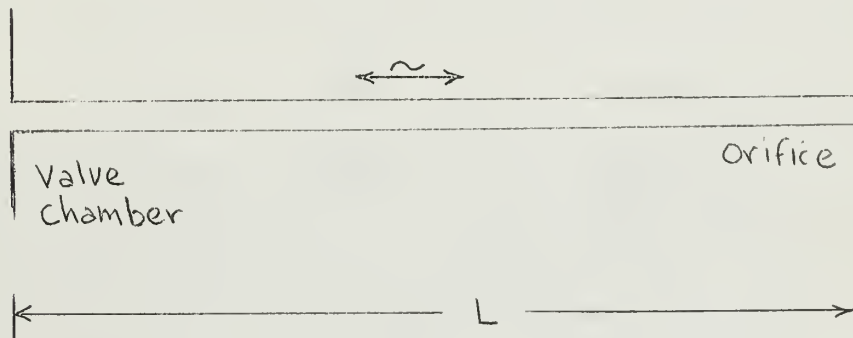
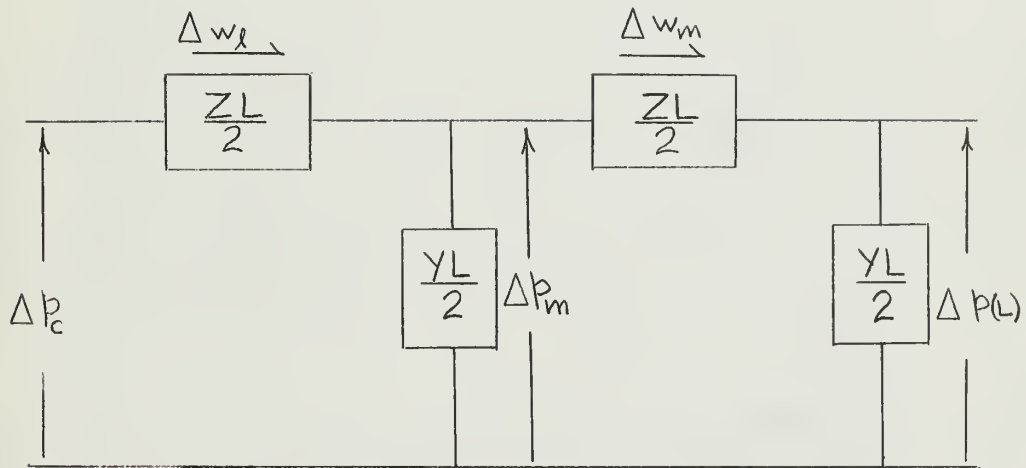






Figure 3.6 Analog Computer Operational Block Diagram

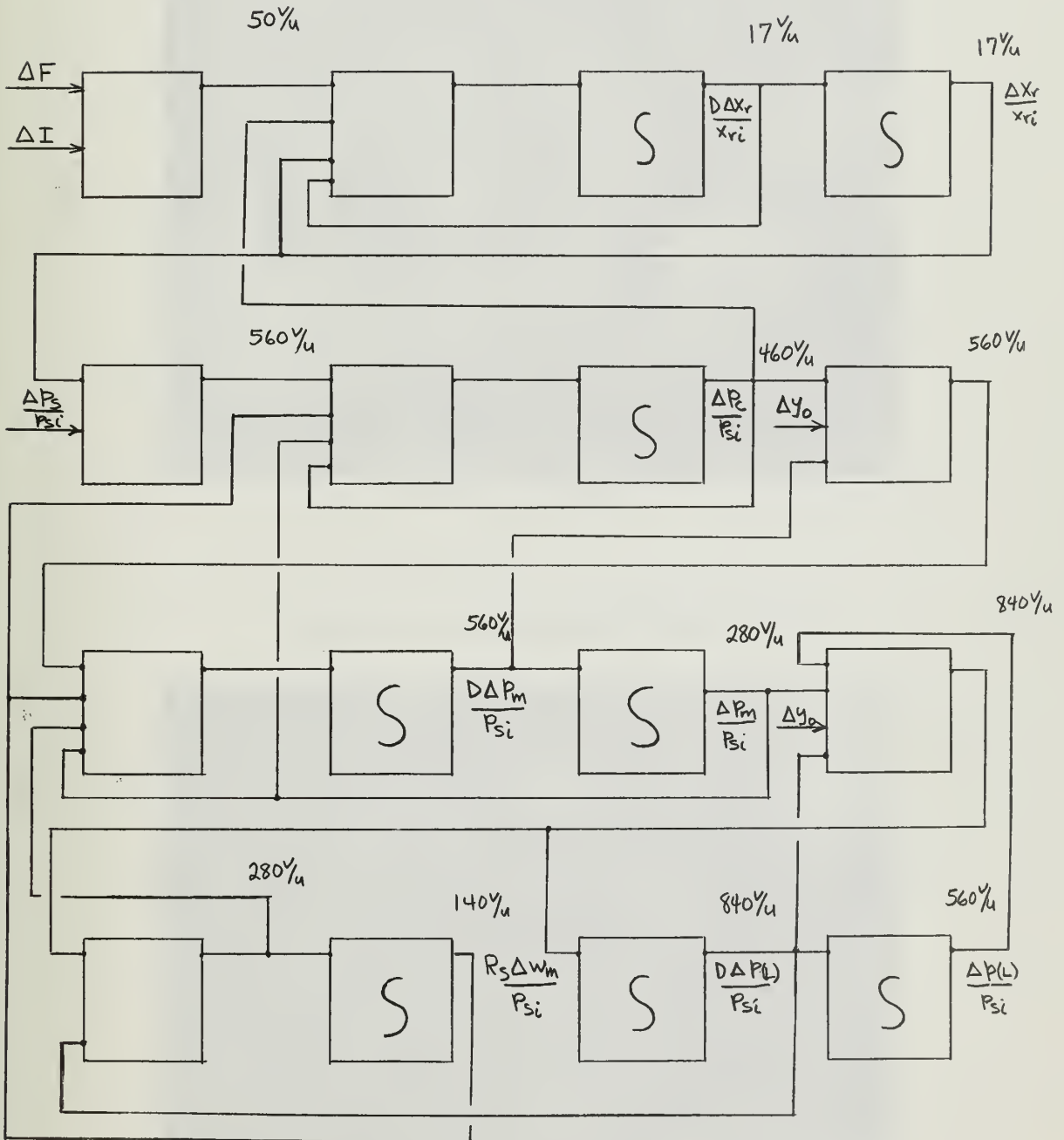




Figure 3.7 Flapper-Nozzle Control Valve

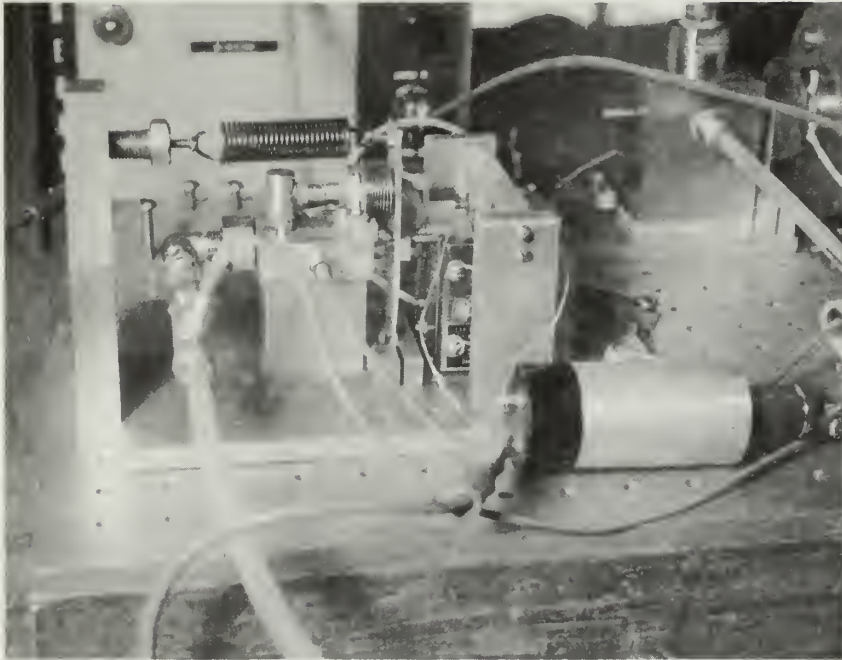


Figure 3.8 Experimental Setup

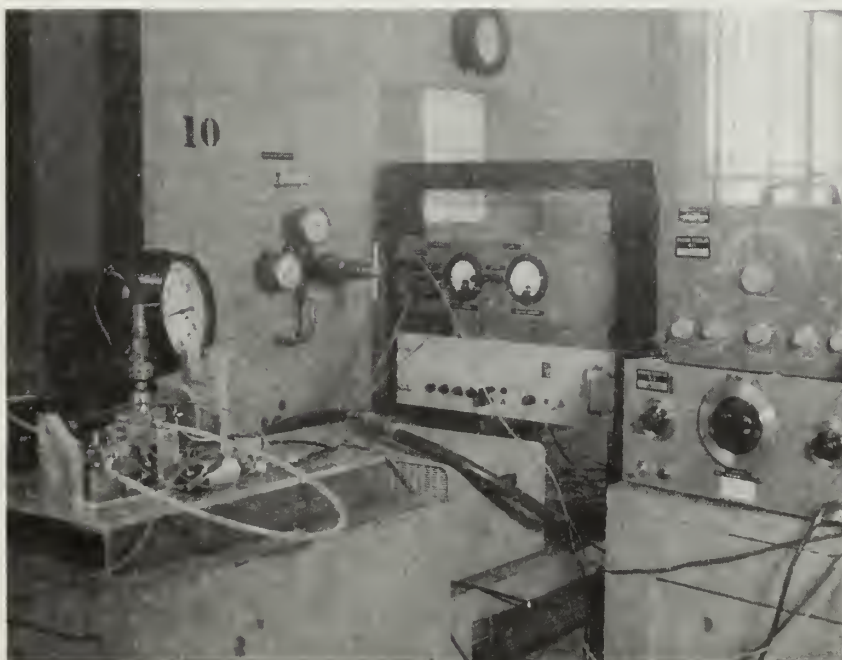




Figure 3.9 Chamber Pressure Frequency Response to Supply Line Noise

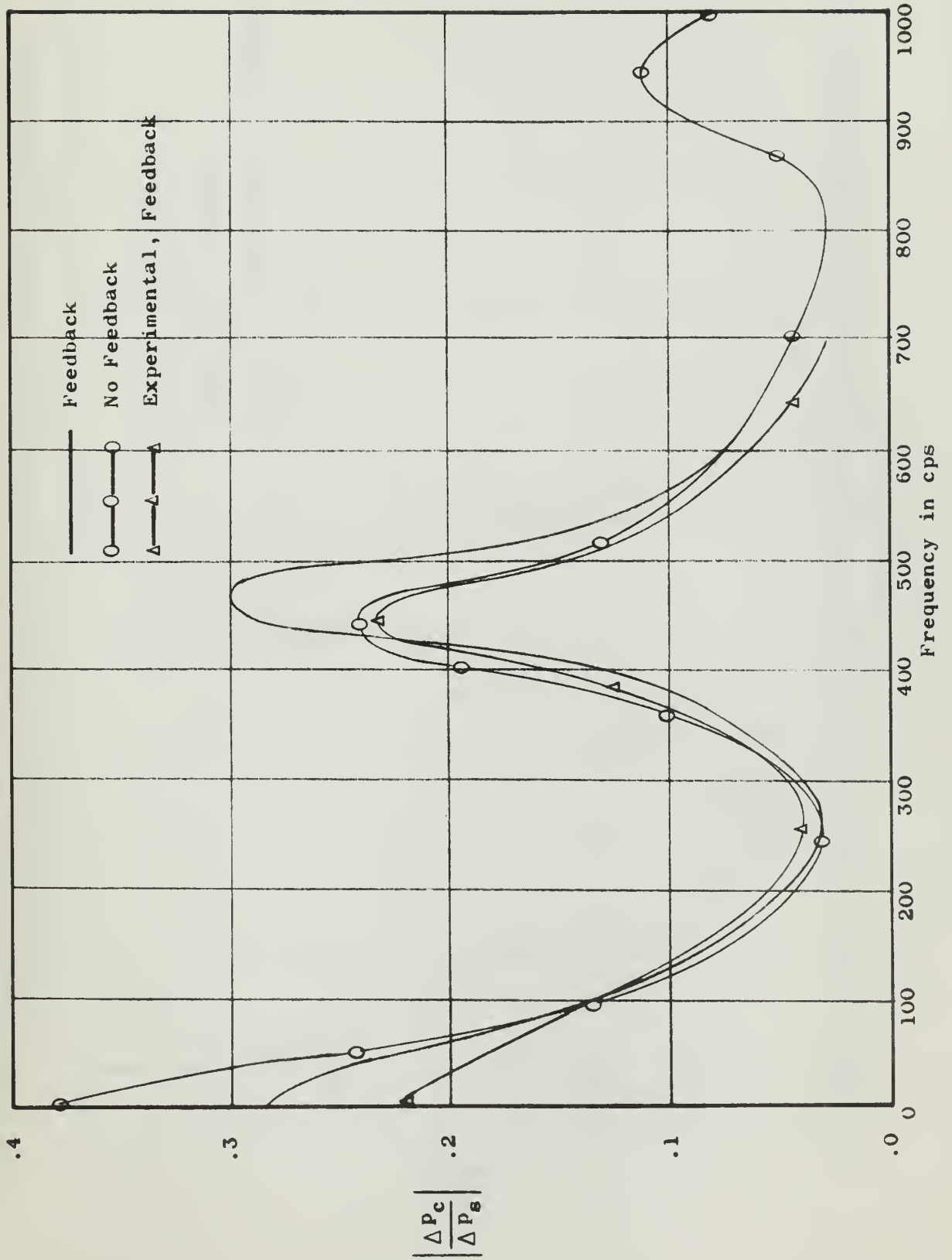




Figure 3.10 Chamber Pressure Frequency Response to Induced Flapper Motion

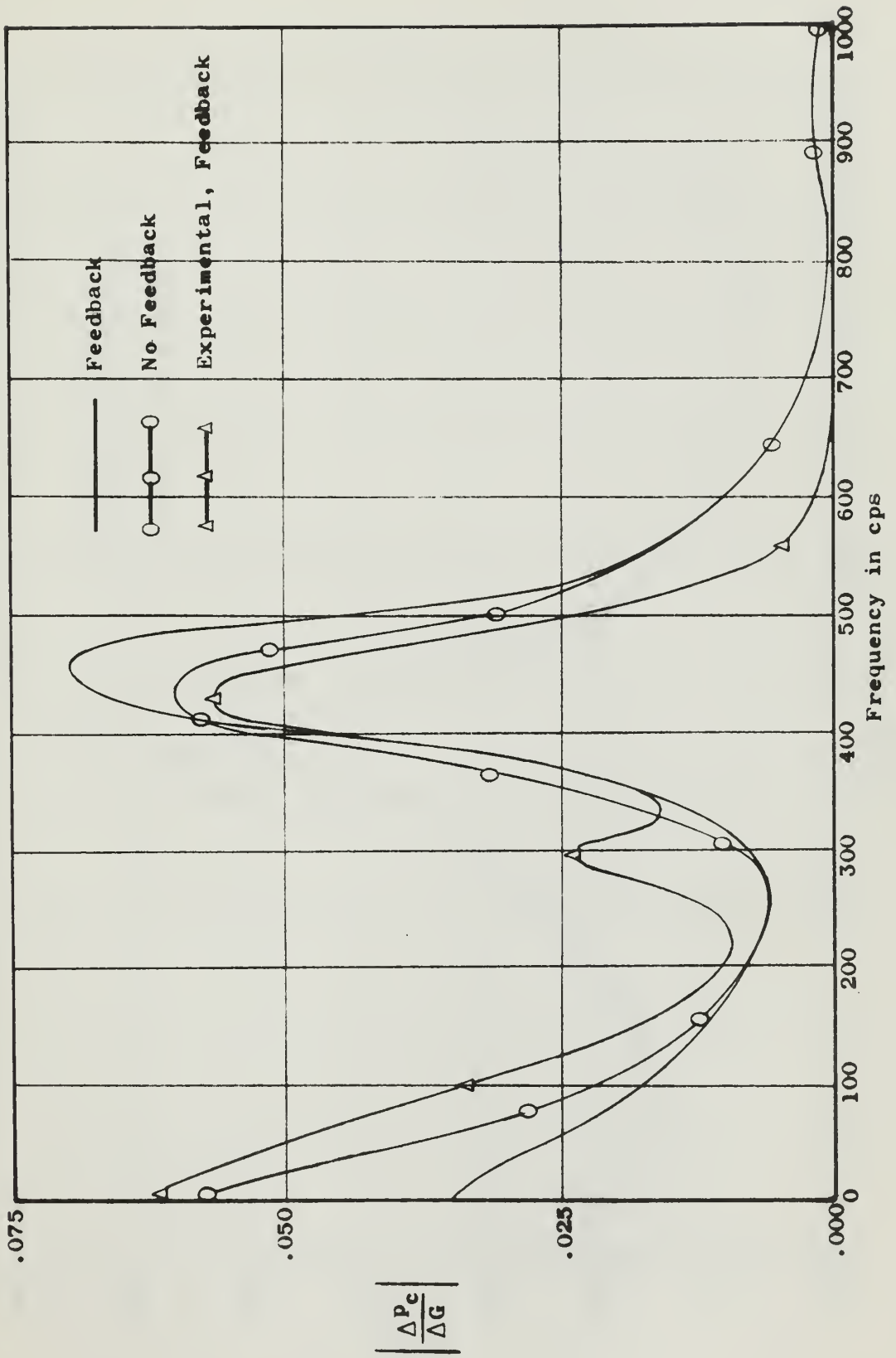
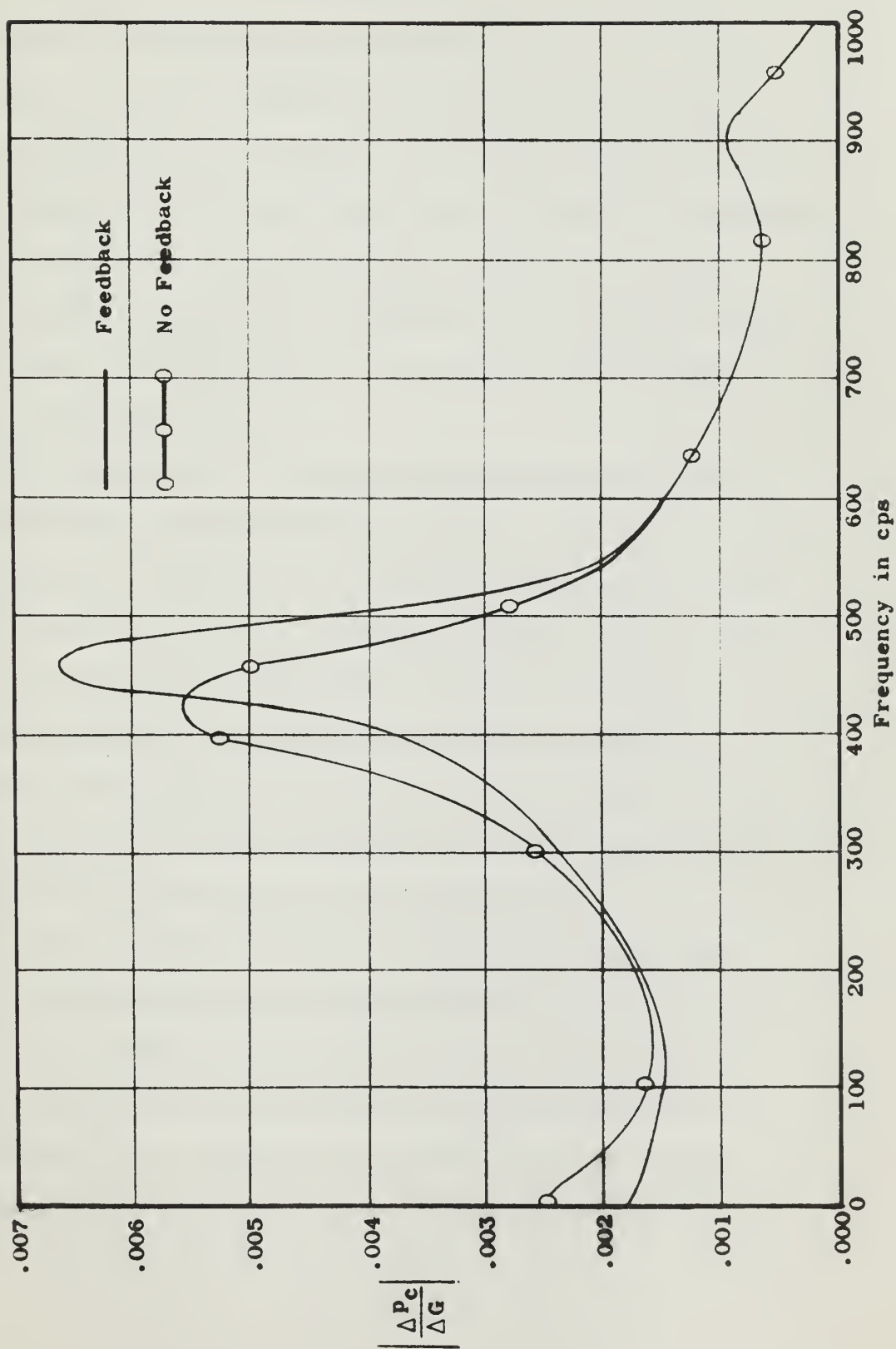






Figure 3.11 Chamber Pressure Frequency Response to Load Line Longitudinal Vibrations





#### 4. CONCLUSIONS

##### 4.1 VIBRATION INDUCED TRANSMISSION LINE NOISE

From the results of Chapter 2 it is concluded that piping subject to white noise environmental vibrations can excite resonant pressure peaks in the contained fluid over a wide band of frequencies. The pressures are caused by induced fluid flow at pipe boundary nonuniformities (bends and area changes) due to the relative motion of the piping. The peaks occur at the various fluid and piping resonant frequencies.

Either longitudinal or transverse piping support vibrations, or a combination, will cause induced pressures. In all cases it is the longitudinal motion at the end nonuniformities that forces the fluid. This is true even for transverse vibrations since the transverse pipe motion excites longitudinal vibrations of the ends at the pipe bending resonant frequencies and at double the resonant frequencies. Since pressures are induced for either type of vibration, a fluid piping system is susceptible to noise generation regardless of its orientation to the vibration field.

The level of induced pressure is proportional to the fluid density, the effective speed of sound in the fluid, and the amount of excitation. Resonant peak levels of .6 psi per g of longitudinal acceleration can be obtained at the lower frequencies for air at 200 psia mean pressure in one quarter inch copper tubing. Preliminary results show that correspondingly higher pressures can



be obtained with liquids due to their higher density. The pressures generated by the first several pipe resonant frequencies when subjected to transverse vibrations are comparable to the longitudinally excited case. However, levels due to transverse double resonant frequency excitation are less by about a factor of two.

Extremely high pressures can be excited when a fluid resonance coincides with that of the piping system. For a more complicated system it is impossible to distinguish between these two types of resonances, but there are still corresponding absolute system resonances that are higher than the others.

#### 4.2 CONTROL VALVE

For the one type of active element<sup>\*</sup> studied while in a vibrating environment, noise introduction into the valve takes place through the supply transmission line, induced motion of the flapper assembly, and for high pressure systems, through vibrations of the transmission line to the load. Since the valve transfer characteristic is that of a first order lag cascaded with a second order system, due to the capacitive chamber and flapper resonance respectively, the noise transfer functions are largest at the low frequencies up to the break frequency and again near the flapper resonant frequency.

---

<sup>\*</sup> A Pneumatic nozzle-flapper control valve.



Force feedback in the way of a bellows arrangement reduces the pressure levels at the lower frequencies. However, it also intensifies those near the flapper resonance. By increasing the feedback enough, it is possible to get amplification of the noise power for frequencies near the flapper resonance. That is to say that in any active element it is possible to convert some of the steady flow power entering the valve into noise power. This phenomenon does not occur in a passive element where signal amplification can take place, but not power amplification.





## 5. RECOMMENDATIONS

### 5.1 FUTURE WORK

Since the results of this study have shown that significant vibration induced pressures can be generated in a fluid control system, further work in this field is warranted. The most fruitful areas for future work are the following. First, it is recommended that extensive experimental work with transversely vibrating pipes be conducted in order to better understand the structural coupling between longitudinal and transverse motion. Data should be taken for various pipe end constraints and different support geometries. Secondly, different types of active elements should be analysed while operating in a vibrating environment. This should include pure fluid elements such as bistable and jet amplifiers, as well as systems with several stages of feedback and amplification. The results should be compared along with those for the flapper-nozzle valve to determine which elements are least susceptible to vibration induced noise. Further experimental work should also be conducted with the flapper-nozzle valve to verify that noise power amplification takes place. Lastly, it is recommended that parallel work be conducted for a hydraulic system. Preliminary work has shown that a liquid system will be even more susceptible to vibration induced noises.

### 5.2 APPLICATION

Information learned in this thesis can be applied in order to reduce a system's susceptibility to noise. Thus, it is recommended that all fluid equipment that will be exposed to strong environmental



vibrations be thoroughly tested before use. The system should be shock mounted if possible. Otherwise it should be mounted on stiff supports so that all resonant frequencies will be high. The transmission lines should also be secured at short intervals in order to decrease transverse vibrations. The installed system, empty of fluid, should then be vibration tested. High induced pressures can be expected at any frequency where strong structural resonances exist. Lastly, the fluid amplifiers should be carefully tested in order to pick those with good transmission characteristics that will not cause noise amplification.



APPENDIX

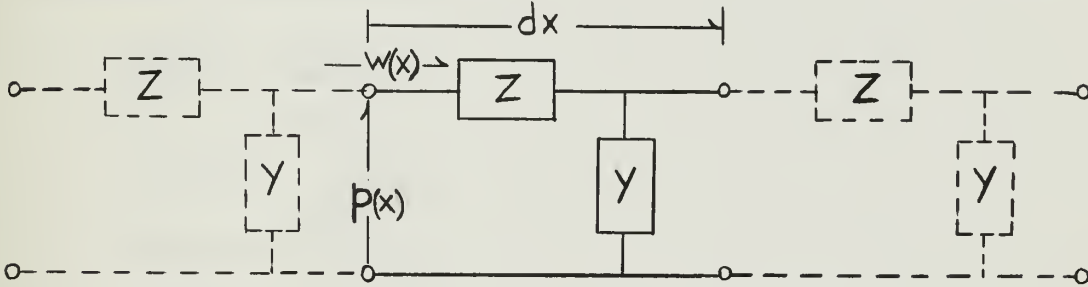


## APPENDIX A

### TRANSMISSION MATRICES

#### A.1 TRANSMISSION MATRIX DEVELOPMENT

A model for a uniform, one-dimensional, distributed system is,\*



where  $Z$  is the series impedance per unit length, and  $Y$  is the shunt admittance. Either or both can contain the operation  $D \equiv \frac{\partial}{\partial t}$ .

Using pressure,  $p$ , and mass flow rate,  $w$ , as variables (force and displacement for pipes) the relations for a micro-element become,

$$\frac{dp}{dx} = -Zw$$

$$\frac{dw}{dx} = -Yp \quad **$$

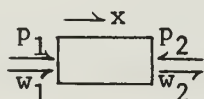
(A.1-1)

or

$$\frac{d}{dx} \begin{bmatrix} p(x) \\ w(x) \end{bmatrix} = - \begin{bmatrix} 0 & Z \\ Y & 0 \end{bmatrix} \begin{bmatrix} p(x) \\ w(x) \end{bmatrix}$$

\* References [15] and [21] give extensive developments containing the material covered in section A.1.

\*\* When working with mechanical and fluid systems, this form of the equations is obtained when the pressure or force variable is taken as compressive and the mass flow rate or displacement variable is taken in the direction of  $x$ . i.e.







Ordinary differential equations are written instead of partial because time is contained in the operator D in the system parameters.

Writing the above matrix equation in compressed form and using matrix algebra, one finds that

$$\frac{d\mathbb{S}(x)}{dx} = -A\mathbb{S}(x)$$

$$\mathbb{S}(x_2) = e^{-Ax_2} \mathbb{C}_0$$

$$\mathbb{S}(x_1) = e^{-Ax_1} \mathbb{C}_0$$

and

$$\mathbb{C}_0 = e^{Ax_2} \mathbb{S}(x_2).$$

Therefore

$$\mathbb{S}(x_1) = e^{A(x_2 - x_1)} \mathbb{S}(x_2) \quad (A.1-2)$$

where  $\mathbb{C}_0$  is the integration constant matrix.

The transmission matrix can be expanded into,\*

$$e^{A(x_2 - x_1)} = \begin{bmatrix} \cosh \gamma(x_2 - x_1) & Z_c \sinh \gamma(x_2 - x_1) \\ \frac{1}{Z_c} \sinh \gamma(x_2 - x_1) & \cosh \gamma(x_2 - x_1) \end{bmatrix}$$

where  $Z_c \equiv \sqrt{Z/Y}$  is defined as the characteristic impedance and

$\gamma \equiv \sqrt{YZ}$  as the propagation operator.

The final expression becomes,

$$\begin{bmatrix} p(x_1) \\ w(x_1) \end{bmatrix} = \begin{bmatrix} \cosh \gamma(x_2 - x_1) & Z_c \sinh \gamma(x_2 - x_1) \\ \frac{1}{Z_c} \sinh \gamma(x_2 - x_1) & \cosh \gamma(x_2 - x_1) \end{bmatrix} \begin{bmatrix} p(x_2) \\ w(x_2) \end{bmatrix}.$$

(A.1-3)

---

\*This can be done by using either the Cayley Hamilton or Sylvester theorems [22].



This transmission matrix is applicable to any uniform, one-dimensional, linear, distributed system of two variables. When working with piping,  $p$  and  $w$  are replaced by  $f$ , force, and  $\xi$ , displacement, respectively.

## A.2 TRANSMISSION MATRIX USING RELATIVE FLOW OR DISPLACEMENT VARIABLES

There are times when working with a system mounted on a vibrating platform when it is more convenient to use flow or displacement variables relative to the platform motion. Thus for distributed fluid and mechanical systems the relations have the form

$$\begin{aligned}\frac{dp}{dx} &= -Zw_r - Zw_o \\ \frac{dw_r}{dx} &= -Yp\end{aligned}\tag{A.2-1}$$

since  $w(x) = w_r(x) + w_o$ . The  $r$  and  $o$  stand for relative to the platform and platform respectively. The platform is rigid so that its motion is independent of position.

Using matrix algebra one obtains from

$$\frac{d}{dx} \begin{bmatrix} p(x) \\ w_r(x) \end{bmatrix} = - \begin{bmatrix} 0 & Z \\ Y & 0 \end{bmatrix} \begin{bmatrix} p(x) \\ w_r(x) \end{bmatrix} + \begin{bmatrix} -Zw_o \\ 0 \end{bmatrix}$$

that

$$\begin{aligned}\frac{d \mathcal{S}(x)}{dx} &= -A \mathcal{S}(x) + C \\ \mathcal{S}(x_2) &= e^{-A x_2} C_o + A^{-1} C \\ \mathcal{S}(x_1) &= e^{-A x_1} C_o + A^{-1} C\end{aligned}$$



and

$$\mathbb{C}_0 = e^{A x_2} \mathbb{S}_{(x_2)} - e^{A x_2} A^{-1} \mathbb{C}.$$

Therefore

$$\mathbb{S}_{(x_1)} = e^{A(x_2 - x_1)} \mathbb{S}_{(x_2)} + \left[ \mathbb{I} - e^{A(x_2 - x_1)} \right] A^{-1} \mathbb{C}. \quad (\text{A.2-2})$$

Now since

$$A^{-1} = \begin{bmatrix} 0 & 1/\gamma \\ 1/Z & 0 \end{bmatrix} \quad \text{and} \quad \mathbb{C} = \begin{bmatrix} -Z w_0 \\ 0 \end{bmatrix}$$

the final expression becomes,

$$\begin{bmatrix} p(x_1) \\ w_r(x_1) \end{bmatrix} = \begin{bmatrix} \cosh \gamma(x_2 - x_1) & Z_c \sinh \gamma(x_2 - x_1) \\ 1/Z_c \sinh \gamma(x_2 - x_1) & \cosh \gamma(x_2 - x_1) \end{bmatrix} \begin{bmatrix} p(x_2) \\ w_r(x_2) \end{bmatrix} + \begin{bmatrix} Z_c \sinh \gamma(x_2 - x_1) w_0 \\ [\cosh \gamma(x_2 - x_1) - 1] w_0 \end{bmatrix}. \quad (\text{A.2-3})$$

It is to be noted that Eq. (A.2-3) can be obtained more directly by substituting the expression  $w(x) = w_r(x) + w_0$  into Eq. (A.1-3). This method is not recommended, however, for more complicated systems involving matrices of higher order. In those cases, application of Eq. (A.2-2) will be more profitable.

### A.3 TRANSMISSION MATRIX WITH TRANSPORT

By introducing wave-scattering variables one can find a good approximate form of the transmission matrix when there is transport

\*For a comprehensive presentation of wave-scattering variables see Paynter [15], pp. 268-271, and Brown [21].



present. This would be useful for cases of mean flow in fluid lines.

Wave-scattering variables can be obtained from the previous expression

$\frac{d\mathcal{S}}{dx} = -A\mathcal{S}$  by obtaining the canonical form of the differential equation by diagonalizing  $A$ . Thus, premultiplying by  $M^{-1}$  gives

$$\frac{d}{dx} M^{-1} \mathcal{S} = - M^{-1} A M M^{-1} \mathcal{S}.$$

Defining  $\mathcal{S}'$  as  $\mathcal{S}' = M^{-1} \mathcal{S}$

leaves  $M^{-1} A M$  as the desired diagonal matrix.

Therefore, for a two variable system,

$$M = \frac{1}{\sqrt{2}} \begin{bmatrix} \sqrt{Z_c} & \sqrt{Z_c} \\ 1/\sqrt{Z_c} & -1/\sqrt{Z_c} \end{bmatrix},$$

$$M^{-1} = \frac{1}{\sqrt{2}} \begin{bmatrix} 1/\sqrt{Z_c} \sqrt{Z_c} \\ 1/\sqrt{Z_c} - \sqrt{Z_c} \end{bmatrix},$$

and

$$\begin{bmatrix} u(x_1) \\ v(x_1) \end{bmatrix} = \begin{bmatrix} e^{\gamma(x_2-x_1)} & 0 \\ 0 & e^{-\gamma(x_2-x_1)} \end{bmatrix} \begin{bmatrix} u(x_2) \\ v(x_2) \end{bmatrix} \quad (\text{A.3-1})$$

since

$$\mathcal{S}'_{(x_1)} = M^{-1} e^{A(x_2-x_1)} M \mathcal{S}'_{(x_2)}$$

and

$$\begin{bmatrix} u(x) \\ v(x) \end{bmatrix} = \mathcal{S}'_{(x)} = M^{-1} \mathcal{S}_{(x)}.$$





For a wavelike transmission line, i.e. fluid line, Eq. (A.3-1) becomes,

$$\begin{bmatrix} u(x_1) \\ v(x_1) \end{bmatrix} = \begin{bmatrix} e^{TD} & 0 \\ 0 & e^{-TD} \end{bmatrix} \begin{bmatrix} u(x_2) \\ v(x_2) \end{bmatrix} \quad (\text{A.3-2})$$

where  $T$  is the wave propagation time between points 1 and 2 and is equal to  $\frac{x_2 - x_1}{c}$  where  $c$  is some characteristic velocity of the wave propagation. When one looks closer it is seen that the scattering matrix contains only a pure time delay and a pure advance operator. Thus writing Eq. (A.3-2) in the time domain it becomes,

$$\begin{aligned} u_2(t) &= u_1(t-T) \\ v_1(t) &= v_2(t-T). \end{aligned}$$

This means that  $u$  is a rightward traveling wave and  $v$  is a leftward traveling wave

$$\begin{array}{ccc} \xrightarrow{u_1} & & \xrightarrow{u_2} \\ \hline \xleftarrow{v_1} & & \xleftarrow{v_2} \end{array}$$

as  $u_2$  is  $u_1$  delayed by  $T$ , and  $v_1$  is  $v_2$  delayed by  $T$ .

Now if one introduces a mean transport velocity  $V$ ,

$$\begin{array}{ccc} \xrightarrow{u_1} & \xrightarrow{V} & \xrightarrow{u_2} \\ \hline \xleftarrow{v_1} & & \xleftarrow{v_2} \end{array}$$

the propagation times will be different for the two directions. For the rightward traveling wave,  $T_r = \frac{x_2 - x_1}{c + V}$ , and for the leftward traveling wave,  $T_l = \frac{x_2 - x_1}{c - V}$ . Now Eq. (A.3-2) becomes



$$\begin{bmatrix} u(x_1) \\ v(x_1) \end{bmatrix} = \begin{bmatrix} e^{T_r D} & 0 \\ 0 & e^{-T_\ell D} \end{bmatrix} \begin{bmatrix} u(x_2) \\ v(x_2) \end{bmatrix},$$

and transforming back to the  $\mathcal{S}$  variables it becomes,

$$\begin{bmatrix} p(x_1) \\ w(x_1) \end{bmatrix} = \frac{1}{2} \begin{bmatrix} \sqrt{Z_c} & \sqrt{Z_c} \\ 1/\sqrt{Z_c} & -1/\sqrt{Z_c} \end{bmatrix} \begin{bmatrix} e^{T_r D} & 0 \\ 0 & e^{-T_\ell D} \end{bmatrix} \begin{bmatrix} 1/\sqrt{Z_c} & \sqrt{Z_c} \\ 1/\sqrt{Z_c} & -\sqrt{Z_c} \end{bmatrix} \begin{bmatrix} p(x_2) \\ w(x_2) \end{bmatrix}.$$

Multiplying gives

$$\begin{bmatrix} p(x_1) \\ w(x_1) \end{bmatrix} = \frac{1}{2} \begin{bmatrix} e^{T_r D} + e^{-T_\ell D} & Z_c (e^{T_r D} - e^{-T_\ell D}) \\ 1/Z_c (e^{T_r D} - e^{-T_\ell D}) & e^{T_r D} + e^{-T_\ell D} \end{bmatrix} \begin{bmatrix} r(x_2) \\ w(x_1) \end{bmatrix}.$$

Now one can make the approximations that

$$T_r = \frac{x_2 - x_1}{c + v} = \frac{x_2 - x_1}{c(1 + \frac{v}{c})} \approx \frac{x_2 - x_1}{c} (1 - \frac{v}{c})$$

and

$$T_\ell = \frac{x_2 - x_1}{c - v} = \frac{x_2 - x_1}{c(1 - \frac{v}{c})} \approx \frac{x_2 - x_1}{c} (1 + \frac{v}{c})$$

since  $\frac{v}{c} \ll 1$  for all cases where the above analysis holds.

Substituting these relations back into the expression gives,

$$\begin{bmatrix} p(x_1) \\ w(x_1) \end{bmatrix} = e^{\frac{-v(x_2 - x_1)D}{c^2}} \begin{bmatrix} \cosh \gamma(x_2 - x_1) & Z_c \sinh \gamma(x_2 - x_1) \\ 1/Z_c \sinh \gamma(x_2 - x_1) & \cosh \gamma(x_2 - x_1) \end{bmatrix} \begin{bmatrix} p(x_2) \\ w(x_2) \end{bmatrix}.$$

(A.3-3)



Thus it can be seen that transport merely introduces a multiplicative factor and that Eq. (A.3-3) approaches Eq. (A.1-3) as  $V \rightarrow 0$ .

When the equations are written in terms of a relative flow or displacement variables one obtains,

$$\begin{aligned} \begin{bmatrix} p(x_1) \\ w_r(x_1) \end{bmatrix} &= e^{\frac{-V(x_2-x_1)D}{c^2}} \left\{ \begin{bmatrix} \cosh \gamma(x_2-x_1) & Z_c \sinh \gamma(x_2-x_1) \\ 1/Z_c \sinh \gamma(x_2-x_1) & \cosh \gamma(x_2-x_1) \end{bmatrix} \begin{bmatrix} p(x_2) \\ w_r(x_2) \end{bmatrix} \right. \\ &\quad \left. + \begin{bmatrix} Z_c \sinh \gamma(x_2-x_1) w_o \\ \left[ \cosh \gamma(x_2-x_1) - e^{\frac{V(x_2-x_1)D}{c^2}} \right] w_o \end{bmatrix} \right\} \quad (A.3-4) \end{aligned}$$

In this case one of the internal terms is altered slightly. Yet this also approaches its corresponding no transport equation, Eq. (A.2-3), as  $V \rightarrow 0$ .



## APPENDIX B

### UNSTEADY MOMENTUM TERM EVALUATION

#### B.1 APPROXIMATE SOLUTION

A simple one-dimensional flow solution can be integrated over the volume between the nozzle and flapper in order to obtain an approximate value for the integral,

$$\frac{\partial}{\partial t} \iiint_{c.v.} \frac{v_x r^{\rho}}{g_o} dV.$$

This is done by assuming that the one-dimensional flow lines are always perpendicular to the slant areas of the right circular and truncated cones into which the volume can be divided, Fig. B.1.

The integration of this volume is done in two parts. The first includes the circular cone volume elements starting at the nozzle opening, and the second consists of the truncated cone elements which end at the curtain area. Dividing the problem this way gives an exact integration of the volume for the first part and a close approximation for the second.

Beginning with the cones, let  $A_s = \pi s R$  be their slant areas where  $R$  is the radius and  $s$  is the slant distance. Then an element of volume is

$$dV = \frac{A_s s d\theta}{3}$$

where  $\frac{1}{3}$  is the factor for a cone, and  $\theta$  is defined in the Figure.

It is also seen that





$$s = \frac{R}{\cos \theta} .$$

Thus, since  $\rho = \frac{w_r}{v_r A_s}$ , these expressions can be put into the first part of the integral to give

$$\begin{aligned} \frac{\partial}{\partial t} \iiint_{(1)} \frac{v_{xr} \rho}{g_o} dV &= \frac{\partial}{\partial t} \int_0^{\theta_0} \frac{v_r \cos \theta w_r A_s R d\theta}{g_o v_r A_s^3 \cos \theta} \\ &= \frac{\partial}{\partial t} \int_0^{\theta_0} \frac{w_r R d\theta}{3 g_o} , \end{aligned}$$

where  $\theta_0 = \tan^{-1} \frac{x_r}{R}$ . Integrating then gives

$$\begin{aligned} \frac{\partial}{\partial t} \int_0^{\theta_0} \frac{w_r R d\theta}{3 g_o} &= \frac{R}{3} \frac{\partial}{\partial t} \frac{w_r \tan^{-1} \frac{x_r}{R}}{g_o} \\ &\approx \frac{1}{3} \frac{\partial}{\partial t} \frac{w_r x_r}{g_o} \end{aligned}$$

since  $\frac{x_r}{R}$  is small and  $\tan^{-1} \frac{x_r}{R} \approx \frac{x_r}{R}$ .

For the truncated cone elements,  $A_s = \pi s(R+r)$  is the slant area and  $r$  is the radius defined in the Figure. An element of volume is then once again

$$dV = \frac{A_s s d\theta}{3}$$

where  $s = \frac{x_r}{\sin \theta}$ .

Thus the remaining part of the integral becomes,

$$\frac{\partial}{\partial t} \iiint_{(2)} \frac{v_{xr} \rho dV}{g_o} = \frac{\partial}{\partial t} \int_{\theta_0}^{\frac{\pi}{2}} \frac{v_r \cos \theta w_r A_s x_r}{g_o v_r A_s \sin \theta} d\theta$$



$$= \frac{\partial}{\partial t} \int_{\theta_0}^{\frac{\pi}{2}} \frac{w_r x_r \cot \theta}{3 g_o} d\theta .$$

Integrating, one obtains,

$$\begin{aligned} \frac{\partial}{\partial t} \int_{\theta_0}^{\frac{\pi}{2}} \frac{w_r x_r \cot \theta}{3 g_o} d\theta &= \frac{\partial}{\partial t} \left( - \frac{w_r x_r}{3} \frac{\ln \sin \theta}{g_o} \right) \\ &= - \frac{1}{3} \frac{\partial}{\partial t} \left( \frac{w_r x_r}{g_o} \ln \frac{x_r}{\sqrt{x_r^2 + R^2}} \right) . \end{aligned}$$

Since  $\frac{x_r}{R}$  is usually about .1 to .3, this expression can be approximated by  $\frac{1}{3} \frac{\partial}{\partial t} \left( \frac{w_r x_r}{g_o} \right)$ , being  $\ln \frac{x_r}{\sqrt{x_r^2 + R^2}} \approx -1$ .

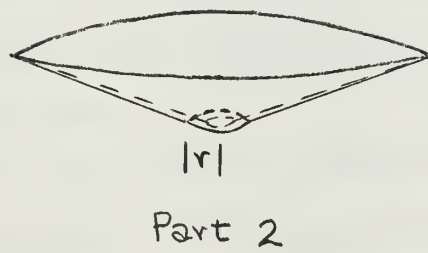
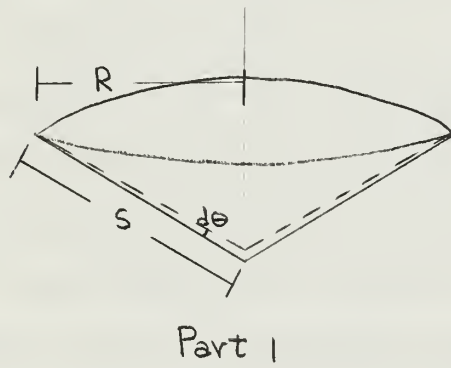
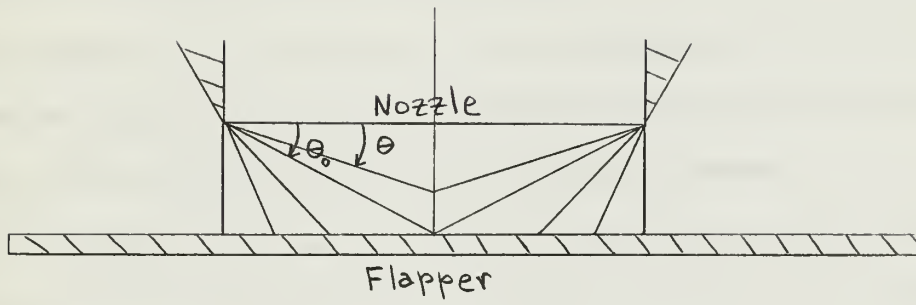
Therefore, adding the two parts of the integral together gives

$$\begin{aligned} \frac{\partial}{\partial t} \iiint_{c.v.} \frac{v_{xr} \rho dV}{g_o} &= \frac{\partial}{\partial t} \iiint_{(1)} \frac{v_{xr} \rho dV}{g_o} + \frac{\partial}{\partial t} \iiint_{(2)} \frac{v_{xr} \rho dV}{g_o} \\ &\approx \frac{\partial}{\partial t} \left( \frac{2}{3} \frac{x_r w_n}{g_o} \right) , \end{aligned}$$

since the relative flow through any slant area is equal to the flow into the nozzle, or  $w_r = w_n$ .



Figure B.1 Elemental Volumes





## APPENDIX C

### COMMENTS ON EXPERIMENTAL PROCEDURES AND INSTRUMENTATION

#### C.1 TRANSMISSION LINE NOISE EXPERIMENTATION

In Chapter 2, the physical set up for experimentally determining the induced pressures in vibrating pipes was described and figures provided. This Appendix contains some additional comments.

While taking data it was necessary to secure the pressure transducer to a nonvibrating support due to the sensitivity of the transducer to vibrations. This was accomplished by having the copper tube terminate in a flexible section of poly-flow tubing which could then be secured. The other end of the piping was attached to the constant pressure reservoir in the same manner.

The vibration generator was made from a 35 watt speaker unit with the cone removed. Extra care was necessary with alignment in order to keep the coil from rubbing while it was in operation. This speaker unit made a very satisfactory vibration shaker that responded well to input signals from both a sinusoidal oscillator and a random noise generator. These input signals were preamplified by a regular high fidelity amplifier before being fed to the shaker. It was necessary to monitor the current going to the shaker coil in order to keep from burning it out.

The mean test pressure level was maintained by use of a regulator reducer that was fed from a high pressure air line. Any fluctuations were damped out by the constant pressure reservoir. A globe valve was installed upstream of the reservoir in order to bleed down the system.





The pressures and accelerations were picked up with Kistler, Model 601-A and Endevco, Model 2215 piezoelectric transducers respectively. The signals then went through buffer amplifiers to the oscilloscope and analyser and recorder. The frequency analyser and level recorder were Brüel and Kjaer, Type 2107 and Type 2305 respectively. This equipment automatically swept through the frequency range with a 6% filter bandwidth and recorded the mean square levels. Averaging time was controlled by the paper feed rate in the recorder.

## C.2 CONTROL VALVE NOISE EXPERIMENTATION

The flapper-nozzle valve built for experimental purposes had a chamber volume of .1 cubic inches. The nozzle diameter was .116 inches while those of the supply and load orifices were .086 and .116 inches respectively. The valve was designed to operate at 100 psia mean supply pressure and with a steady state flapper displacement of .005 inches.

The flapper displacement was controlled by a Midwestern, Type 11 F torque motor that operated from a 300 volt d.c. American Measurement and Control servo amplifier, Model 652. The flapper displacement was measured by using a Decker Unit, Type 902-1. This capacitive pickup had the advantage of not imposing any unwanted force on the flapper.

Pressure measurements were obtained with the same piezoelectric transducers previously mentioned. Readings could be taken in the valve chamber and just upstream of the supply orifice. The supply air was



provided through another flapper-nozzle valve whose load was the test valve. In order to maintain this mean supply pressure at 100 psia, it was necessary to operate the first valve supply pressure at 467 psia due to the large mass flow rate required by the test valve.

Data analysis was accomplished with the same equipment mentioned in the previous section.



BIBLIOGRAPHY

1. Blackburn, J.F., Reethof, G., and Shearer, J.L., Fluid Power Control, M.I.T. Press, Cambridge, 1960.
2. Lee, S.-Y. and Blackburn, J.F., "Contribution to Hydraulic Control, 1-Axial Forces on Control-Valve Pistons", Transactions ASME, Vol. 74, August 1952.
3. Lee, S.-Y. and Blackburn, J.F., "Contributions to Hydraulic Control, 2-Transient-Flow Forces and Valve Instability", Transactions ASME, Vol. 74, August 1952.
4. Frederiksen, E., "Pulsating Air Flow in Pipe Systems", (In Danish with English summary) I Kommission hos Teknisk Forlag, Kobenhavn, 1954.
5. Ezekiel, F.D., "Effect of a Hydraulic Conduit with Distributed Parameters on Control-Valve Stability", Sc.D. Thesis, M.I.T. June 1955.
6. Brown, F.T., "The Transient Response of Fluid Lines", Journal of Basic Engineering, Transactions ASME Series D. Vol. 84, December 1962.
7. D'Souza, A.F., and Oldenburger, R., "Dynamic Response of Fluid Lines", Journal of Basic Engineering, Transactions ASME Series D, Vol. 86, September 1964.
8. Silberman, E., "The Effect of Tube Vibrations on Flow Through Tubes", University of Minnesota, St. Anthony Falls Hydraulic Laboratory, Project Report No. 27, November 1951.
9. Lipner, N. and Fay, F.B., "Acoustic Waves Generated by the Motion of Piping Containing a Fluid", Shock and Vibration Bulletin Part III, U.S. Naval Research Laboratory, January 1966.



10. Noiseux, D.V., Dietrich, C.W., Eichler, E., and Lyon, R.H., "Random Vibration Studies of Coupled Structures in Electronic Equipments", Bolt Beranek and Newman, Inc., Report No. 1061, October 1963.
11. Smith, P.W., Jr. and Lyon, R.H., "Sound and Structural Vibrations", NASA Report CR-160, March 1965.
12. Crandall, S.H. (ed.), Random Vibration, M.I.T. Press, Cambridge 1958.
13. Crandall, S.H. (ed.), Random Vibration, Vol. 2, M.I.T. Press, Cambridge, 1963.
14. Crandall, S.H. and Mark, W.D., Random Vibration in Mechanical Systems, Academic Press, New York, 1963.
15. Paynter, H.M., Analysis and Design of Engineering Systems, M.I.T. Press, Cambridge, 1961.
16. Crandall, S.H. (ed.), A Unified Approach to Dynamics via Hamilton's Principle, School of Engineering, M.I.T., Cambridge, 1962.
17. Jacobsen, L.S. and Ayre, R.S., Engineering Vibrations, McGraw-Hill, New York, 1958.
18. Long, R.H., Jr., "Experimental and Theoretical Studies of Transverse Vibration of a Tube Containing Flowing Fluid", Journal of Applied Mechanics, ASME, Vol. 22, March 1955.
19. Brown, F.T., "Pneumatic Pulse Transmissions with Bistable-Jet Relay Reception and Amplification", Sc.D. Thesis, M.I.T., May 1962.
20. Den Hartog, J.P., Mechanical Vibrations, 4th ed., McGraw-Hill, New York, 1956.





21. Brown, F.T., "A Unified Approach to the Analysis of Uniform One-Dimensional Distributed Systems", paper submitted for presentation at the 1966 Annual Winter Meeting of the ASME.
22. Pipes, L.A., Matrix Methods for Engineering, Prentice-Hall, Englewood Cliffs, 1963.
23. Pawlak, R.J., "A Continued Study of Pneumatic Flapper Valves", S.M. Thesis, M.I.T., September 1959.



BIOGRAPHICAL NOTE

The author was born in Los Angeles, California on 20 June 1935, and attended local schools through the secondary level. After obtaining a congressional appointment he entered the United States Naval Academy in July 1953 from which he graduated in June 1957 with a Bachelor of Science degree and a commission as an Ensign in the United States Navy. He also received the American Society of Naval Engineers Award for standing highest in his class in those courses most basic to naval engineering. Upon graduation he served two years in the Engineering Department of the cruiser USS LOS ANGELES (CA-135) and then as Engineer Officer of the destroyer USS COGSWELL (DD-651) for another two years. During those four years he made five cruises to the Western Pacific Area. He was then ordered in May 1961 to the Massachusetts Institute of Technology, Course XIII-A, Naval Construction and Engineering, from which he graduated in June 1964 with a Master of Science degree in Mechanical Engineering and a Naval Engineer degree. He received the Brand Award from the American Society of Naval Engineers for standing first in Course XIII-A in the class of 1964.

In August 1959 he married the former Edna Elisabeth Ann Gulick of Whittier, California.

He is a member of Tau Beta Pi, Sigma Xi, and the American Society of Naval Engineers.



6 DEC 66  
5 AUG 69

815868

87696

Thesis  
A4289 Alvarez  
Fluid control system  
behavior in a randomly  
vibrating environment.

6 DEC 66  
5 AUG 69

DISP  
SI

Thesis

A4289 Alvarez

Fluid control system  
behavior in a randomly  
vibrating environment.

87896

thesA4289

Fluid control system behavior in a random



3 2768 001 89852 1

DUDLEY KNOX LIBRARY